Structural Characterization of CENP-C Cupin Domains at Regional Centromeres Reveals Unique Patterns of Dimerization and Functions for the Inner Pocket

by

Jennifer Kui-Lok Chik

A dissertation submitted in partial fulfillment
of the requirements for the degree of
Doctor of Philosophy
(Cellular and Molecular Biology)
in the University of Michigan
2019

Doctoral Committee:

Assistant Professor Uhn-Soo Cho, Chair
Professor Yali Dou
Associate Professor Ajit P. Joglekar
Associate Professor Raymond C. Trievel

Jennifer Kui-Lok Chik

jchik@umich.edu

ORCID iD: 0000-0003-4968-5082

Acknowledgments

There are a multitude of people that I must thank and acknowledge who have helped me throughout my graduate school journey. This work would not have been possible without each of these individuals, and I will always be truly grateful for their support.

First and foremost, a big thank you to Uhn-Soo for allowing me to join the lab and taking a genuine interest in my development and growth as a scientist. I truly appreciate your support over the years, and I have learned so much under your guidance.

I would also like to thank each of my committee members, Dr. Yali Dou, Dr. Ajit Joglekar, and Dr. Ray Trievel for your advice and insight over the years. Thank you for providing me with feedback that was always constructive and for encouraging me to think of my project from different points of view. I always left my committee meetings feeling reassured and eager to move my project forward.

I must also acknowledge all the past and present members of the Cho Lab. Everyone was incredibly welcoming from day one and created a positive lab environment that was a joy to work in. Thank you for always being there for me and never hesitating to help me troubleshoot experiments or guide me in the right direction.

The Cellular and Molecular Biology Program is a wonderful program with so many diverse scientific points of view, and I am incredibly proud to have been a part of it. Thank you to Dr. Bob Fuller, Dr. Kathy Collins, Cathy Mitchell, Margarita Bekiares, Pat Ocelnik, Jessica Kijek, Jim Musgrave, and Lauren Perl for helping me navigate

through graduate school and always ensuring that everything went smoothly behind the scenes.

I must also acknowledge each of the collaborators who have contributed to this work. Thank you to Dr. Lakxmi Subramanian and her lab, Ben Meinen, Dr. Phil Koldewey, and Dr. Barbara Mellone for helping me bring this cupin domain project to life. We certainly would not have been able to create this story without your time and effort.

Without my undergraduate research mentors, Dr. Lori Robins and Dr. Barry Stoddard, I would not be here today. My research experiences as an undergraduate were invaluable and were instrumental in my decision to pursue graduate school. I can only hope that I will one day be able to positively impact students' lives in the same way that you have inspired mine.

I am incredibly lucky to have friends, old and new, who have never failed to be my constant pillars of support and encouragement. Thanks for never hesitating to lend an ear when I needed one most. I will always treasure the many laughs, adventures, and great meals that we shared together.

Lastly, I must thank my family. There are no adequate words to describe how much you all mean to me. I am so thankful for your encouragement and unwavering support throughout this journey. Thank you for always believing that I had the potential to make it this far. I am forever grateful that I get to call you all my family.

Table of Contents

List of Tables

List of Figures

Abstract

Cell division is vital to the development and well-being of all living organisms. This process must occur without error and depends on the equal and accurate division of genetic material to daughter cells. If chromosomes fail to segregate properly, the consequences are often severe and can include cell death, birth defects, and cancer.

The centromere and kinetochore are two factors that are required for the successful completion of cell division. The centromere is a unique chromosomal region that is required for specifying the location of kinetochore assembly. In turn, the kinetochore, a multi-protein complex, assembles onto the centromere during cell division and facilitates the formation of functional microtubule attachments.

Interestingly, while the functions of both the centromere and kinetochore are highly conserved throughout evolution, their underlying organization and composition vary greatly between organisms. *Saccharomyces cerevisiae* possess unique point centromeres that are genetically defined by a 125 bp DNA sequence. On the other hand, the majority of other eukaryotes possess much larger regional centromeres whose locations are epigenetically specified by the histone H3 variant, CENP-A. As each organism has its own unique centromere and kinetochore composition, their kinetochore proteins likely possess differing mechanisms of recruitment and function. Consequently, their respective kinetochore proteins may possess variations in structure to accommodate these differences.

CENP-C is a particularly interesting inner kinetochore component to study due to its evolutionary conservation and scaffolding roles that connect the inner and outer kinetochores. At its C-terminus, CENP-C harbors a conserved cupin domain that has an established role in CENP-C homodimerization. Although the crystal structure of the *Saccharomyces cerevisiae* Mif2^{CENP-C} cupin domain has been determined, it is not yet known whether this domain is structurally conserved within organisms with regional centromeres. Therefore, whether the structural and functional role of the cupin domain is conserved throughout evolution, requires investigation.

This dissertation focuses on the structural conservation of the CENP-C cupin domain and elucidating its functional significance beyond dimerization. Here, I report the crystal structures of two CENP-C cupin domains from organisms with regional centromeres, *Schizosaccharomyces pombe* and *Drosophila melanogaster*. While the central jelly roll architecture is conserved among the three determined CENP-C cupin domain structures, the cupin domains from organisms with regional centromeres contain additional structural features to facilitate dimerization. In addition, analysis of the *Schizosaccharomyces pombe* Cnp3^{CENP-C} cupin domain *in vitro* and *in vivo* shows the inner pocket formed by its jelly roll fold functions as a binding surface for the meiosis-specific protein, Moa1. Thus, these results unveil the evolutionarily conserved and novel features of the CENP-C cupin domain, as well as its additional role as a recruitment factor.

Chapter 1: Introduction

1.1 Summary

Kinetochores are macromolecular protein structures that build upon the chromosomal centromere and form a functional link between the chromosome and microtubules during cell division. Thus far, over 100 human kinetochore proteins have been discovered. Remarkably, these proteins must all work together to ensure the even and accurate division of genetic material during the cell cycle. As the consequences of aberrant genetic division are severe, it is essential to gain a full understanding of the composition and regulation of kinetochore proteins within their respective organisms. Here, basic summaries of centromere types are presented along with a review of core kinetochore components and their respective recruitment and interaction information.

1.2 Centromeres

The centromere is the designated chromosomal site for kinetochore assembly and is thus, indirectly responsible for attaching the chromosome to microtubules during cell division. The term “centromere” was first coined in 1936 and since then, much progress has been made in regards to elucidating their fundamental structure and the significant factors required for function [1]. While the function of the centromere is highly conserved throughout evolution, the underlying DNA sequence and organization diverge greatly among organisms. Even so, a well conserved feature of eukaryotic centromeres is the

presence of the histone H3 variant, CENP-A. In a subset of centromeric nucleosomes, CENP-A replaces H3 and epigenetically specifies the location of the centromere.

1.2.1 CENP-A

The most significant factor in establishing centromeric identity and ensuring the successful recruitment of kinetochore components is the centromere-specific histone H3 variant, CENP-A. CENP-A shares 49% sequence identity with canonical histone H3 and replaces H3 to form an octameric nucleosome along with histones H4, H2A, and H2B [2]. Disruption of CENP-A function shows severe defects in proper chromosome segregation and reveals that CENP-A is essential for viability [3-7]. In the majority of cases, the presence of CENP-A is responsible for epigenetically specifying the centromeric location. Analysis of dicentric human chromosomes showed that CENP-A is only found at the active centromere, regardless of whether the active centromere possesses alpha satellite DNA [8-10]. Additionally, human neocentromeres are not established on any particular DNA sequence or alpha satellite DNA but rely on the presence of ectopically positioned CENP-A nucleosomes [11, 12]. Together, these studies point to the epigenetic specification of the centromere as the sequence of centromeric DNA is not sufficient to specify the location.

Similar to other histone proteins, CENP-A possesses a characteristic histone fold **(Figure 1.1A)**. The loop 1 and helix 2 regions of CENP-A are termed the CENP-A targeting domain (CATD) and are responsible for centromeric localization **(Figure 1.1A)** [13, 14]. In comparison to H3, CENP-A also features a slightly elongated L1 region where two solvent accessible residues, Arg 80 and Gly 81, are shown to be required for maintaining a stable CENP-A population at the centromere [2].

Overexpression of CENP-A results in its localization to non-centromeric loci [15-17]. In *Drosophila melanogaster* cells, non-centromeric CENP-A is sufficient to recruit proteins and build a kinetochore that can form stable attachments to microtubules [16]. However, in human cells, only a small subset of kinetochore proteins are recruited to CENP-A specified ectopic sites [17].

The overall structure of the CENP-A nucleosome is very similar to a canonical H3 containing nucleosome. The crystal structure of the human CENP-A nucleosome shows an octameric structure with DNA wrapped around the core particle in a left-handed manner **(Figure 1.1B)** [2]. In canonical nucleosomes, the loop before the N-terminal helix of H3 makes interactions with the wrapping DNA to stabilize its entry and exit from the core particle. However, CENP-A possesses a shorter loop and N-terminal helix in comparison to its H3 counterpart. Consequently, the DNA present in the CENP-A nucleosome structure is disordered at either end, indicating that the flexible DNA may contribute to a unique chromatin organization compared to the rest of the chromosome [2].

It is worth noting that CENP-A does not occupy 100% of centromeric nucleosomes. In *Schizosaccharomyces pombe,* estimations range from 2–21 CENP-A nucleosomes per 10–12 kb centromeric region [18, 19]. Meanwhile, *D. melanogaster* is estimated to possess 42 CENP-A nucleosomes over its 200–500 kb centromeric region [20]. Additionally, analysis of linear chromatin has shown that stretches of CENP-A nucleosomes are interspersed with regions of canonical nucleosomes [21-23]. Electron microscopy and immunofluorescence images of mitotic chromosomes have shown that the CENP-A nucleosomes are not scattered throughout the centromeric region, but

instead cluster toward the chromosomal surface where the kinetochore will eventually assemble [22, 24]. In contrast to the distinct 146 bp laddering seen from the digestion of non-centromeric chromatin, centromeric chromatin from fission yeast shows smearing when digested with MNase [25-28]. Together, these studies indicate that the centromere possesses unique chromatin organization that maximizes the accessible surface area of CENP-A nucleosomes for kinetochore recognition.

1.2.2 Point Centromeres

Budding yeasts and importantly, *Saccharomyces cerevisiae*, possess point centromeres that are unique, in that the centromeric location is genetically specified by a 125 bp DNA sequence that is sufficient for function, rather than the presence of CENP-A nucleosomes [29-31]. Point centromeres possess only one CENP-A nucleosome, and the kinetochore that subsequently assembles on this location attaches to a single microtubule [32-34].

The 125 bp sequence that specifies *S. cerevisiae* centromeres consists of three conserved DNA elements, CDEI, CDEII, and CDEIII **(Figure 1.2)**. CDEI consists of a PuTCACPuTG consensus sequence and binds to the transcription factor Cbf1 [35]. CDEII is a 78–84 bp AT-rich stretch of DNA that surrounds the centromeric nucleosome [36]. CDEIII, the most critical of the conserved elements, features a TGTTT(T/A)TGNTTTCCGAAANNNAAAAA consensus sequence and binds to the CBF3 complex, a foundational component in *S. cerevisiae* kinetochore assembly [37]. Overall, *S. cerevisiae* is thought to possess a relatively simplistic centromere in comparison to those of other eukaryotes.

1.2.3 Regional Centromeres

The majority of other eukaryotes, including *S. pombe, D. melanogaster,* and humans, possess regional centromeres. While the organization of each regional centromere varies greatly between organisms, they all share core features, including repetitive DNA sequences, characteristic post-translational modifications of centromeric and flanking chromatin, and kinetochores that bind to multiple microtubules [21, 38-46]

In comparison to the point centromeres of *S. cerevisiae, S. pombe* possess relatively large centromeres ranging from 35 to 110 kb across three chromosomes [47]. The *S. pombe* centromere can be characterized into three regions: cnt, imr, and otr **(Figure 1.2)** [38]. At the center of each chromosomal centromere lies a non-repetitive region named the central core (cnt). The cnt is surrounded on either side by the innermost repeats (imr) whose sequences are unique to each chromosome. Together, the cnt and imr regions are named the central domain, and this region is where CENP-A nucleosomes are deposited, and consequent kinetochore assembly takes place [27, 48]. Moreover, this region is marked by H3K4 methylation [43]. Lastly, the imr is flanked by H3K9 methylated heterochromatic repeats (otr), which complete the boundaries of the centromeric region and consist of two types of repeating elements, dg and dh [42, 43, 49]. The orientation and number of the dg and dh elements vary with each chromosome and contribute to the main differences in centromeric size [47].

Human centromeres are AT-rich regions that span significant chromosomal regions consisting of alpha satellite DNA [39]. At its most basic level, alpha satellite DNA consists of differing 171 bp sequences that are repeated in a “head-to-tail” pattern [50]. A cluster of these repeats is then characterized as a higher order repeat, that itself

is repeated and becomes known as a higher order array. At human centromeres, CENP-A nucleosomes are interspersed with H3K4 di-methylated (H3K4me2) canonical nucleosomes [21-23]. Meanwhile, H3K9 is modified with methylation marks in flanking chromatin [21].

D. melanogaster centromeres have been less well characterized but a 420 kb functional centromere was isolated from the Dp1187 minichromosome and was found to possess satellite DNA with two characteristic repeating sequences, AATAT and TTCTC [40, 41]. Like *S. pombe* and human centromeres, *D. melanogaster* centromeres are characterized by the presence CENP-A nucleosomes scattered in between regions of canonical nucleosomes [22]. Similar to human centromeres, *D. melanogaster* shows H3K4me2 marks in the central region and H3K9 methylation markers in the surrounding chromatin [21].

1.2.4 Holocentromeres

Caenorhabditis elegans and certain plant and insect lineages possess holocentromeres. In contrast to both point and regional centromeres, which only occupy a distinct region of the chromosome, holocentromeres are unique in that the centromere spans the entire length of the chromosome **(Figure 1.2)**. Accordingly, both CENP-A and microtubule attachments have been found to line the full extent of the chromosome [5, 51].

1.3 **Overview of Kinetochore Composition and Function**

Along with CENP-A, the first kinetochore components were discovered using sera from patients with CREST syndrome, a type of scleroderma. The sera were found to contain auto antibodies for what we now know as CENPs A, B, and C [52, 53]. Early

electron microscopy images of the kinetochore showed a trilaminar structure with two electron dense regions [54, 55]. These sections can now be classified as the inner and outer kinetochores, CCAN (**C**onstitutive **C**entromere **A**ssociated **N**etwork) and the KMN Network (**K**nl1 complex, **M**is12 complex, and **N**dc80 complex) respectively **(Figure 1.3)**.

1.3.1 The Inner Kinetochore (CCAN)

The inner kinetochore, or the **C**onstitutive **C**entromere **A**ssociated **N**etwork (CCAN), is made up of sixteen proteins that localize to the centromeric region throughout the cell cycle [56, 57]. By building a stable foundation, the inner kinetochore serves as a physical link between the chromosomal centromere and the outer kinetochore. These proteins can be further categorized into five subcomplexes: CENP-C, CENP-L-N, CENP-T-W-S-X, CENP-H-I-K-M, and CENP-O-P-Q-R-U **(Figure 1.4)**.

As more research has been done concerning the regulation of CCAN components, the perception regarding their recruitment has evolved from a linear assembly process to one of a concerted effort, where multiple proteins contribute to the centromeric localization of one subcomplex. The localization of the vast majority of the CCAN subcomplexes is extremely interconnected. With the exception of CENP-C, other CCAN subcomplexes rely on the presence of more than one subcomplex for recruitment during mitosis [58]. Additionally, mechanisms of CCAN protein localization differ between interphase and mitosis, indicating that CCAN may go through a remodeling process as the cell cycle progresses.

1.3.1.1 CENP-C

CENP-C can be broadly classified as a scaffolding protein and is considered to be the initiating factor for kinetochore assembly after CENP-A. CENP-C is one of two

CCAN components to directly recognize CENP-A nucleosomes and interacts with the CENP-A C-terminal tail as well as the acidic patch of H2A and H2B [59]. After CENP-A chromatin has been established, CENP-C is the first kinetochore component to be recruited to the centromere and is additionally required for the recruitment of all other CCAN components during mitosis [58].

CENP-C has been found to directly interact with multiple CCAN subcomplexes including CENP-L-N and CENP-H-I-K-M [58, 60-62]. Additionally, the N-terminus of CENP-C binds directly to the Mis12 complex and therefore serves as a direct link between the inner and outer kinetochores [63-66]. Lastly, at its C-terminus, CENP-C possesses a characteristic cupin domain that is used for homodimerization [67]. However, the functional contribution of this conserved cupin domain to kinetochore assembly has not yet been fully elucidated.

Taken together, this data establishes CENP-C as a foundational protein that has a critical role in kinetochore assembly. CENP-C biology will be discussed in further detail in the following chapter.

1.3.1.2 CENP-L-N

The structure of the truncated *S. cerevisiae* CENP-L-N complex shows that CENP-L is comprised of α-helices and a ten stranded β-sheet which is extended via β-augmentation by the C-terminus of CENP-N [61]. CENP-N, along with CENP-C, is one of two kinetochore components to directly recognize CENP-A nucleosomes [34]. The CENP-N N-terminus recognizes CENP-A nucleosomes through the L1 loop of the CATD and thus, does not interact with canonical H3 nucleosomes [58, 68, 69]. There is evidence from multiple model organisms that the CENP-L-N complex binds to CENP-C

in vitro [58, 60, 61, 70, 71]. Biochemical reconstitution of the two complexes shows that CENP-L-N and CENP-H-I-K-M also interact *in vitro* [58].

During interphase, the interaction between CENP-A and CENP-N is sufficient for kinetochore localization [58]. However, the CENP-L-N complex also requires an interaction with CENP-C for centromere localization during mitosis in addition to its interaction with CENP-A [58]. Therefore, the mechanisms of centromeric localization vary depending on the state of the cell cycle.

1.3.1.3 CENP-T-W-S-X

The CENP-T-W-S-X complex is composed of four histone-fold proteins that have been proposed to form a unique nucleosome-like structure at the centromere. On their own, CENP-T-W forms a heterodimer while CENP-S-X forms a heterotetramer [72]. However, when all four proteins are mixed, one CENP T-W heterodimer replaces one CENP-S-X heterodimer resulting in a CENP-T-W-S-X heterotetramer composed of one of each of the respective proteins [72]. In contrast to canonical nucleosomes, the CENP-T-W-S-X complex positively supercoils DNA [73].

Like CENP-C, CENP-T connects directly to the outer kinetochore via the Mis12 complex but also has unique roles in interacting with the Ndc80 complex [17, 74]. The N-terminal region of CENP-T binds directly to the Ndc80 complex and thus, acts as a direct link between the inner and outer kinetochores, similar to CENP-C [74]. Although CENP-A is required for epigenetically specifying the centromeric location in most centromeres, it is not necessarily required for kinetochore assembly once CENP-C and CENP-T have been established [17]. When the endogenous centromere is inactivated, and CENP-C and CENP-T are artificially tethered to ectopic chromosomal sites, the

KMN Network is recruited and chromosomes proceed through cell division [17]. Therefore, CENP-C and CENP-T are considered to be the foundational proteins in kinetochore assembly.

Like other CCAN components, CENP-T-W-S-X has interdependencies when it comes to its centromeric localization. Specifically, based on knockdown studies, CENP-T-W-S-X requires CENP-C, CENP-H-I-K-M, and CENP-L-N for localization to the centromere during mitosis [58]. Along the same lines, CENP-T-W has been shown to bind to the CENP-H-I-K-M complex *in vitro* [58, 75].

1.3.1.4 CENP-H-I-K-M

Negative staining of the CENP-H-I-K-M complex reveals an overall shape that features a foundational base (CENP-I-M) and a head with a nose (CENP-H-K) [75]. CENP-M has a similar structure to GTPases but does not show the characteristic GTPase conformational changes or enzymatic activity [75]. CENP-H is predicted to be a coiled-coil protein with a central nuclear localization signal [71, 76]. Crosslinking studies show that CENP-M binds only to CENP-I and does not interact with CENP-H or CENP-K. Meanwhile, CENPs H, I, and K all interact with one another [75].

As these proteins form a stable subcomplex, the alteration of any of the components disrupts centromeric localization of the entire complex [56, 57, 75, 77]. CENP-H-K interacts directly with hydrophobic motifs in the CENP-C PEST (Pro-Glu-Ser-Thr) region [58, 62]. However, the interaction with CENP-C is not sufficient for centromeric localization of the complex [58]. In addition to CENP-C, the CENP-H-I-K-M subcomplex requires both CENP-L-N and CENP-T-W-S-X for centromeric localization [56, 58].

1.3.1.5 CENP-O-P-Q-R-U

Reconstruction of the complex via negative stain electron microscopy revealed that the CENP-O-P-Q-R-U has a wide base domain (CENP-Q-U) and a head domain (CENP-O-P) at the other end of the complex [78]. The *Kluyveromyces lactis* CENP-O-P structure shows a heterodimeric complex where each protein is composed of double RWD domains [79].

Structural reconstruction of a 26 protein kinetochore complex revealed that the CENP-O-P-Q-R-U complex binds to both the CENP-H-I-K-M and CENP-L-N complexes [78]. Based on pulldown data, CENP-O-P forms the required interactions to bind the subcomplex to other CCAN components [78]. Even though the *S. cerevisiae* homolog of the CENP-O-P-Q-R-U complex, COMA, has been shown to bind to the Mis12 complex, it is not known if this interaction is widely conserved in higher eukaryotes [65, 66, 80]. Even though they are part of a CCAN complex, CENP-Q-U has been found to bind to microtubules, and this activity seems to work in cooperation with the Ndc80 complex to enhance overall kinetochore-microtubule binding activity. [78, 81, 82]. In *S. cerevisiae*, the phosphorylation of CENP-P is indirectly required for the loading of centromeric cohesin [83].

Each complex member seems to require the others for stability, as the reduced expression of any of the complex proteins results in reduced complex localization to the centromere [78]. CENP-O-P-Q-R-U is likely to be one of the last CCAN components to be recruited to the inner kinetochore, as its knockdown does not significantly affect the localization of other CCAN proteins [58]. Corroborating the structural data, knockdown

of CENP-H, CENP-L, or CENP-N via RNAi prevents localization of the CENP-O-P-Q-R-U complex [78].

1.3.2 The Outer Kinetochore (KMN Network)

The outer kinetochore attaches directly to microtubules and regulates checkpoint signaling. The KMN Network is named after its main components, the **K**nl1 complex, the **M**is12 complex, and the **N**dc80 complex **(Figure 1.5)** [84]. Unlike CCAN, the KMN Network does not localize to the centromere throughout the cell cycle. Members of the KMN Network begin to associate with kinetochores during late interphase and dissociate during telophase [85].

1.3.2.1 The Mis12 Complex

The Mis12 complex consists of four proteins, Mis12, Nsl1, Nnf1, and Dsn1, that function together as a scaffolding complex to connect the inner and outer kinetochores through interactions with CENP-C, the Knl1 complex, and the Ndc80 complex.

The crystal structures of both the human Mis12 complex and *K. lactis* homolog, MIND complex, have been determined [65, 66]. Both structures revealed that each of the Mis12 complex proteins possess a similar protein fold with N-terminal helical hairpins and longer helices moving towards the C-terminal end [65, 66]. Within the Mis12 complex, the components form two subcomplexes Mis12/Nnf1 and Dsn1/Nsl1. Each subcomplex is created through the interaction of the N-terminal helical hairpins that result in the formation of four-helix bundles and two designated head domains. Head 1 and Head 2 are made up of Mis12/Nnf1 and Dsn1/Nsl1, respectively **(Figure 1.6A)**. After the head groups, the two subcomplexes become increasingly intertwined through alpha-helical interactions moving towards the C-terminus. Thus, the entire

complex forms an elongated Y-shape with the termini of all four complex proteins oriented in the same manner (e.g., all the N-termini face one side and the C-termini face the other).

CENP-C interacts with Mis12 through Head 1 interactions. In *K. lactis*, this interaction is sufficient for high-affinity binding [65]. However, in humans, secondary interactions through the helical connector of the Dsn1/Nnf1 subcomplex and the N-terminal helix of Mis12 are required [66]. Uniquely, the *K. lactis* COMA complex interacts with the MIND complex via Ame1 (CENP-U homolog), and this interaction is compatible with Mif2 (CENP-C homolog)/MIND binding [65, 80]. Interestingly, Dsn1 is also phosphoregulated by Aurora B kinase to make the Head 1 region available for CENP-C and Ame1 binding [65, 66]. The C-terminal region of *S. cerevisiae* Dsn1 was also found to be sufficient for binding to the Ndc80 complex via Spc24/25 [65]. In humans, the C-terminal tail of Nsl1 has been found to interact with the Ndc80 complex and the Knl1 complex via Spc24/25 and the C-terminal tail of Knl1, respectively [86]. Lastly, there is evidence for CENP-T and its phosphorylation state influencing Mis12 recruitment. The phosphorylation via CDK1 of human CENP-T at Ser 201 was found to be critical for Mis12 complex binding *in vitro* and *in vivo* [87].

In contrast to the two other protein complexes within the outer kinetochore, the Mis12 complex does not bind directly to microtubules [84]. Even so, cells with depleted Mis12 complex subunits show severe defects in microtubule attachment and aberrant division of chromosomes, likely due to the reliance of the other two KMN Network complexes on the Mis12 complex for recruitment [88].

1.3.2.2 The Knl1 Complex

The Knl1 complex is made up of two proteins, Knl1 and Zwint. Knl1, the largest protein within the KMN network, can be broadly characterized as a scaffold for a variety of proteins involved in the regulation of spindle assembly checkpoint signaling **(Figure 1.6B)**. Knl1 possesses a variety of functional domains that aid in its function. Knl1 binds to microtubules through a conserved basic patch at its N-terminus [89]. Accordingly, Knl1 depleted cells are unable to form stable kinetochore-microtubule attachments [90]. The N-terminal region also possesses SILK and RVSF motifs that are important for the recruitment and association of protein phosphatase 1 (PP1), which removes Aurora B kinase phosphorylation [91]. The two KI motifs that are also found at the N-terminal region of Knl1 serve as important binding sites for Bub1 and BubR1, two proteins that function as spindle assembly checkpoint kinases [92, 93]. At its N-terminal and central regions, Knl1 possesses characteristic Met-Glu-Leu-Thr (MELT) repeats that recruit Bub3 and Bub1 when phosphorylated by Mps1 [94-96]. The C-terminal region of Knl1 contains a coiled-coil region for Zwint binding [86, 92, 97]. While the majority of Knl1 is thought to be relatively unstructured, its C-terminus possesses an RWD domain that is responsible for its kinetochore localization via its interaction with Nsl1 of the Mis12 complex [86, 90, 92, 97].

Similar to Knl1, Zwint is responsible for recruiting regulatory proteins to the kinetochore. Specifically, ZW10, a component of the trimeric Rod–Zwilch–Zw10 (RZZ) complex, is reliant upon Zwint for kinetochore localization [98, 99]. In turn, the RZZ complex is responsible for recruiting regulatory checkpoint MAD proteins and indirectly recruiting dynein to the kinetochore [100, 101]. Knl1 and Zwint localization seem to be

at least partially interdependent, with Knl1 having a larger effect on Zwint localization [102].

In cells where the Knl1 complex is depleted/deleted, the phenotype mirrors those of cells with missing checkpoint proteins. Thus, further reinforcing the role of the Knl1 complex as a scaffold that recruits regulatory checkpoint proteins to the kinetochore. Knl1 knockdown cells show defects in cell cycle checkpoints and increased incidence of chromosome missegregation, a phenotype very similar to cells with both Bub1 and BubR1 affected by RNAi [90]. Similarly, cells show a checkpoint defect when is Zwint depleted [98, 99].

1.3.2.3 The Ndc80 Complex

The Ndc80 complex consists of four proteins assembled as two sets of dimers, Ndc80/Nuf2 and Spc24/Spc25 whose primary roles are to microtubule binding and kinetochore interactions, respectively **(Figure 1.6C)** [65, 74, 84, 103]. Each of the Ndc80 components feature a globular head followed by a stretch of α-helices. Through coiled-coil interactions, the complex forms an overall shape similar to a 57 nm elongated dumbbell with the globular domains at either end [104]. The globular domains of both Ndc80 and Nuf2 are calponin homology domains while Spc24 and Spc25 possess RWD domains [103, 105, 106]. The reconstituted KMN Network binds to microtubules with higher affinity compared to the individual Knl1 complex and Ndc80 complex *in vitro* [84]. Thus, microtubule binding is likely a cooperative effort between complexes within the outer kinetochore.

In accordance with its function, depletion of Ndc80 complex components results in cells that are unable to form stable kinetochore-microtubule attachments and disruption of the kinetochore's characteristic trilaminar structure [107, 108].

The Ndc80 complex interacts directly with the Mis12 complex and its kinetochore localization occurs downstream of other KMN Network complexes [109]. The Spc24/25 subcomplex interacts with the Mis12 complex via Dsn1 [65, 110]. Spc24/25 also bind directly to the N-terminal region of CENP-T, though this interaction seems to be mutually exclusive with the interaction with the Mis12 complex [17, 74, 87, 110]. Therefore, there are two separate pathways for the recruitment of the Ndc80 complex.

1.3.3 Conservation of Kinetochore Proteins Between Model Organisms

While the kinetochore itself is a highly conserved structure throughout evolution, the individual proteins and subcomplexes are not necessarily well conserved, especially within the inner kinetochore **(Table 1.1)**. CENP-C is the most conserved CCAN component within higher eukaryotes. Interestingly, both *D. melanogaster* and *C. elegans* kinetochores are missing all CCAN components except for CENP-C [111, 112]. The evolutionary or functional justification for these simpler kinetochores is an aspect of kinetochore biology that still needs to be addressed. In addition to being the lone scaffold within the inner kinetochore, CENP-C may be especially important in these organisms as this CENP-C mediated pathway is the only way to recruit the Ndc80 complex without the presence of CENP-T. Notably, recent discoveries have shown that some insect lineages do not possess CENP-A or CENP-C homologs [113]. The exception being dragonflies that may have a CENP-C homolog that has developed a divergent CENP-C motif sequence [113]. Even without the components to build the

canonical foundation of the kinetochore, the majority of these lineages still possess CCAN components such as CENP-L, CENP-N, and CENP-I [113]. All of the insects with this unique kinetochore makeup made the transition from monocentric to holocentric centromeres at some point during evolution [113]. Because CENP-A and CENP-C are traditionally critical components in kinetochore assembly, it would be interesting to elucidate the recruitment mechanisms and interactions of kinetochore components within these unique insect lineages. Perhaps some of the protein interactions and the hierarchy of protein recruitment are conserved with those of traditional kinetochores.

Members of the KMN Network are better conserved than those of CCAN across organisms **(Table 1.1)**. However, the composition of the *D. melanogaster* outer kinetochore is not composed of traditional KMN Network components. The *D. melanogaster* Mis12 complex has no known Dsn1 homolog and instead possesses one of two Nnf1 subunits [114-116]. Additionally, the *D. melanogaster* kinetochore does not possess any known homolog of Zwint. Interestingly, all of the divergent insect lineages missing CENP-A and CENP-C still possess Mis12, Ndc80, and Spc25 homologs [113].

As CCAN components are primarily seen as scaffolding proteins, it is not surprising that they are less conserved in comparison to the outer kinetochore components. As long as a connection can be formed between the centromere and the KMN Network, the resulting partial kinetochore may still be functional. On the other hand, the KMN Network proteins may need to be highly conserved because they perform two specific and vital roles: the regulation of checkpoint signaling as well as the binding and regulation of microtubule attachments.

Finally, although certain kinetochore proteins may be conserved from organism to organism, that does not guarantee that the homologs perform identical functions. For example, the *S. cerevisiae* homologs of CENP-Q and CENP-U are essential proteins [80]. In contrast, CENP-Q and CENP-U have a relatively minor role in kinetochore assembly in HeLa cells as knockout of these proteins still results in the recruitment of most core kinetochore proteins [56, 58, 80]. The reason for this discrepancy may be due to the the unique interaction between the MIND and COMA complexes in *S. cerevisiae* [65, 66, 80]. Thus, protein homologs likely have varying degrees of significance in different systems.

In *C. elegans,* Knl1, along with the Mis12 complex, forms a platform for the assembly of the Ndc80 complex [84]. However, in other organisms, Knl1 does not play a role in the interaction between the Ndc80 and Mis12 complexes [86, 117, 118]. Additionally, it has been established that CENP-T interacts with the Ndc80 complex via Spc24/25. However, the requirement of CENP-T phosphorylation for this interaction is organism dependent. Human and chicken proteins show a requirement for CENP-T phosphorylation in order to interact with the Ndc80 complex while *S. cerevisiae* does not [17, 74, 110].

In summary, throughout evolution, organisms have developed both centromeres and kinetochores with differing degrees of conservation. While many of the interactions are conserved, by necessity, some unique kinetochores must have different methods of kinetochore regulation. Therefore, the thorough investigation and comparison of kinetochore proteins from different organisms is required to understand the complete mechanisms of kinetochore function and assembly.

1.3.4 Disease Implications of Aberrant Chromosome Division and Kinetochore Dysfunction

Since kinetochores have a significant role in the accurate division of genetic material, it is not surprising that one of the most common consequences of kinetochore dysfunction is genomic instability, which in turn, can lead to aneuploidy. Aneuploidy, the possession of an abnormal number of chromosomes, is causative of a plethora of significant consequences to cells and the organism as a whole. Aneuploidies can be sorted into two classes: constitutional aneuploidy (occurring in all cells of the organism, likely inherited from parental germ cell) and somatic aneuploidy (only occurring in a subset of the organism's cells, caused by errors in cell division). Whether a cell is missing chromosomes or possesses too many, aneuploidy can have detrimental effects due to the subsequent changes in gene dosage. A variety of kinetochore-associated factors can be causative of aneuploidy including defects in microtubule attachment and impaired signaling of cell cycle checkpoints.

Cases of constitutional aneuploidy often lead to severe consequences including miscarriage and birth defects that can lead to mental retardation and developmental impairment. It is estimated that approximately one-third of miscarried pregnancies are due to aneuploidy and approximately 0.3% of live births are aneuploid [119]. The most common aneuploidies of live births are Down Syndrome (trisomy 21), Triple X syndrome (XXX), Klinefelter Syndrome (XXY), and XYY Syndrome (XYY) [119]. However, trisomy of the vast majority of chromosomes is incompatible with life. The incidence of individuals born with trisomies is higher than monosomies, as all autosomal monosomies are embryonic lethal.

Aneuploidy is a hallmark feature of cancer cells. It is estimated that approximately 90% of solid tumors and approximately 75% of hemopoietic cancers are aneuploid [120]. The presence of aneuploidy can alter the gene dosage of oncogenes and tumor suppressors, which are each required for keeping the other in balance. Not surprisingly, the overexpression of kinetochore components has also been found in certain cancers. Elevated CENP-A expression has been found in many cancers including colorectal, breast, ovarian, and lung [121, 122]. CENP-H has been found to be expressed at elevated levels in primary colorectal cancer tissues [123]. Ndc80, originally known as Hec1 (highly expressed in cancer), was discovered by its interaction with the Retinoblastoma tumor suppressor via yeast two-hybrid and has been found to have elevated expression levels in cervical and colon cancer cell lines, as well as breast tumor tissue [124-126]. Additionally, Ndc80 overexpression is sufficient to induce tumor formation in inducible mouse models [127].

Individual kinetochore proteins have also been implicated in disease phenotypes. Fanconi Anemia is a serious disorder that is characterized by bone marrow failure, physiological abnormalities, increased susceptibility to cancer, and overall genomic instability [128]. The Fanconi Anemia pathway has roles in DNA repair, specifically in the repair of interstrand crosslinks. The vast majority of the mutations associated with the disease phenotype are within a core complex of proteins required for initiating the repair cascade, termed the Fanconi Anemia core complex [128]. CENP-S has been shown to bind to FANCM, a core complex component, and CENP-S depletion resulted in impaired activation of the Fanconi Anemia pathway [129].

Lastly, CENPs A, B, and C were first discovered from the autoimmune sera of CREST syndrome patients [52, 53]. While CREST Syndrome is not thought to be a result of aberrant regulation of these proteins and it is not known why patients generate these antibodies, it is worth noting that detection of these proteins in patient sera is still used as a diagnostic tool today.

1.4 **Figures**

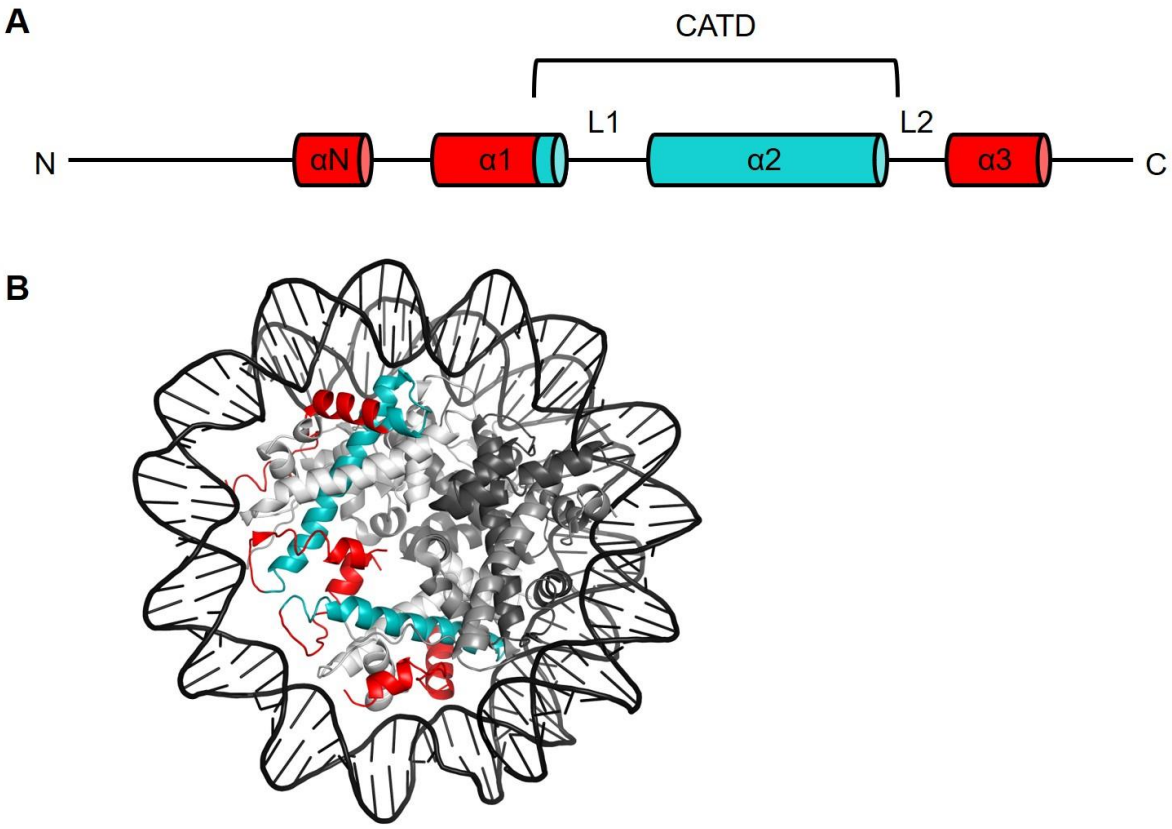

Figure 1.1 Structure of CENP-A nucleosomes.A. Secondary structure representation of CENP-A. The CENP-A targeting domain (CATD) is responsible for centromeric localization and consists of the loop 1 and helix 2 regions (teal). **B.** Crystal structure of the octameric human CENP-A nucleosome (PDB ID: 3AN2) [2]. CENP-A is colored red while its CATD is represented in teal. The remaining six histones H4, H2A, and H2B are shown in varying shades of gray.

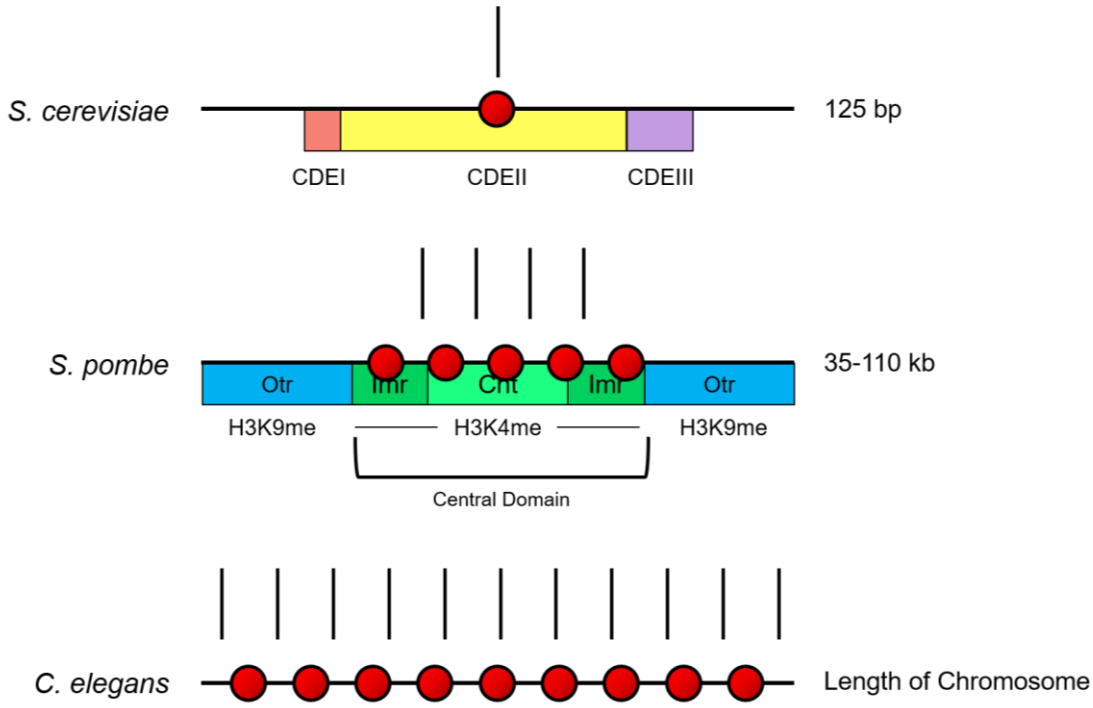

Figure 1.2 Centromeric structure and organization varies greatly between organisms.
S. cerevisiae, S. pombe, and C. elegans are used as representative model organisms for point, regional, and holocentromeres, respectively. CENP-A nucleosomes are represented by red circles and microtubules are shown as black lines.

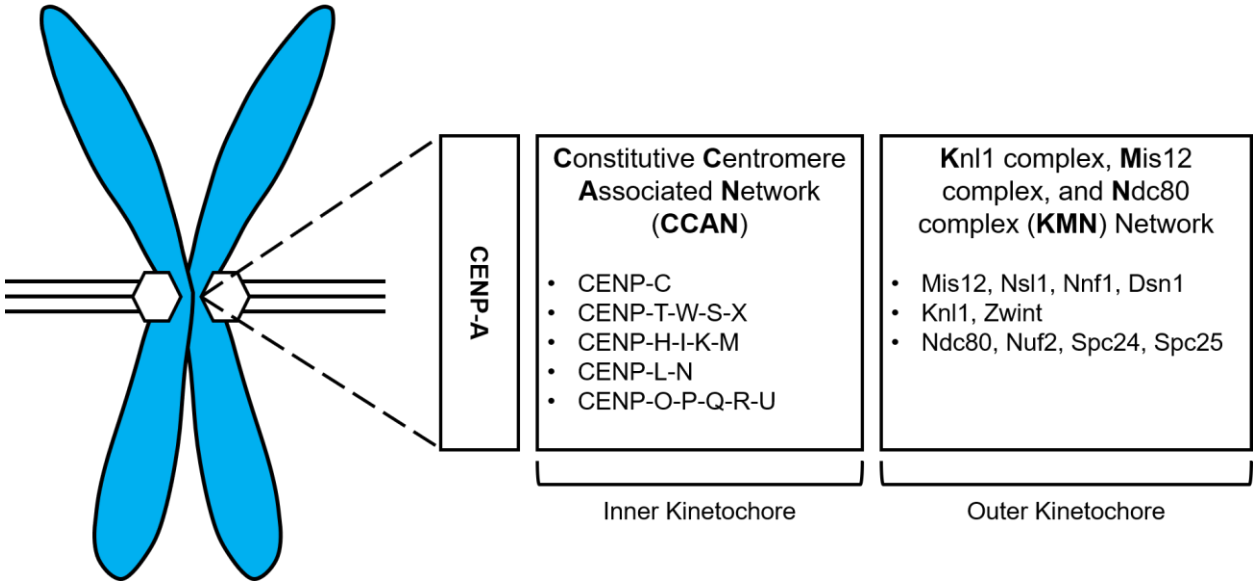

Figure 1.3 Basic organization of the kinetochore and its major subcomplexes.
The inner kinetochore (CCAN) builds upon CENP-A nucleosomes and forms a stable foundation for kinetochore assembly. The outer kinetochore (KMN Network) forms stable microtubule attachments and regulates checkpoint signaling.

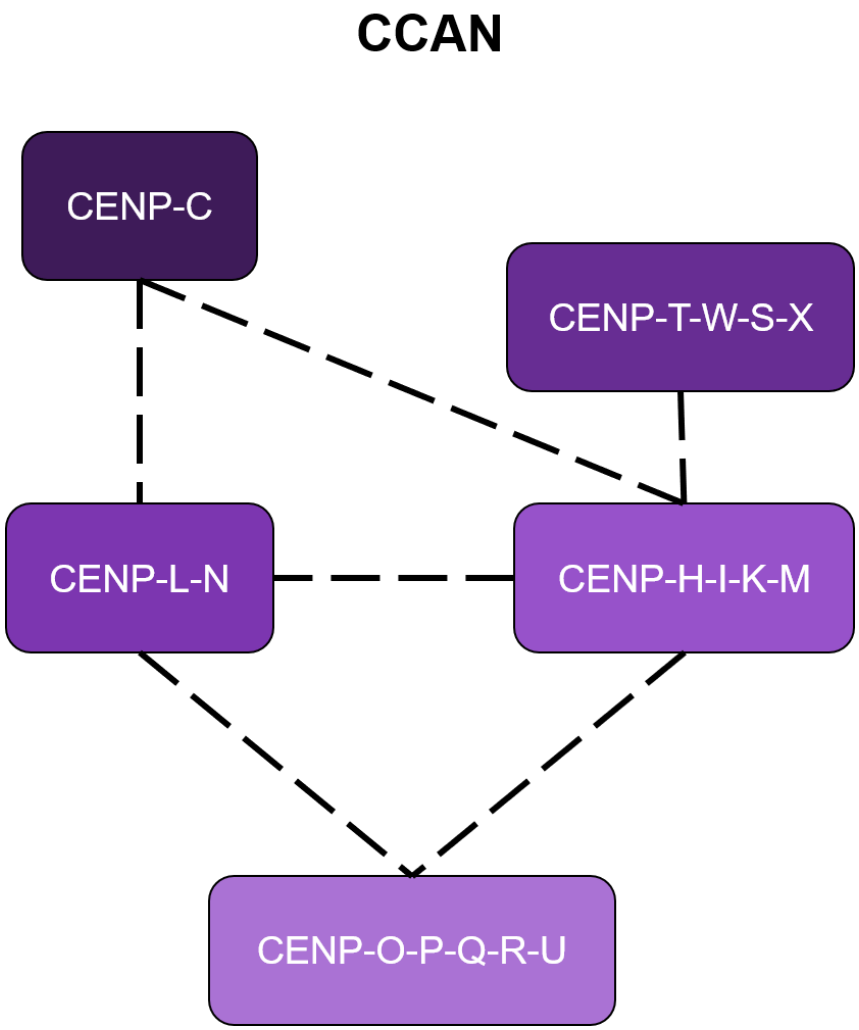

Figure 1.4 Summary of physical interactions between CCAN subcomplexes.

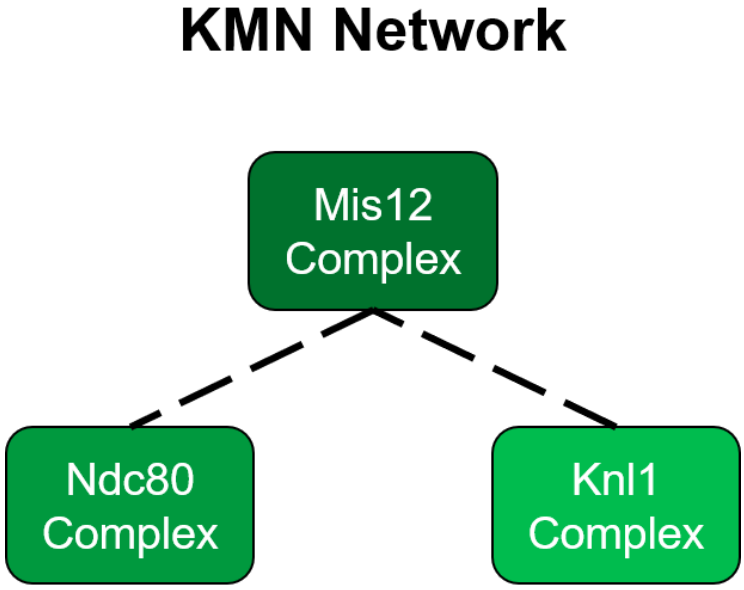

Figure 1.5 Summary of physical interactions between KMN Network subcomplexes.

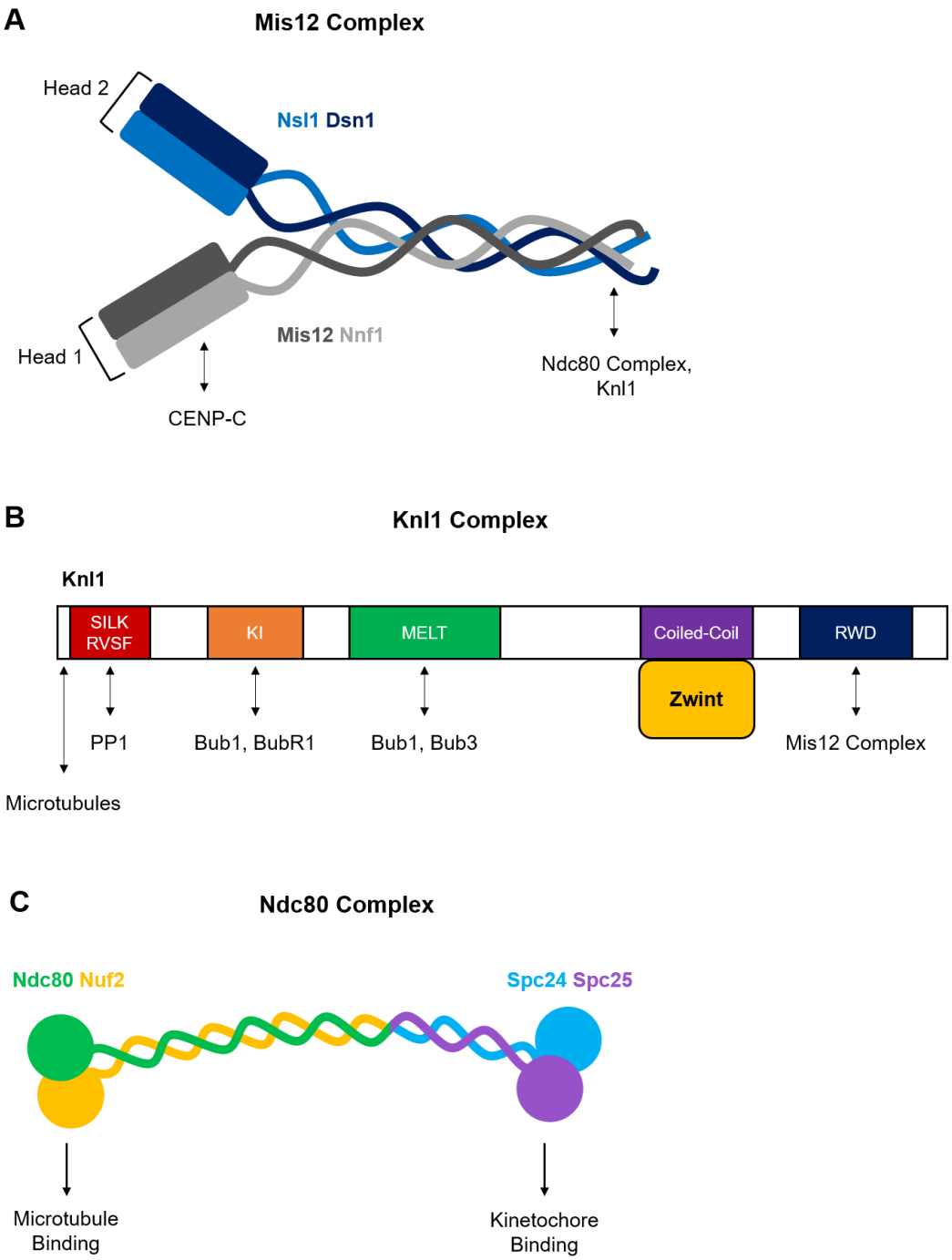

Figure 1.6 Cartoon representations of KMN Network subcomplexes.
A. The Mis12 complex serves as a central connection point within the KMN Network and forms a Y-shaped complex with two head domains at the N-terminus. **B.** The Knl1 complex is a protein scaffold for spindle assembly checkpoint signaling proteins. **C.** The Ndc80 complex features globular domains on either side of its characteristic dumbbell shape and has primary roles in microtubule binding.

Table 1.1 CCAN and KMN Network equivalents between common eukaryotic model organisms.
Modified from [130].

	Protein	Human	*S. pombe*	*S. cerevisiae*	*D. melanogaster*	*C. elegans*
	CENP-A	CENP-A	Cnp1	Cse4	Cid	HCP-3
CCAN	CENP-C	CENP-C	Cnp3	Mif2	CENP-C	HCP-4
	CENP-N	CENP-N	Mis15	Chl4		
	CENP-T	CENP-T	Cnp20	Cnn1		
	CENP-W	CENP-W	New1	Wip1		
	CENP-S	CENP-S	Mhf1	Mhf1		
	CENP-X	CENP-X	Mhf2	Mhf2		
	CENP-L	CENP-L	Fta1	Iml3		
	CENP-H	CENP-H	Fta3	Mcm16		
	CENP-K	CENP-K	Sim4	Mcm22		
	CENP-I	CENP-I	Mis6	Ctf3		
	CENP-M	CENP-M				
	CENP-O	CENP-O	Mal2	Mcm21		
	CENP-P	CENP-P	Fta2	Ctf19		
	CENP-Q	CENP-Q	Fta7	Okp1		
	CENP-R	CENP-R				
	CENP-U	CENP-U	Mis17	Ame1		
KMN Network	Mis12	Mis12	Mis12	Mtw1	Mis12	Mis12
	Nsl1	DC8	Mis14	Nsl1	Kmn1	KBP-2
	Nnf1	PMF1	Nnf1	Nnf1	Nnf1a, Nnf1b	KBP-1
	Dsn1	Dsn1	Mis13	Dsn1		KNL3
	Knl1	KNL1	Spc7	Spc105	Spc105R	KNL1
	Zwint	Zwint-1	Sos7	Kre28		KBP-5
	Ndc80	Hec1	Ndc80	Ndc80	Ndc80	Ndc80
	Nuf2	Nuf2	Nuf2	Nuf2	Nuf2	Nuf2
	Spc24	Spc24	Spc24	Spc24	Kmn2	KBP-4
	Spc25	Spc25	Spc25	Spc25	Spc25	KBP-3

Chapter 2: Characterization of Regional Centromere CENP-C Cupin Domains from *S. pombe* and *D. melanogaster*

2.1 Introduction

2.1.1 CENP-C

CENP-C, a foundational inner kinetochore protein, is known to localize to the centromere by directly recognizing CENP-A nucleosomes and subsequently participating in the recruitment of both inner kinetochore (CCAN) and outer kinetochore (KMN Network) components. CENP-C is an essential gene in multiple model organisms with the exception of *S. pombe* [60, 131-133]. While viable, Cnp3 (CENP-C homolog) null *S. pombe* cells exhibit severe phenotypes such as cold and thiabendazole sensitivity and quickly acquire suppressor mutations in order to lessen cellular stress [60]. CENP-C significance is evidenced from cellular studies, as when CENP-C function is disrupted the resulting cells exhibit severe defects in chromosome segregation [134-137]. Additionally, the injection of HeLa cells with anti-CENP-C antibodies prevents the correct assembly of the kinetochore and results in metaphase-arrested cells [138].

Structurally, little is known about CENP-C. This is likely because the majority of CENP-C is predicted contain intrinsically disordered protein regions, meaning that they are disordered in the absence of binding partners **(Figure 2.1)** [139, 140]. However, multiple CENP-C sub-domains, particularly within the human protein, have been characterized that emphasize its functional significance as a scaffolding protein in

kinetochore assembly **(Figures 1.4 and 2.2A)**. The N-terminal regions of CENP-C can be broadly classified as the regions required for the assembly of a functional kinetochore. The CENP-C N-terminal domain binds directly to the Mis12 complex and thus, acts as a point of recruitment and a physical link to the outer kinetochore [63, 64]. While the sequence of the CENP-C N-terminus is not well conserved, this Mis12 complex interaction is preserved throughout organisms [63, 80, 116].

Downstream of the N-terminus is a PEST (Pro-Glu-Ser-Thr) domain, enriched in proline, glutamate, serine and threonine residues, that binds to the CENP-H-I-K-M complex [58, 62]. CENP-C has also been shown to bind to the CENP-L-N complex [58, 60, 61, 70, 71]. However, the CENP-C region required for CENP-L-N binding has not been well characterized. This CENP-C region is likely located close to the region required for CENP-H-I-K-M binding [58, 70]. The central region of human CENP-C binds to CENP-A nucleosomes through the CENP-A C-terminus [141]. However, the function of this region is not likely to be highly conserved as the equivalent region of chicken CENP-C is dispensable and has no discernable consequences on cell viability in DT40 cells [70].

In contrast to the evolutionarily divergent sequence at the N-terminal regions, the CENP-C C-terminus contains two conserved regions: the CENP-C motif and the cupin domain **(Figure 2.2)**. The CENP-C motif is the hallmark feature of CENP-C homologs and is used for CENP-A recognition [59, 142]. CENP-C binding has also been shown to remodel and change the overall shape of the CENP-A nucleosome structure [143, 144]. Lastly, the cupin domain at the C-terminal end of the protein is used for CENP-C homodimerization [67, 145].

The human CENP-C protein has two characterized centromere localization domains. One at the central region and one at the C-terminus **(Figure 2.2A)**. Unsurprisingly, the residues required for localization within the CENP-C central region overlap with the central CENP-A binding domain [141, 146-148]. A C-terminal region containing the CENP-C motif and the cupin domain has also been shown to be required for centromeric localization [148, 149]. Specifically, the CENP-C motif contains a conserved arginine residue that has been shown to be required for CENP-C localization in multiple organisms [60, 133, 150]. Accordingly, this arginine residue is important for maintaining binding affinity to the nucleosome [59].

CENP-C has also been characterized as a DNA binding protein. While human CENP-C does not show affinity for a specific DNA sequence *in vitro*, the central and C-terminal domains have been shown to bind to alpha satellite DNA *in vivo* [141, 146, 148, 151, 152]. As expected, these DNA binding regions overlap with those required for centromeric localization.

There is evidence for kinetochore dynamics and remodeling throughout the cell cycle as CCAN recruitment dependencies change from interphase to mitosis. In mitotic cells, all other CCAN components require CENP-C for recruitment to the centromere [58]. Meanwhile, CENP-C localization does not seem to depend on any other proteins besides CENP-A [58]. However, during interphase, CENP-C recruitment depends on the CENP-H-I-K-M and CENP-L-N complexes [58, 70, 153, 154]. Accordingly, the regions of CENP-C required for centromeric localization change depending on the state of the cell cycle. It has been shown in chicken DT40 cells that CENP-C residues 166–324 (a region upstream of the central domain) and CENP-C residues 601–864 (the

CENP-C motif and cupin domain) are the required regions for centromeric localization in interphase and mitosis, respectively [70].

Paradoxically, studies have also implicated that CENP-C is involved in the CENP-A recruitment mechanism, as depletion of CENP-C results in a decreased CENP-A population at the centromere [58, 143]. Additionally, the C-terminal region of CENP-C, including the CENP-C motif and the cupin domain, interacts with Mis18BP1 [155, 156]. The human Mis18 complex, comprised of Mis18α, Mis18β, and Mis18BP1, acts as a licensing factor for the deposition of CENP-A into centromeric chromatin [157]. Consequently, depletion of CENP-C reduces centromeric localization of the Mis18 complex [158]. The *D. melanogaster* CENP-C cupin domain binds to Cal1, an evolutionarily distinct CENP-A chaperone and likely the functional homolog of the Mis18 complex [20].

2.1.2 Cupin Domain

The CENP-C cupin domain, the main focus of this dissertation, is part of the large and extremely diverse cupin superfamily. The term cupin is derived from the Latin term “cupa,” meaning small barrel and was named due to the characteristic shape of the proteins [159]. Specifically, members of the cupin family are characterized by two metal binding histidine motifs ($GX_5HXHX_{3,4}EX_6G$ and $GX_5PXGX_2HX_3N$) that are separated by an intervening loop region of variable size [160, 161]. Altogether, the cupin fold consists of six total β-strands, two within each motif and two within the loop region. Members of the cupin family have been discovered in archaea, eubacteria, and eukaryota and have been found with and without enzymatic activity [162]. Additionally, cupin domain

proteins perform a variety of functions including roles as transcription factors, isomerases, dioxygenases, and germins [163-166].

CENP-C cupin domains along with the CENP-C motif are well conserved across organisms suggesting that the cupin domain possesses functional importance [142]. While members of the cupin domain superfamily have been found in a variety of oligomeric states, the CENP-C cupin domain has only been found to be dimeric [67, 167]. The structure of the *S. cerevisiae* Mif2 (hereafter referred to as *Sc*Mif2^{CENP-C}) cupin domain has previously been determined and reveals a homodimeric complex composed of two nine-stranded jelly roll monomers **(Figure 2.3A)** [67]. When the *Sc*Mif2^{CENP-C} cupin domain is deleted or dimerization is disrupted through point mutations, cells show a temperature sensitive phenotype [67]. Thus, indicating that the cupin domain has a designated role in cellular biology.

As stated in Chapter 1, centromere and kinetochore composition varies significantly from organism to organism. Here, we present the crystal structures of the *S. pombe* Cnp3 (hereafter referred to as *Sp*Cnp3^{CENP-C}) and *D. melanogaster* CENP-C (hereafter referred to as *Dm*CENP-C) cupin domains at 2.52 Å and 1.81 Å resolutions, respectively. While we find a conserved dimeric core structure within each cupin domain, we find that both the *Sp*Cnp3^{CENP-C} and *Dm*CENP-C cupin domains possess additional and unique structural features. Particularly, the *Sp*Cnp3^{CENP-C} cupin domain features a distinct β-hairpin at the N-terminal side of the jelly roll core, which is essential for maintaining the stability of the dimeric state *in vitro* and has mitotic roles *in vivo*.

2.2 **Materials and Methods**

2.2.1 Purification of the SpCnp3^{CENP-C} Cupin Domain

N-terminal His-MBP tagged Cnp3 489–643 was cloned into the pET3a vector and expressed in Escherichia coli Rosetta (DE3) cells using PA-5052 (native protein) or PASM-5052 (Selenium-labeled protein) auto-inducible media [168]. Harvested cells were resuspended in 30 mM Tris-HCl (pH 8.0), 500 mM NaCl, and 3 mM β-mercaptoethanol with protease inhibitor cocktails. After sonication on ice for 2 min, soluble lysate was recovered by centrifugation at 34,541 x g for 1 hr. Lysate was applied to a cobalt affinity column (Takara) pre-equilibrated with Buffer A (30 mM Tris-HCl (pH 8.0), 500 mM NaCl, 3 mM β-mercaptoethanol). The resin was subsequently washed with Buffer A, a high salt buffer (30 mM Tris-HCl (pH 8.0), 1 M NaCl, 3 mM β-mercaptoethanol), and once more with Buffer A before eluting with the elution buffer (30 mM Tris-HCl (pH 8.0), 500 mM NaCl, 300 mM imidazole, and 3 mM β-mercaptoethanol). The N-terminal His-MBP tags were cleaved by Tobacco Etch Virus protease (1:100 ratio) while dialyzing in 30 mM Tris-HCl (pH 8.0), 100 mM NaCl, 1 mM dithiothreitol (DTT) at 4 °C overnight. The cleaved tags were removed with secondary cobalt and amylose (New England Biolabs) affinity columns. The amylose column flow through fraction was applied to the HiTrap Q HP anion exchange column (GE Healthcare) with a NaCl gradient (50 mM to 1 M NaCl) and fractions containing the S. pombe Cnp3 cupin domain were pooled. Pooled fractions were concentrated using an Amicon Centrifugal Filter (Millipore Sigma) and applied to a HiLoad 16/600 Superdex 200 pg size exclusion chromatography column (GE healthcare) pre-equilibrated with 30 mM Tris-HCl (pH 8.0), 100 mM NaCl, 1 mM tris(2-carboxyethyl)phosphine (TCEP).

Desired fractions were pooled, applied to a final amylose column to remove any remaining MBP, and the collected flow through was concentrated for crystallization and subsequent biochemical assays.

2.2.2 Purification of the DmCENP-C Cupin Domain

The overall cloning and protein expression procedure of native and selenomethionine-substituted *D. melanogaster* CENP-C cupin domains (residues 1244–1411 and 1190–1411) was the same as the *S. pombe* Cnp3 cupin domain, described above. The native CENP-C 1190-1411 protocol did not require the HP-Q column before being applied to the Superdex 200 column.

2.2.3 Crystallization and Structure Determination of the SpCnp3^{CENP-C} Cupin Domain

Crystals of the *S. pombe* Cnp3 cupin domain were grown using the hanging drop diffusion method at room temperature. Plate-shaped crystals were obtained by mixing purified proteins (12.7 mg/ml) with 0.1 M HEPES (pH 7.0), 20% PEG 3350, and 6% (w/v) Trimethylamine N-oxide dihydrate in a 1:1 ratio (v/v). The reservoir solution was made up of 0.25 M potassium fluoride, 0.125 M HEPES (pH 7.0), and 25% PEG 3350. Crystals were cryo-protected in reservoir solution with a final concentration of 35% PEG 3350 and flash-frozen in liquid nitrogen. A 2.52 Å dataset of a selenomethionine (SeMet)-substituted *S. pombe* Cnp3 cupin domain crystal was collected at Advanced Photon Source (APS) on beamline 21-ID-G (LS-CAT) at the wavelength of the selenium anomalous peak position (λ=0.9786 Å). The dataset was indexed and scaled using XDS and it belonged to the space group of P 4_12_12 with the unit cell size of a = 55.16 Å, b = 55.16 Å, c = 206.64 Å, $\alpha = \beta = \gamma = 90^o$ [169, 170]. The electron density map was

generated via PHENIX.autosol **(Figure 2.4A)** [171]. The initial model was built using PHENIX.autobuild and the model building and structure refinement were done using programs COOT and PHENIX.refine, respectively **(Figure 2.4B)** [172-174]. The final refined model has a Rwork/Rfree of 0.217/0.251 and the Ramachandran analysis was done using MolProbity with the result of 97.43 (favored), 2.57 (allowed), and 0.00 % (outlier) **(Figures 2.4C and 2.5)** [175].

2.2.4 Crystallization and Structure Determination of the DmCENP-C Cupin Domain

Purified native *D. melanogaster* CENP-C cupin domain protein (residues 1244–1411) at 19.7 mg/ml was used for crystallization using the hanging drop diffusion method. Ridged oval-shaped crystals were obtained by mixing protein with 0.2 M NaCl, 0.1 M MES (pH 6.0), 15 % (v/v) Pentaerythritol propoxylate (5/4 PO/OH) in a 1:1 ratio (v/v). SeMet-substituted crystals of this short CENP-C cupin domain were grown in the same condition by providing native crystals as microseeds. These crystals were then cryo-protected in 0.2 M NaCl, 0.1 M MES (pH 6.0), 15 % (v/v) Pentaerythritol propoxylate (5/4 PO/OH) containing 20% glycerol as a cryo-protectant and quickly frozen in liquid nitrogen. The 2.63 Å SAD dataset of the *D. melanogaster* CENP-C cupin domain (residues 1244–1411) was collected at APS using beamline 21-ID-G at the wavelength of 0.9786 Å. The collected data was further processed using Mosflm and Aimless [176, 177]. The diffracted crystal belonged to the space group $P3_121$ with the unit cell dimensions of a = 86.24 Å, b = 86.24 Å, c = 112.24 Å, $\alpha = \gamma = 90^{o}$ and $\beta = 120^{o}$. The initial SAD map was generated using PHENIX.autosol **(Figure 2.6A)** [171]. Using PHENIX.autobuild, an initial model was obtained and was further manually built and refined using the program COOT and PHENIX.refine, respectively **(Figure 2.6B)** [172-

174]. The obtained model was used for molecular replacement against the native dataset of *D. melanogaster* CENP-C cupin domain (residues 1190–1411), which diffracted to 1.81 Å resolution.

The native crystals of the *D. melanogaster* CENP-C cupin domain (residues 1190–1411) were grown by mixing purified proteins (21 mg/ml) and the precipitation solution (0.1 M MOPS (pH 7.0) and 12% (w/v) PEG 4000) in a 1:1 ratio (v/v) using the hanging drop diffusion method at room temperature. Crystals were further cryo-protected with a final concentration of 35% (w/v) PEG 4000 and frozen in the liquid nitrogen. Dataset was collected at a 0.9786 Å wavelength under cryogenic conditions at APS using beamline 21-ID-G. The 1.81 Å native dataset of the space group $P2_12_12_1$ and unit cell dimensions of a = 51.93 Å, b = 61.72 Å, c = 87.92 Å, $\alpha = \beta = \gamma = 90^o$ was indexed and scaled using the program XDS [169, 170]. The initial phases were calculated by molecular replacement (Phaser) using the model built from the short construct of the *D. melanogaster* CENP-C cupin domain (residues 1190–1411) as a search model **(Figure 2.6C)** [178]. Further model building and the refinement was done using the program COOT and PHENIX.refine, respectively [173, 174]. Residues 1190–1269 were likely proteolytically cleaved during the crystallization process and were not visible within our structure. The R_{work} and R_{free} values of the final refined model of *D. melanogaster* CENP-C cupin domain (residues 1190–1411) were 0.196 and 0.232, respectively **(Figure 2.6D)**. The final model has the Ramachandran plot of favored/allowed/disallowed with 98.14/1.86/0.00 % based on MolProbity **(Figure 2.7)** [175].

2.2.5 Sedimentation Velocity Analytical Ultracentrifugation (SV-AUC)

SV-AUC was carried out using 420 µl loaded into two-sector Epon centerpieces with 1.2 cm path-length (Beckman Coulter, Indianapolis, USA) in an An60Ti rotor in a Beckman Optima Xl-I analytical ultracentrifuge and run at 22 °C or 6 ºC after at least 2h of temperature equilibration prior to sedimentation. Measurement was completed in intensity mode. Sedimentation was monitored by absorbance at 280 nm at 42 krpm. Samples were prepared as mentioned.

All SV-AUC data were analyzed using UltraScan 4 software, version 4.0 and fitting procedures were completed on XSEDE clusters at the Texas Advanced Computing Center (Lonestar, Stampede) through the UltraScan Science Gateway (https://www.xsede.org/web/guest/gateways-listing) [179]. The partial specific volume (vbar) of all species was estimated within UltraScan III based on the protein sequence. Raw intensity data were converted to pseudo-absorbance by using the intensity of the air above the meniscus as a reference and edited. Next, 2-dimensional sedimentation spectrum analysis (2DSA) was performed to subtract time-invariant noise and the meniscus was fit using ten points in a 0.05-cm range [180]. A sedimentation coefficient distribution of 1 to 20 for the *Dm*CENP-C cupin domain 1 to 50 for MBP *Sp*Cnp3^{CENP-C} Cupin or 0.5 to 5 for the *Sp*Cnp3^{CENP-C} cupin domain was fitted. Arrays were fit using an S range of 1-20, 1-50 or 0.5-5 S, an f/f0 range of 1–4 with 64 grid points for each, 10 uniform grid repetitions and 400 simulation points. 2DSA was then repeated at the determined meniscus to fit radially invariant and time-invariant noise together using ten iterations.

N-terminal His-MBP tagged Cnp3 489–643 was cloned into the pET3a vector and expressed in *Escherichia coli* Rosetta (DE3) cells using PA-5052 [168]. Harvested cells were resuspended in 30 mM Tris-HCl (pH 8.0), 500 mM NaCl, and 3 mM β-mercaptoethanol with protease inhibitor cocktails. After sonication on ice for 1.5 min, soluble lysate was recovered by centrifugation at 34,541 x g for 1 hr. The lysate was applied to a cobalt affinity column (Takara) pre-equilibrated with Buffer A (30 mM Tris-HCl (pH 8.0), 500 mM NaCl, 3 mM β-mercaptoethanol). The resin was subsequently washed with Buffer A, a high salt buffer (30 mM Tris-HCl (pH 8.0), 1 M NaCl, 3 mM β-mercaptoethanol), and once more with Buffer A before eluting with the elution buffer (30 mM Tris-HCl (pH 8.0), 500 mM NaCl, 300 mM imidazole, and 3 mM β-mercaptoethanol). The elution was concentrated using an Amicon Centrifugal Filter (Millipore Sigma) and applied to a HiLoad 16/600 Superdex 200 pg size exclusion chromatography column (GE healthcare) pre-equilibrated with 30 mM Tris-HCl (pH 8.0), 500 mM NaCl, 1 mM tris(2-carboxyethyl)phosphine (TCEP). Desired fractions were diluted to differing $O.D._{280}$ values for AUC analysis. The purification protocol was identical for the MBP Cnp3 $Cupin^{\Delta DS}$ samples.

2.2.6 S. pombe Strains and Growth Assays

Standard methods were used for fission yeast growth, genetics and manipulation [181]. Gene deletion, tagging and mutagenesis were carried out by either the lithium acetate transformation method or electroporation. Truncations within the *Sp*$Cnp3^{CENP\text{-}C}$ cupin domain were generated by PCR-based methods, and integrated at the endogenous *cnp3* genomic locus using either a *ura4* or *natMX* selection marker targeted to the 3'UTR of *cnp3* [182]. Five-fold serial dilutions of the indicated strains

were spotted onto YES media supplemented with or without the indicated concentrations of thiabendazole (TBZ) and incubated at the indicated temperatures for 3–7 days. Genotypes of *S. pombe* strains used in this study are listed in **Table 2.1**.

2.3 **Results**

2.3.1 Structural Determination of the S. pombe and D. melanogaster CENP-C Cupin Domains

To elucidate the evolutionarily conserved and/or differentiating features of the CENP-C cupin domain between organisms with point and regional centromeres, we determined the crystal structures of CENP-C cupin domains belonging to two organisms with regional centromeres: *S. pombe* (*Sp*Cnp3^{CENP-C}) and *D. melanogaster* (*Dm*CENP-C). The crystal structure of the *Sp*Cnp3^{CENP-C} cupin domain (residues 489–643) was determined by single-wavelength anomalous diffraction (SAD) with selenomethionine-substituted protein to calculate initial phases. The electron density map at 2.52 Å resolution was used for model building, and the final model was refined at R_{work}/R_{free} values of 0.217/0.251, respectively **(Figures 2.3B and 2.4, Table 2.2)**. Residues 489–493 of the *Sp*Cnp3^{CENP-C} cupin domain structure were not visible due to their flexible nature. The initial model of *Dm*CENP-C cupin domain (residues 1244–1411) was built based on the 2.63 Å resolution electron density map calculated from SAD phases using selenomethionine-labeled protein **(Figure 2.6A)**. This model was then used for molecular replacement against a 1.81 Å native dataset collected from crystals of a longer *Dm*CENP-C cupin domain construct (residues 1190–1411) **(Figure 2.6C)**. The electron density for additional residues was visible after molecular replacement. After

building the additional residues, the final model was refined at R_{work}/R_{free} values of 0.196/0.232 **(Figures 2.3C and 2.6D, Table 2.2)**.

2.3.2 Structural Comparison of CENP-C Cupin Domains at Point and Regional Centromeres

The structural core of both the *Sp*Cnp3^{CENP-C} and *Dm*CENP-C cupin domains shows a dimeric complex where each monomer forms a jelly roll fold consisting of nine β strands that form two antiparallel β sheets **(Figure. 2.8A)**. The five-stranded sheet (β1-β5) participates in dimerization, while the remaining four strands (β1'- β4') complete the jelly roll fold to form the characteristic shape of the cupin domain. We find that the core nine-stranded fold of the CENP-C cupin domains from organisms possessing point centromeres (*Sc*Mif2^{CENP-C} cupin domain; PDB ID: 2VPV) is well preserved evolutionarily with those with regional centromeres (*Sp*Cnp3^{CENP-C} and *Dm*CENP-C), showing Cα R.M.S. differences of 2.02 Å (*Sc*Mif2^{CENP-C} vs. *Sp*Cnp3^{CENP-C} (532–625; 158 Cα residues)) and 1.93 Å (*Sc*Mif2^{CENP-C} vs. *Dm*CENP-C (1320–1411; 161 Cα residues)) **(Figure 2.8B)**. In both *Sp*Cnp3^{CENP-C} and *Dm*CENP-C cupin domains, the two β-sheets (β1-β5 and β1'-β4') within the jelly roll fold create a pocket-like surface that is often used as a site for metal ion binding in other cupin proteins [183-185].

Although the core jelly roll folds are conserved, the CENP-C cupin domains from organisms with regional centromeres exhibit additional features at their N- and C-terminal ends. The *Sp*Cnp3^{CENP-C} cupin domain features a β-hairpin and a short α-helix at its N-terminal side and an additional α-helix on the C-terminal end of the jelly roll **(Figure 2.8)**. The *Dm*CENP-C cupin domain possesses two extra α-helices and an extra β-strand at the N-terminal side of the jelly roll **(Figure 2.8)**. These additional

features have not been observed in the *Sc*Mif2^{CENP-C} cupin domain. Since the *Sc*Mif2^{CENP-C} cupin domain construct that was used for crystallization (residues 365–530) was longer than that within the determined structure (residues 437–530), residues 365-436 of the *Sc*Mif2^{CENP-C} cupin domain are likely to be disordered.

Additionally, despite the high level of conservation in the overall architecture of the jelly roll fold, the primary sequence of residues within the dimer interface is not well preserved amongst the three CENP-C cupin domain structures **(Figure 2.9)**. The *Sc*Mif2^{CENP-C} cupin domain mainly relies on hydrophobic interactions along the interface for dimer formation. While the *Sp*Cnp3^{CENP-C} cupin domain does possess hydrogen bonding between chains at its dimerization interface, this does not seem to be the major interaction required for dimerization. Instead, the *Sp*Cnp3^{CENP-C} and *Dm*CENP-C cupin domains primarily rely on hydrogen bond interactions formed by their additional secondary structures outside of the jelly roll fold to maintain their dimeric state.

Taken together, although the overall structural features of the *Sc*Mif2^{CENP-C} (point centromere) cupin domain are well preserved in the *Sp*Cnp3^{CENP-C} and *Dm*CENP-C (regional centromere) cupin domains, the interactions at the dimer interface are not conserved. The cupin domains from organisms with regional centromeres also have additional structural components. We propose that these additional features may further reinforce the dimerization in the CENP-C cupin domains at regional centromeres.

2.3.3 Additional Secondary Structures in the CENP-C Cupin Domains from Organisms with Regional Centromeres Contribute to Dimerization and Protein Stability

The structural comparison of *Sc*Mif2^{CENP-C} cupin domain with the *Sp*Cnp3^{CENP-C} and *Dm*CENP-C cupin domains revealed that organisms with regional centromeres

encode CENP-C cupin domains that possess secondary structures in addition to the jelly roll folds **(Figure 2.8)**. Two β-strands at the N-terminus of the *Sp*Cnp3^{CENP-C} cupin domain form a β-hairpin structure and then participate in domain swapping between monomers. This unexpected domain swapped region (DS) is likely to further enforce the dimerization of the *Sp*Cnp3^{CENP-C} cupin domain. This is evidenced by the formation of multiple hydrogen bonds between the backbones of the DS2 β-strand and the adjacent β5-strand of the opposing chain **(Figure 2.10A)**. Specifically, the backbones of residues Y524 and V522 in DS2 hydrogen bond to the backbones of residues V599 and I601 in β5-strand, respectively. DS1 residues E505 and L507 also hydrogen bond with nearby loops via the sidechains of N588 and N606, respectively. Additionally, the backbones of L526 and D597, residues that are located in adjacent loops, also participate in hydrogen bonding **(Figure 2.10A)**. T628, D627, and R634, residues within the C-terminal helical region of the *Sp*Cnp3^{CENP-C} cupin domain, further contribute to the dimeric state by interacting with residues along the opposite chain.

A similar domain swapping feature is also observed within the *Dm*CENP-C cupin domain as a loop in place of the β-hairpin at its corresponding position. Although not as structurally well defined as the *Sp*Cnp3^{CENP-C} β-hairpin, this loop structure may similarly contribute to stabilizing dimerization with several hydrogen bond interactions through a combination of side chain and backbone interactions between the overlapping loop and the adjacent β-strands of the opposing chain. S1305 and S1307 respectively hydrogen bond with E1387 and M1385 of β5 of the opposing chain. N1303 hydrogen bonds with H1377 and S1378 of strand β4’ while S1298 and S1300 both interact with V1379 of strand β4’. A1297, S1308, and A1309 all form hydrogen bonds with loop regions

adjacent to strands β5 and β4' **(Figure 2.10B)**. Lastly, residues D1274, E1277, and R1288, from the N-terminal *Dm*CENP-C helical region contribute to dimerization through interactions with surrounding loops via K1402, R1288, and E1277, respectively **(Figure 2.10C)**.

The calculated surface area of the dimer interface of the *Sc*Mif2^{CENP-C} cupin domain is 720.4 Å^2 [186]. The corresponding surface areas within the *Sp*Cnp3^{CENP-C} and *Dm*CENP-C cupin domains are 2711.2 Å^2 and 1807.9 Å^2, respectively **(Figure 2.11)** [186]. The differences in interface surface area between CENP-C cupin domains from organisms with point vs. regional centromeres strongly indicate that the dimerization of CENP-C cupin domains at regional centromeres needs to be further strengthened by the additional secondary structure components.

2.3.4 The Dimeric State of the CENP-C Cupin Domain is Evolutionarily Conserved In Vitro

To analyze the oligomeric state of the *Sp*Cnp3^{CENP-C} and *Dm*CENP-C cupin domains, sedimentation velocity analytical ultracentrifugation (SV-AUC) was employed. SV-AUC analysis of purified *Sp*Cnp3^{CENP-C} and *Dm*CENP-C cupin domains each showed a single peak with estimated molecular weights (M.W.) of 34 kDa (expected M.W. of the monomer is 16.8 kDa) and 52 kDa (expected M.W. of the monomer is 24.9 kDa), respectively **(Figure 2.12A)**. This demonstrates that both cupin domains form homodimers in solution, similar to the *Sc*Mif2^{CENP-C} cupin domain [67].

2.3.5 The Domain Swapped Region is Essential to Maintain the Dimeric State and Structural Integrity of the SpCnp3$^{CENP\text{-}C}$ Cupin Domain

To further investigate the functional role of the unique *Sp*Cnp3$^{CENP\text{-}C}$ β-hairpin structure, an N-terminally truncated construct of the *Sp*Cnp3$^{CENP\text{-}C}$ cupin domain was generated by removing the domain swapped region (Cnp3 Cupin$^{\Delta DS}$; residues 532–643) and subsequently subjected to SV-AUC analysis **(Figure. 2.12B)**. Analysis of maltose binding protein (MBP)-tagged Cnp3 Cupin$^{\Delta DS}$ shows distinct peak shifts in comparison to MBP-tagged wild type (WT) *Sp*Cnp3$^{CENP\text{-}C}$ cupin domain (residues 489–643) with a lower molecular weight population as well as a higher molecular weight population **(Figure 2.12C)**. The latter is likely to be higher molecular weight aggregates. Notably, cleavage of the MBP tag from MBP-tagged Cnp3 Cupin$^{\Delta DS}$ for further purification resulted in protein aggregation that was unable to be further purified. This is in stark contrast to the tag cleavage and purification of the WT *Sp*Cnp3$^{CENP\text{-}C}$ cupin domain (residues 489–643) that could be purified in large amounts and crystallized without any issues with protein stability.

In order to investigate whether the domain swapped region is required for *Sp*Cnp3$^{CENP\text{-}C}$ function *in vivo*, we generated *S. pombe* strains expressing internally truncated mutants of *Sp*Cnp3$^{CENP\text{-}C}$, from the *cnp3* endogenous locus. *cnp3*$^{\Delta 493–531}$ cells expressed the *Sp*Cnp3$^{CENP\text{-}C}$ protein selectively missing the domain swapped region alone, i.e. residues 493–531 which form part of the N-terminus within the solved *Sp*Cnp3$^{CENP\text{-}C}$ cupin domain structure. Similarly, *cnp3*$^{\Delta 478–531}$ cells expressed the *Sp*Cnp3$^{CENP\text{-}C}$ protein missing residues 478–531, which we predicted would additionally eliminate the disordered region preceding the domain swapped region. A strain

expressing a C-terminally truncated mutant *cnp3*$^{\Delta 489–end}$ eliminating the entire cupin domain of *Sp*Cnp3^{CENP-C}, i.e. residues 489–643, was also generated as a control. While *cnp3*$^{\Delta 493–531}$ and *cnp3*$^{\Delta 478-531}$ cells displayed very little cold sensitivity when compared with *cnp3Δ* cells, they showed hypersensitivity to the microtubule depolymerizing drug thiabendazole (TBZ) much like *cnp3Δ* cells, suggesting that mitotic chromosome segregation is disrupted in the absence of the domain swapped region within *Sp*Cnp3^{CENP-C} **(Figure 2.13)**. These results suggest that the domain swapped region within the cupin domain is essential for *Sp*Cnp3^{CENP-C} function *in vivo*.

Taken together, we conclude that unlike the *Sc*Mif2^{CENP-C} cupin domain, the jelly roll fold architecture alone is not sufficient to maintain the stability of the *Sp*Cnp3^{CENP-C} cupin dimer. The domain swapped region at the N-terminus of the *Sp*Cnp3^{CENP-C} cupin domain plays an important role in stabilizing and maintaining the dimeric state of the *Sp*Cnp3^{CENP-C} cupin domain and is essential for its function *in vivo*.

2.4 **Discussion**

Here, we present and analyze the structures of CENP-C cupin domains from two evolutionarily distinct organisms with regional centromeres *Sp*Cnp3^{CENP-C} and *Dm*CENP-C. Along with the previously published crystal structure of the *Sc*Mif2^{CENP-C} cupin domain, these three structures originate from organisms with diverse centromere architecture and kinetochore composition. We sought to define and distinguish the conserved and unique structural features of the CENP-C cupin domain at two different types of centromeres, point and regional, in order to gain a better understanding of the evolutionary conservation of CENP-C cupin domain function.

Through structural comparison, we found that the core nine-stranded jelly roll fold is conserved among these structures. However, the mechanisms of dimerization differ between cupin domains associating with regional vs. point centromeres due to the former relying on secondary structures additional to the jelly roll fold, and thus, creating a larger dimerization interface.

2.4.1 Comparison of the CENP-C Cupin Domain Dimer Interface in Organisms with Point and Regional Centromeres

One clear distinction between CENP-C cupin domains at point and regional centromeres is the interactions at the dimer interface. The *Sc*Mif2^{CENP-C} (point centromere) cupin domain, forms a dimer through the jelly roll fold, which is likely sufficient to form the *Sc*Mif2^{CENP-C} dimer **(Figure 2.3A)**. CENP-C cupin domains at regional centromeres, however, seem to require additional secondary structures to form a stable dimer, with a larger dimer interface surface **(Figures 2.3 and 2.11)**. The *Sp*Cnp3^{CENP-C} cupin domain possesses an additional secondary structure element, namely a β-hairpin (domain swapped region) N-terminal to the jelly roll fold. Our experiments both *in vitro* and *in vivo* demonstrate that this additional secondary structure element is essential for the stability and function of *Sp*Cnp3^{CENP-C}. Deletion of the Mif2^{CENP-C} cupin domain in *S. cerevisiae* results in a temperature sensitive phenotype [67]. Analogously, deletion of the Cnp3^{CENP-C} cupin domain (*cnp3*$^{\Delta 489\text{-end}}$) in *S. pombe* results in mild cold sensitivity, and hypersensitivity to thiabendazole suggesting that dimerization mediated by the cupin domain is essential for *Sp*Cnp3^{CENP-C} function *in vivo* **(Figure 2.13)**.

Similar to *Sp*Cnp3^{CENP-C}, the *Dm*CENP-C cupin domain also contains additional loop and helical structures to aid in dimerization. The comparison of dimer interfaces across the three analyzed orthologous CENP-C cupin domains further supports our observation that the cupin domains associated with regional centromeres possess dimerization interfaces over twice the size of the *Sc*Mif2^{CENP-C} interface (point centromere) **(Figure 2.11)**. The point centromere has a well-defined centromeric DNA sequence bound by a single CENP-A^{Cse4} nucleosome while, the regional centromere is composed of a larger centromeric DNA sequence (several kilobases to several megabases) with multiple CENP-A nucleosomes sporadically incorporated together with canonical histone H3 nucleosomes [22, 23, 32]. In fact, CENP-A nucleosomes have been shown to cluster towards the centromeric surface in order to maximize their accessible surface area for inner kinetochore recognition [22, 24]. Accordingly, several models have been proposed to explain how CENP-A and H3 centromeric nucleosomes are organized [187]. The potential role of CENP-C in organizing CENP-A nucleosomes at the regional centromere has been proposed in an earlier study [141]. In this model, CENP-C utilizes its CENP-A recognition domain and cupin domain to function as a bridge to connect neighboring CENP-A nucleosomes. In comparison to the point centromere, bridging of CENP-A nucleosomes at the regional centromere may require a larger and stronger dimerization interface. Indeed, former studies have shown that CENP-C depletion in HeLa cells affects the size, shape, and structural integrity of the inner kinetochore plate in electron micrographs [108].

2.5 Author Contributions

Data from this chapter has been submitted to the Journal of Biological Chemistry. J.K.C. purified proteins, obtained the crystals, solved and refined the structures, analysed data, and wrote the manuscript; V.M. and P.K.G. generated *S. pombe* strains, performed cold sensitivity and TBZ sensitivity assays; B.A.M. and P.K. performed SV-AUC analyses; S.A. assisted with structural determination; B.G.M. cloned and analysed *D. melanogaster* CENP-C cupin; L.S. designed experiments for *S. pombe in vivo* analysis, analysed data, and wrote the manuscript; and U-S.C. directed the project, designed experiments, analysed data, and wrote the manuscript.

2.6 Acknowledgements

We thank the staff at the Advanced Photon Source LS-CAT beamlines for their advice and assistance with data collection and Dr. James C. A. Bardwell for the use of his analytical ultracentrifuge. We are grateful to the Yeast Genetic Resource Center (YGRC), National Bioresource Project (NBRP), Japan for *S. pombe* strains, and Prof. Robin Allshire for the anti-Cnp1^{CENP-A} antibody. This work was supported by grants (N019154-00 and DK111465) to U-S.C, and a QMUL start-up grant and BBSRC grant BB/R00868X/1 to L.S. B.G.M is supported by R01GM-108829. J.K.C. was supported by the NIH Cellular and Molecular Biology Training Grant T-32-GM007315 and the Rackham Graduate Student Precandidate and Candidate Research Grants.

The atomic coordinates and structure factors for the *Sp*Cnp3^{CENP-C} cupin domain (PDB ID: 6O2D) and *Dm*CENP-C cupin domain (PDB ID: 6O2K) have been deposited in the Protein Data Bank (http://www.pdb.org/).

2.7 Figures

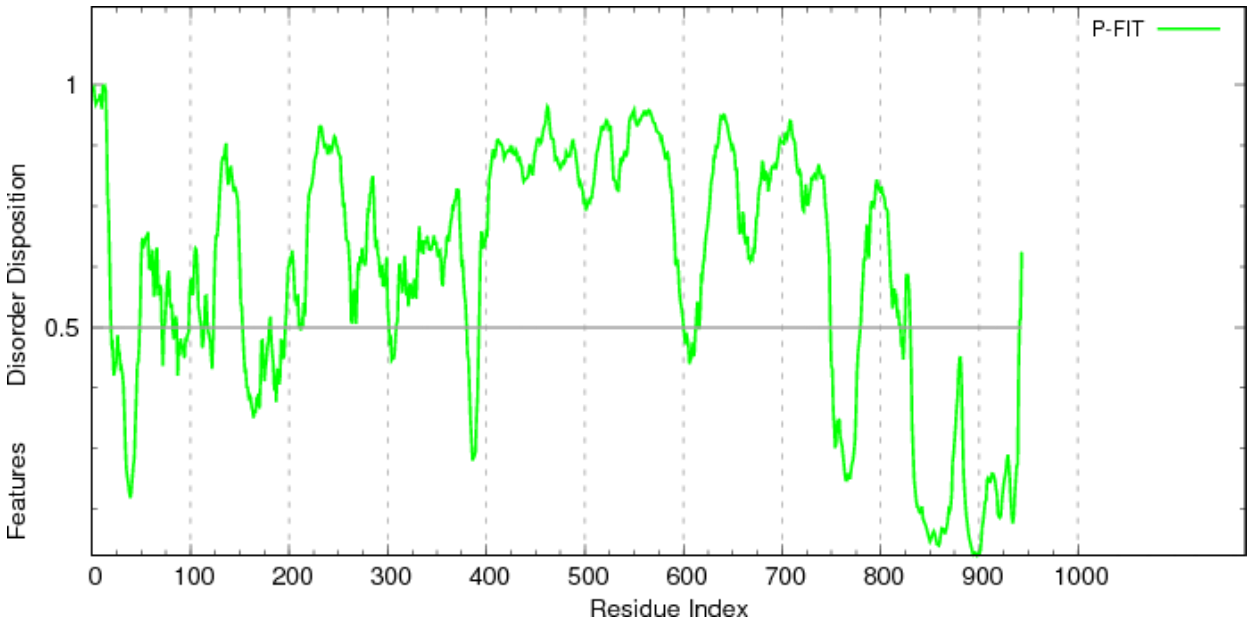

Figure 2.1 The majority of human CENP-C is predicted to be disordered.
Disorder prediction of human CENP-C. A score above 0.5 indicates that these residues are likely to be disordered in the structure. The C-terminal cupin domain is the most structurally ordered region within human CENP-C. Prediction was created using PONDR-FIT [139].

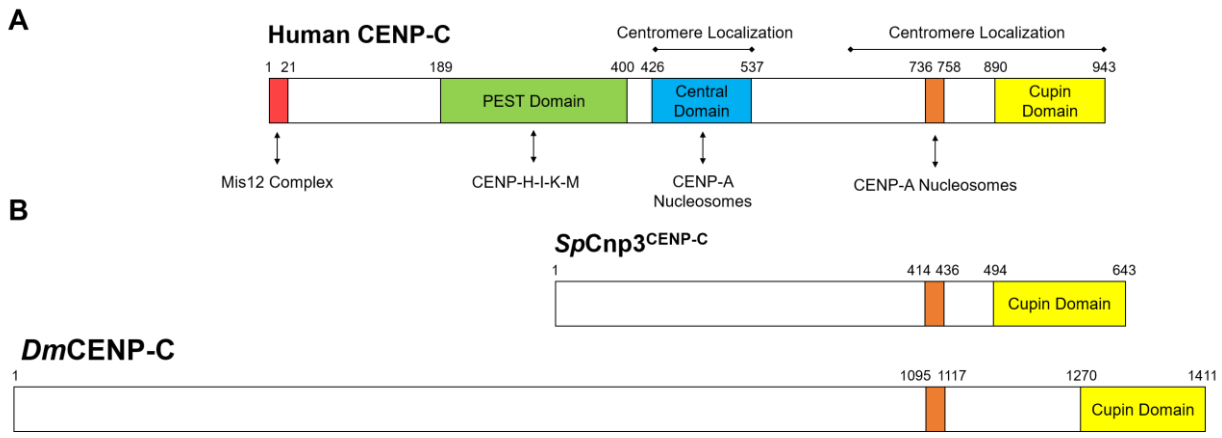

Figure 2.2 CENP-C harbors two conserved domains at its C-terminus.
A. Functional domains of human CENP-C and the regions required for centromere localization.Known binding partners are indicated by the double-headed arrows. The CENP-L-N binding region is not well defined but likely resides near the PEST domain. **B.** The *Sp*Cnp3^{CENP-C} and *Dm*CENP-C proteins also contain a CENP-C motif and cupin domain at their C-termini. The functional domains and binding partners for the *S. pombe* and *D. melanogaster* proteins are less well defined. CENP-C motifs for each protein are represented in orange.

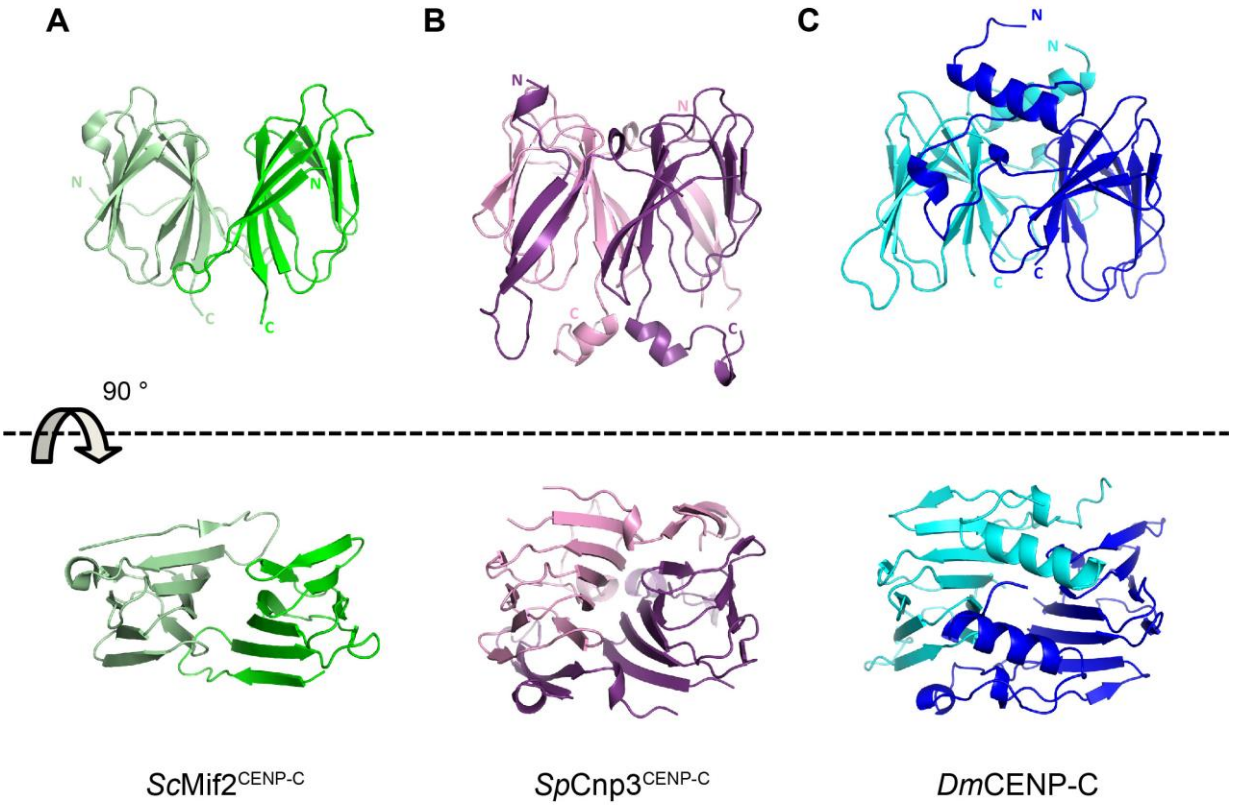

Figure 2.3 Side and aerial views of CENP-C cupin domain crystal structures.
A. Crystal structure of the *Sc*Mif2^{CENP-C} cupin domain (PDB ID: 2VPV) [67]. Monomers are colored in green and light green. **B.** Crystal structure of the *Sp*Cnp3^{CENP-C} cupin domain (PDB ID: 6O2D). Monomers are colored in purple and pink. **C.** Crystal structure of the *Dm*CENP-C cupin domain (PDB ID: 6O2K). Monomers are colored in blue and cyan. Illustrations of protein structures used in all figures were generated with PyMOL (Delano Scientific, LLC). Both N- and C-termini are labeled**.**

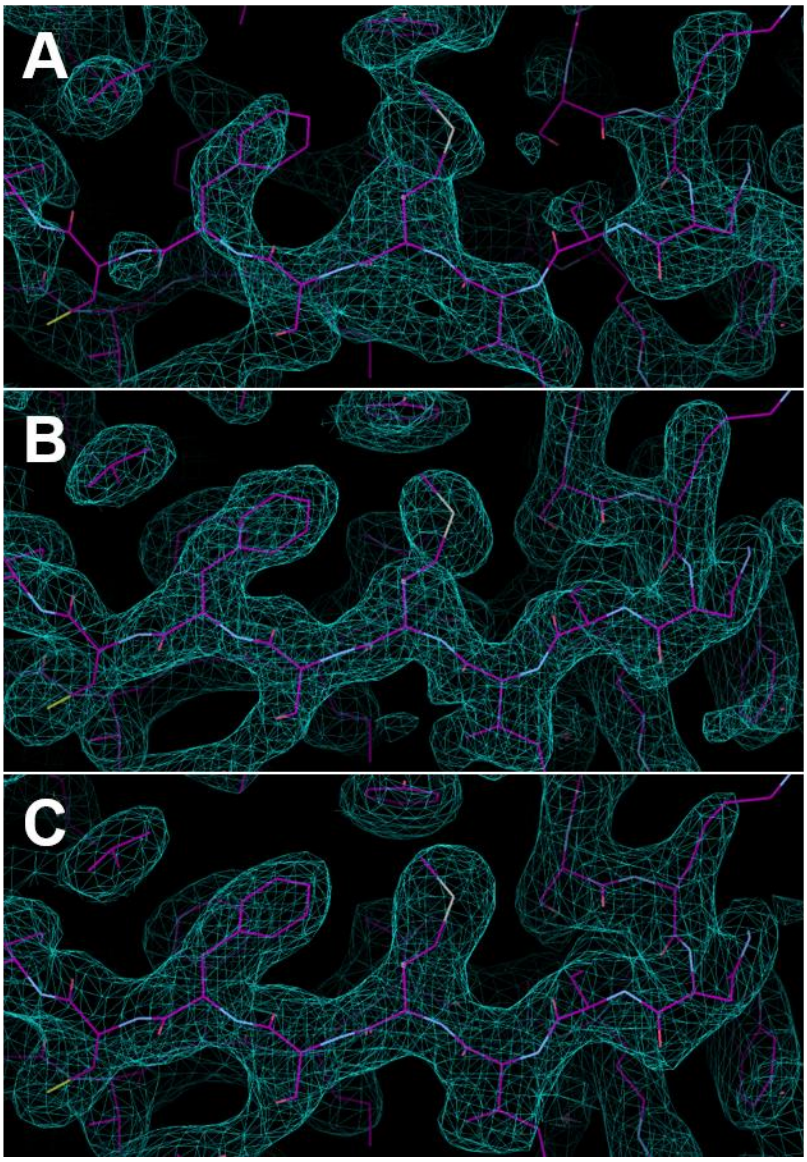

Figure 2.4 Electron density map quality through each stage of *Sp*Cnp3^{CENP-C} cupin domain structural determination.
All 2Fo-Fc maps (teal) are contoured to 1σ and overlaid with the final *Sp*Cnp3^{CENP-C} cupin domain model (fuschia). **A.** Initial SAD map determined from *Sp*Cnp3^{CENP-C} cupin domain selenium sites. **B.** Autobuild output. **C.** Final refinement. All maps and models were visualized using the program Coot [173].

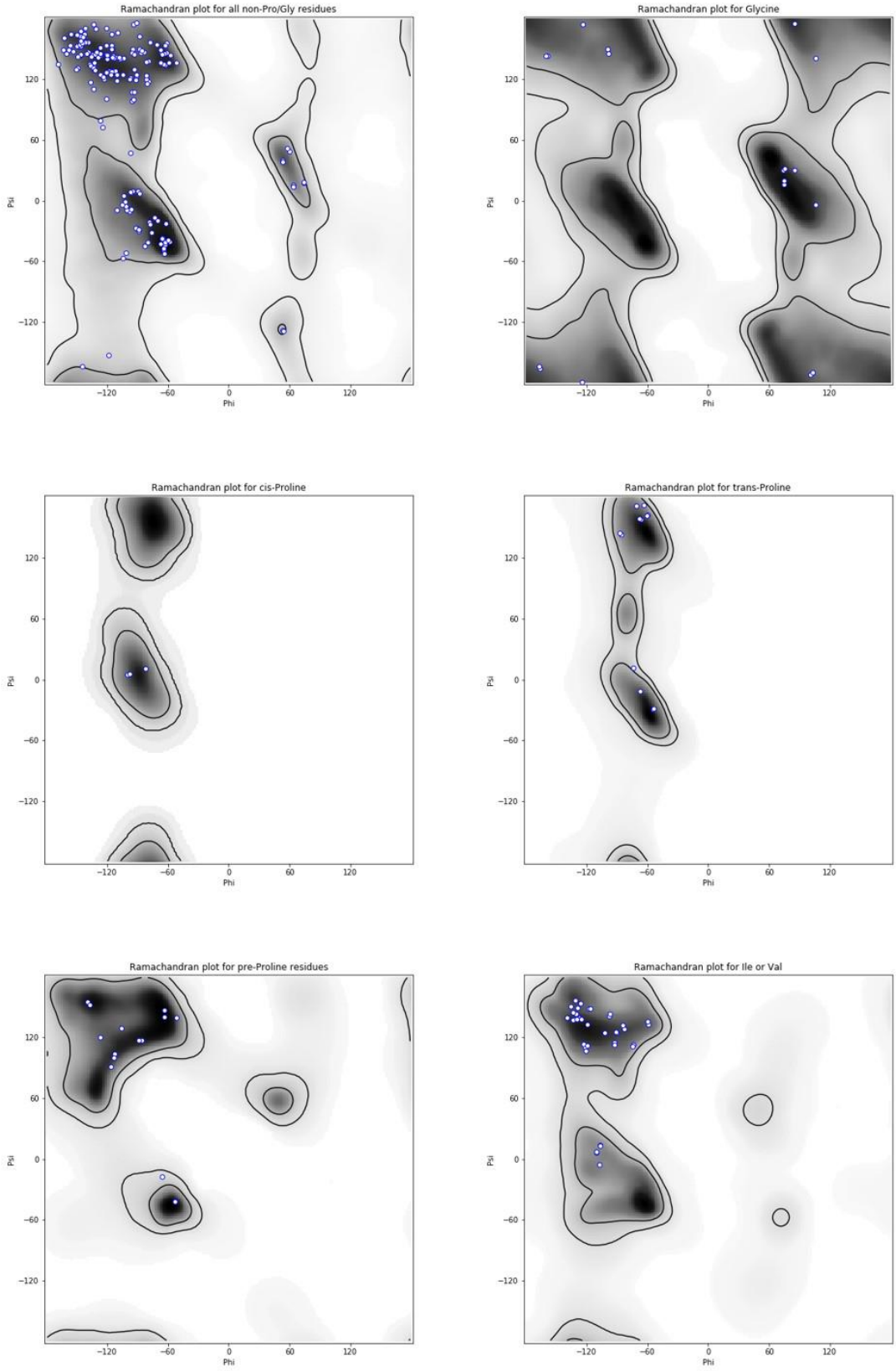

Figure 2.5 Ramachandran plots of the final *Sp*Cnp3^{CENP-C} cupin domain model.
Plots were generated using MolProbity [175].

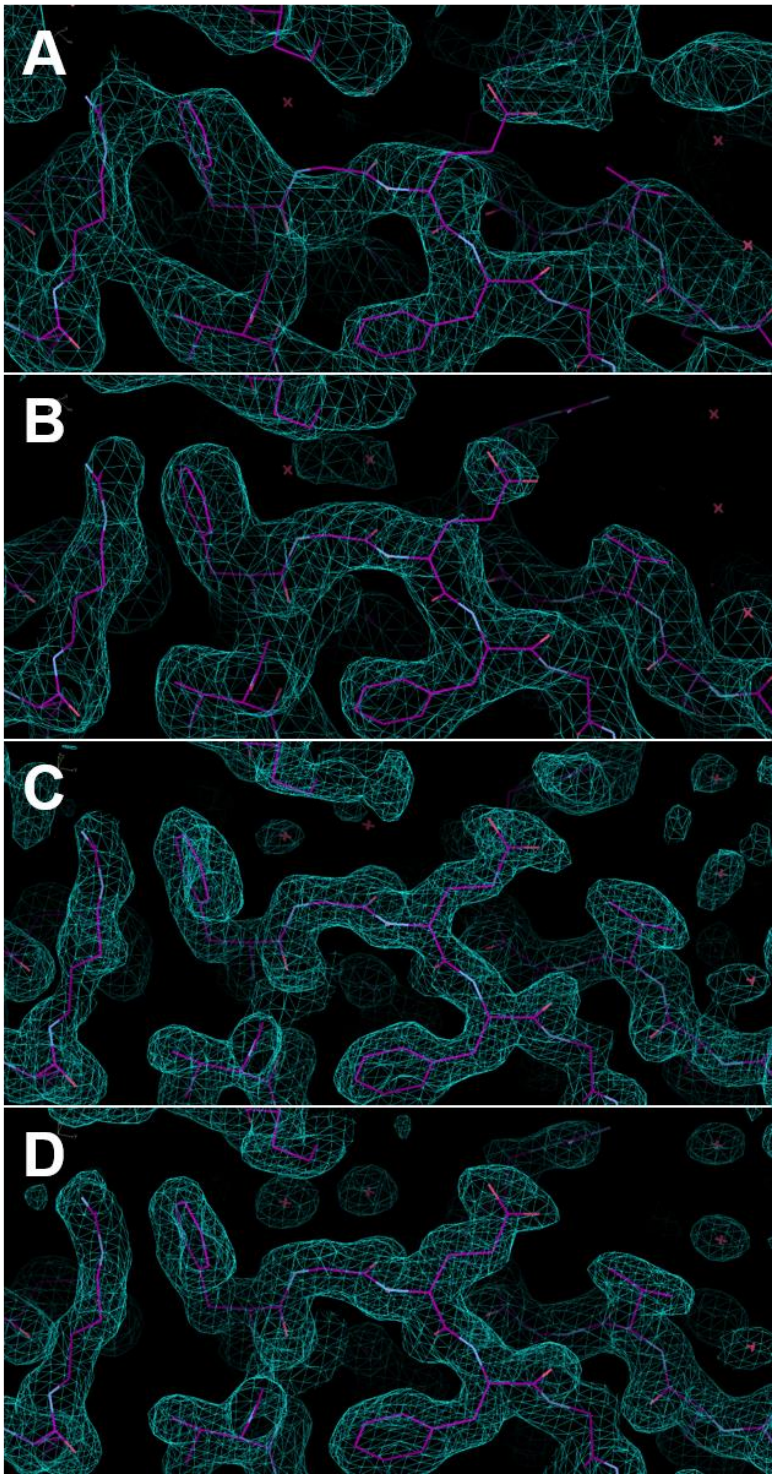

Figure 2.6 Electron density map quality through each stage of *Dm*CENP-C cupin domain structural determination.
All 2Fo-Fc maps (teal) are contoured to 1σ and overlaid with the final DmCENP-C cupin domain (residues 1190—1411) model (fuschia). **A.** Initial SAD map determined from SeMet *Dm*CENP-C residues 1244—1411 selenium sites. **B.** Autobuild output. **C.** Phaser output after molecular replacement into a native *Dm*CENP-C residues 1190—1411 dataset. **D.** Final refinement. All maps and models were visualized using the program Coot [173].

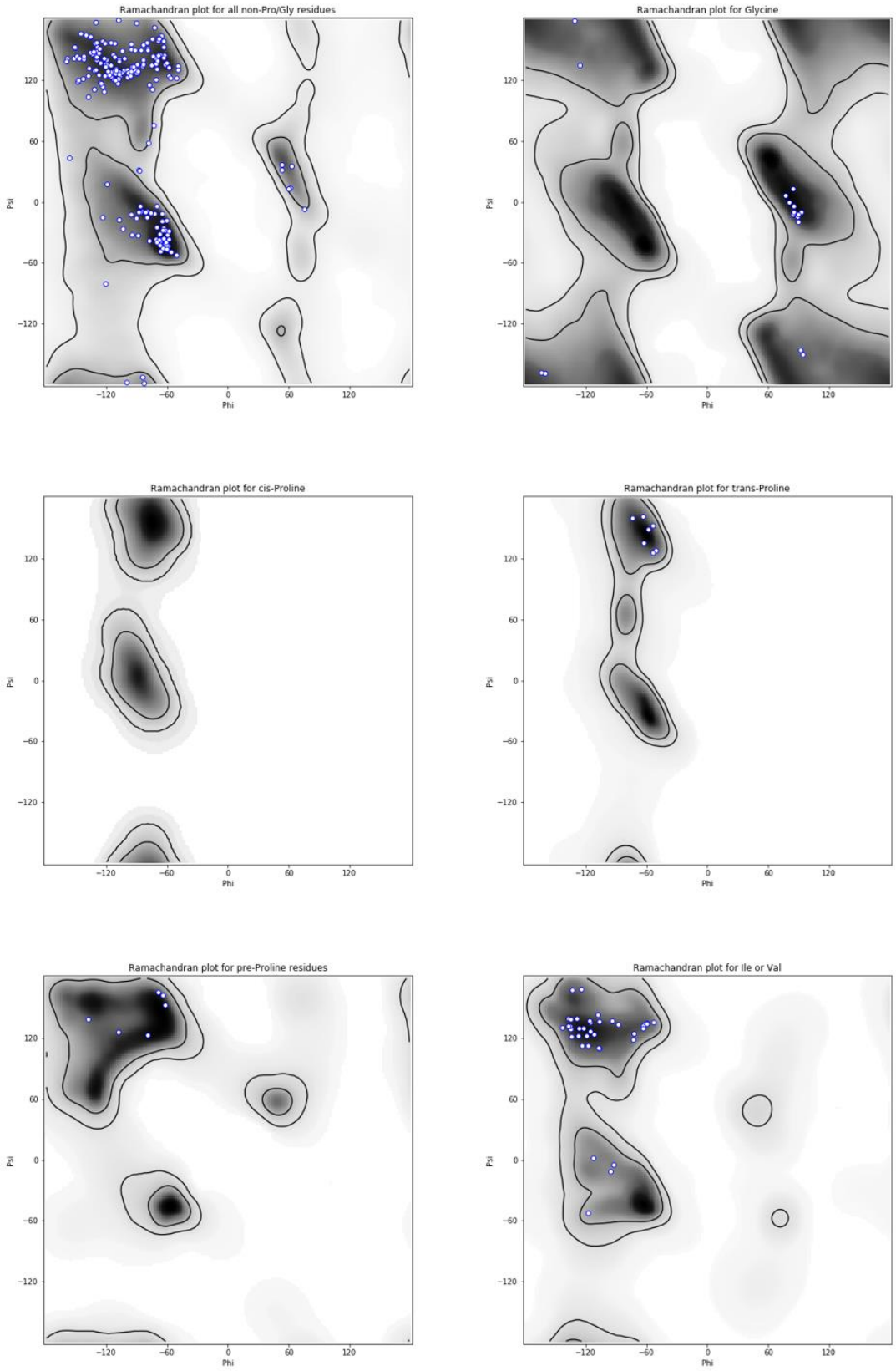

Figure 2.7 Ramachandran plots of the final *Dm*CENP-C cupin domain (residues 1190—1411) model. Plots were generated using MolProbity [175].

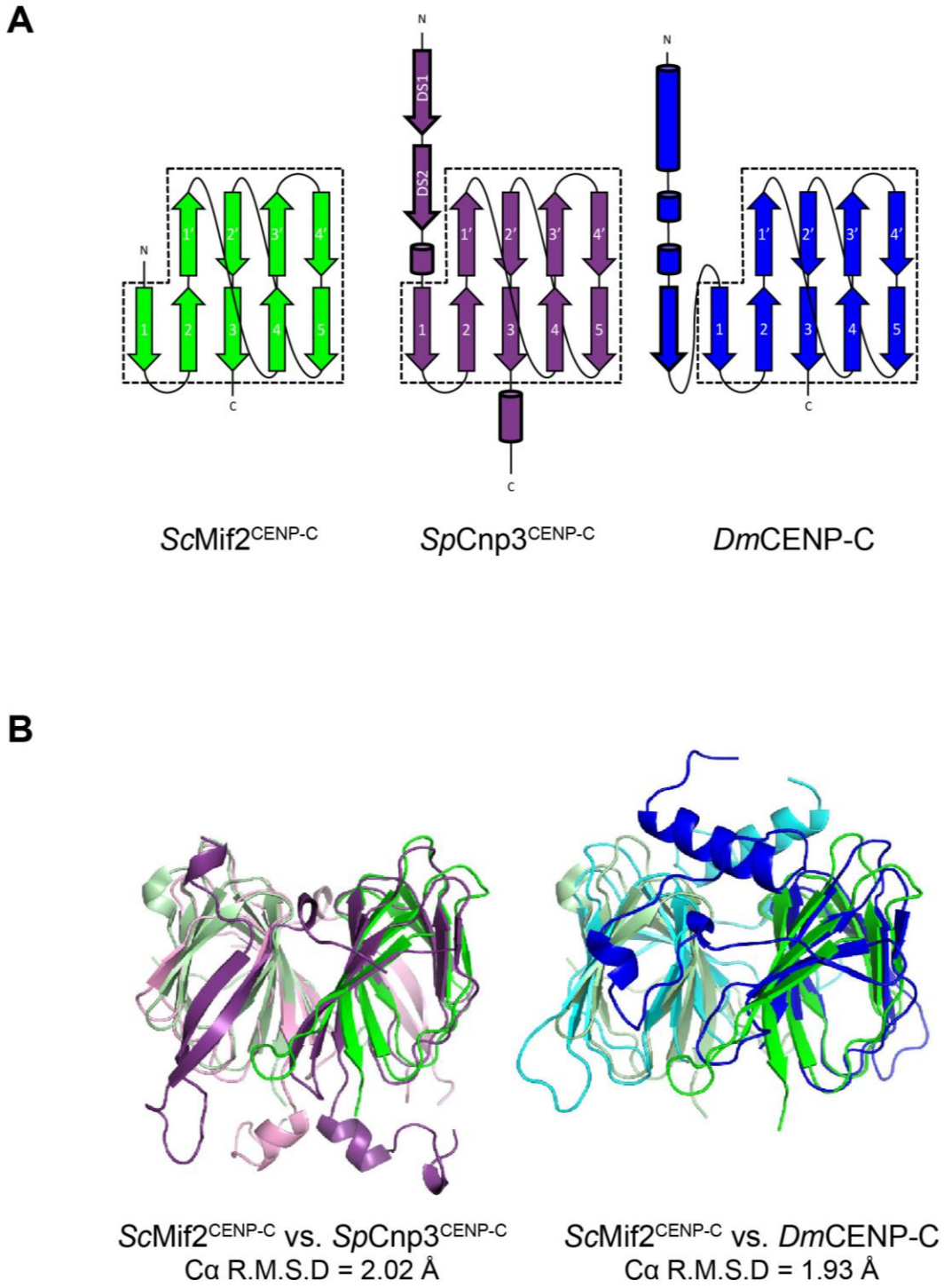

Figure 2.8 CENP-C cupin domains from point and regional centromeres share a core jelly roll fold.
A. Secondary structure representations of the *Sc*Mif2^{CENP-C}, *Sp*Cnp3^{CENP-C}, and *Dm*CENP-C cupin domains. The conserved jelly roll fold is comprised of nine β strands. β strands 1-5 participate in dimerization while β strands 1'-4' complete the rest of the conserved jelly roll fold (dashed boxes). The regional centromere CENP-C cupin domains of *S. pombe* and *D. melanogaster* possess additional secondary structures shown in cylinders (α-helix) and arrows (β-strand) with bold outlines. **B.** The core jelly roll fold of the *Sc*Mif2^{CENP-C} cupin domain (residues 437–530) overlays well with the core fold of the *Sp*Cnp3^{CENP-C} cupin domain (residues 532–625, Cα R.M.S.D. = 2.02 Å) as well as with the core fold of the *Dm*CENP-C cupin domain (residues 1320–1411, Cα R.M.S.D. = 1.93 Å).

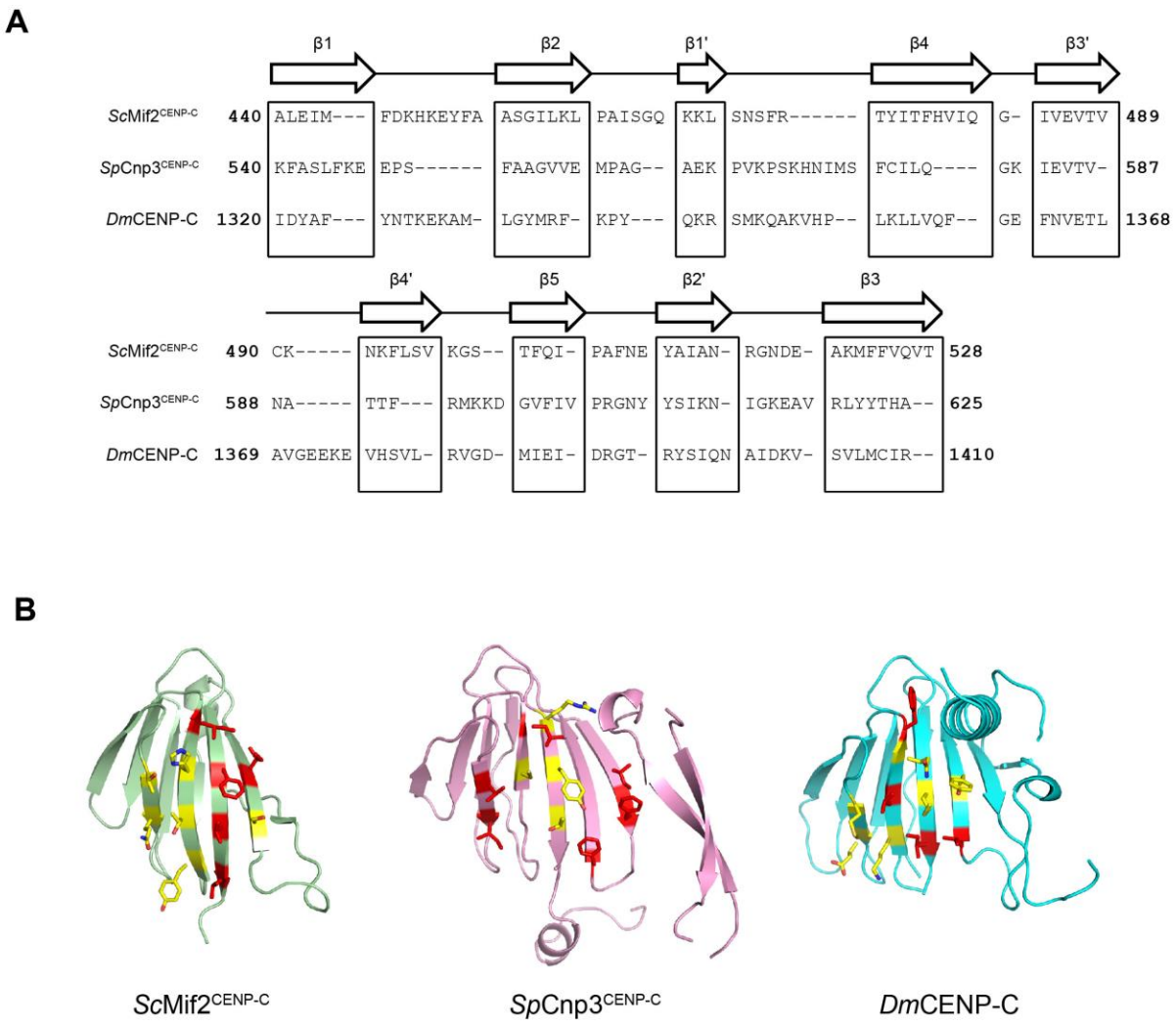

Figure 2.9 The residues lining CENP-C cupin domain dimer interfaces are not conserved.
A. The amino acid sequences of the *Sc*Mif2^{CENP-C}, *Sp*Cnp3^{CENP-C}, and *Dm*CENP-C cupin domain core folds are represented with their location within the secondary structure. Residues lining the cupin domain dimerization interface of β strands 1-5 are not well conserved. **B.** The interfacing residues of point and regional point centromere CENP-C cupin domains along β strands 1-5 are shown as sticks. Nonpolar (red) and polar (yellow) interface sidechains are shown.

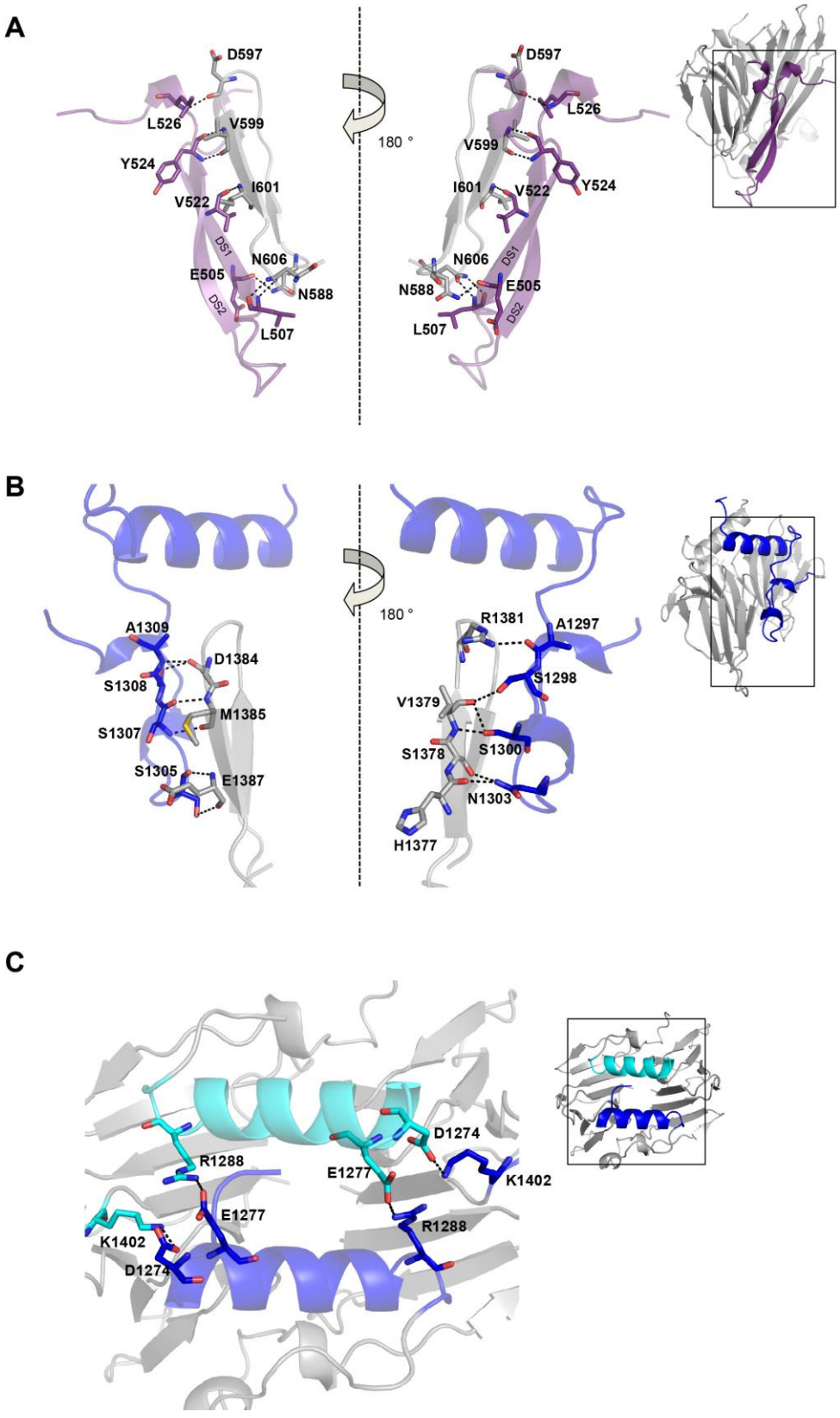
A
D597
L526
V599
Y524
I601
V522
DS1
N606
E505
N588
DS2
L507
180 °
D597
L526
V599
I601
V522
Y524
N606
DS1
N588
E505
DS2
L507
B
A1309
D1384
S1308
M1385
S1307
S1305
E1387
180 °
R1381
A1297
S1298
V1379
S1378
S1300
N1303
H1377
C
D1274
R1288
E1277
K1402
E1277
R1288
K1402
D1274

Figure 2.10 CENP-C cupin domains from organisms with regional centromeres possess additional interactions mediated by their extra secondary structure features.
A. Zoom in of the *Sp*Cnp3^{CENP-C} domain swapped region to highlight the interactions (dashes) and interacting residues (sticks) between the β hairpin (purple) and the β strands of the opposite chain (grey). **B.** Zoom in of the *Dm*CENP-C N-terminal region to highlight the interactions (dashes) and interacting residues (sticks) between the loop region (blue) and the β strands of the opposite chain (grey). **C.** Zoom in of the *Dm*CENP-C N-terminal helices to highlight the residues (sticks) and interactions (dashes) between the two chains (blue, cyan).

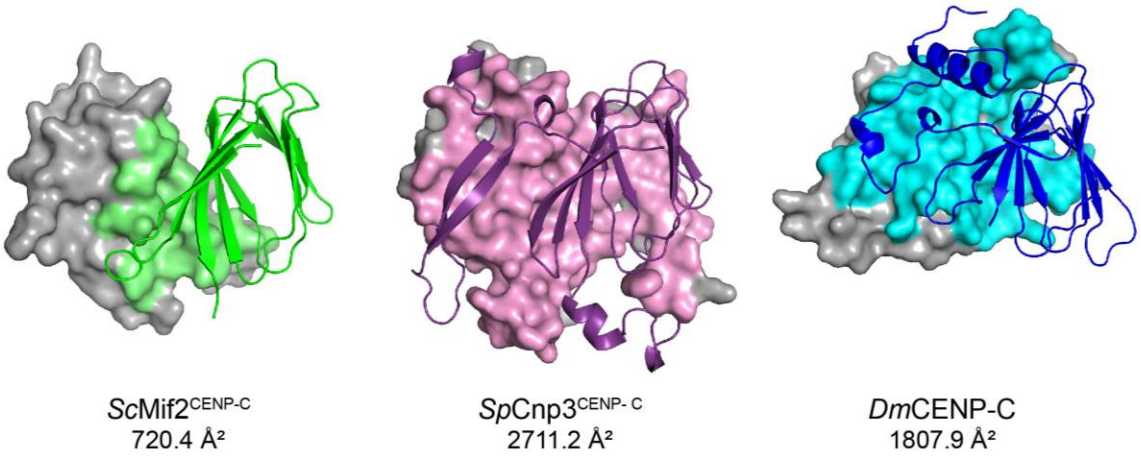

Figure 2.11 CENP-C cupin domains at regional centromeres (*Sp*Cnp3^{CENP-C} and *Dm*CENP-C) possess more expansive dimer interfaces than that at point centromeres (*Sc*Mif2^{CENP-C}).
One monomer in each structure is represented as a cartoon, and interfacing residues are colored accordingly within the grey surface representation of the opposite monomer. Dimer interface areas were calculated using PISA at the European Bioinformatics Institute. (http://www.ebi.ac.uk/pdbe/prot_int/pistart.html).

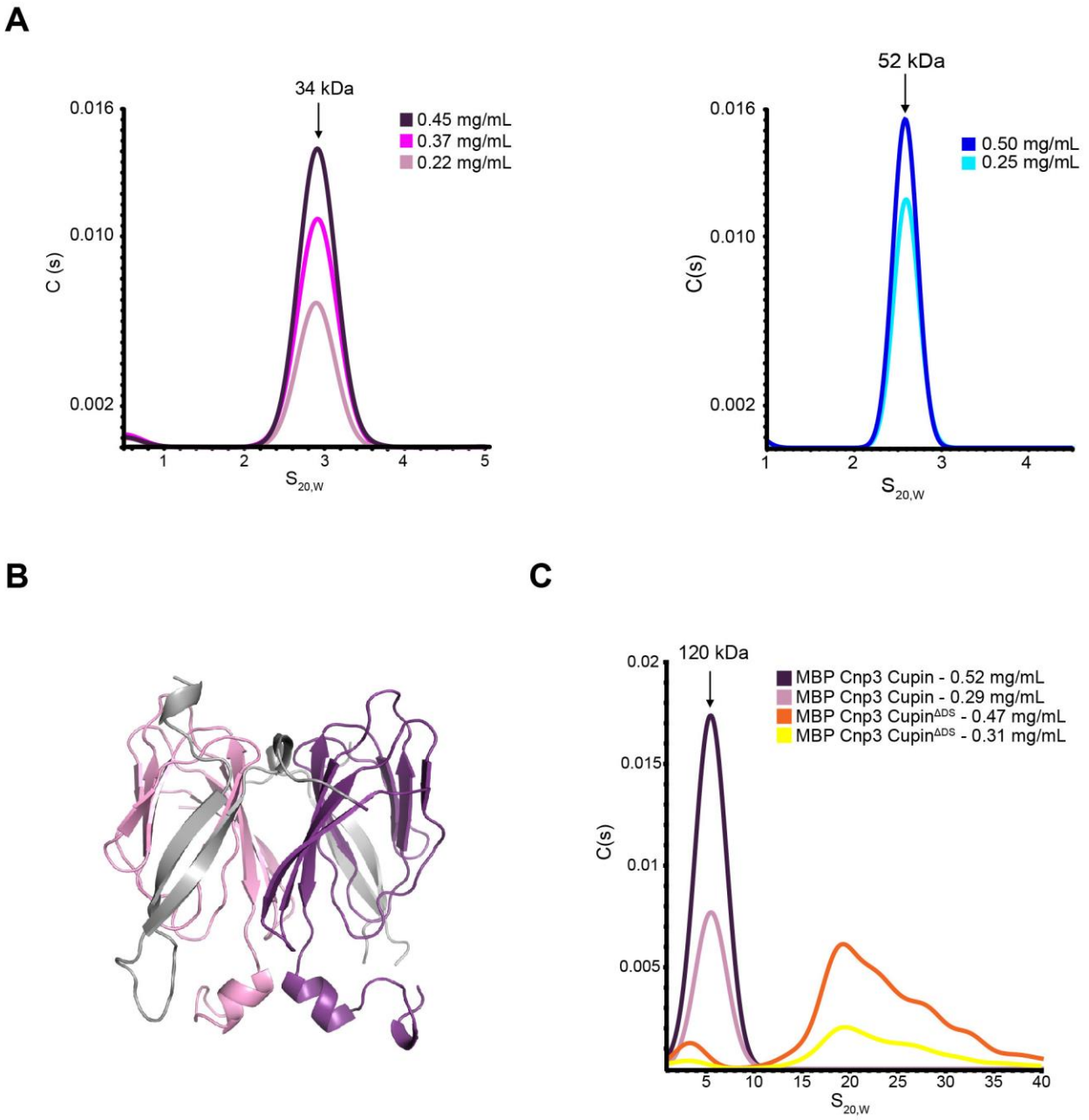

Figure 2.12 CENP-C cupin domains encoded by organisms with regional centromeres are dimeric *in vitro*. **A.** SV-AUC analysis of the *Sp*Cnp3^{CENP-C} (left) *and Dm*CENP-C (right) cupin domains shows that both are dimeric *in vitro.* Colors represent samples of differing concentrations. The expected molecular weight of the *Sp*Cnp3^{CENP-C} cupin monomer is 16.8 kDa. The expected molecular weight of the *Dm*CENP-C cupin monomer is 24.9 kDa. **B.** The MBP-tagged *Sp*Cnp3^{CENP-C} Cupin$^{\Delta DS}$ construct (532–643) does not contain the N-terminal β hairpin (grey) of the *Sp*Cnp3^{CENP-C} cupin domain. This construct was used for SV-AUC analysis to determine the significance of the *Sp*Cnp3^{CENP-C} DS region. **C.** SV-AUC analysis of the purified MBP-tagged *Sp*Cnp3^{CENP-C} Cupin$^{\Delta DS}$ protein (orange, yellow) reveals that it sediments as higher molecular weight aggregates. MBP-tagged *Sp*Cnp3^{CENP-C} cupin (purple, pink) continues to sediment as a dimeric population. Expected molecular weight of the MBP-tagged *Sp*Cnp3^{CENP-C} cupin monomer is 62.4 kDa.

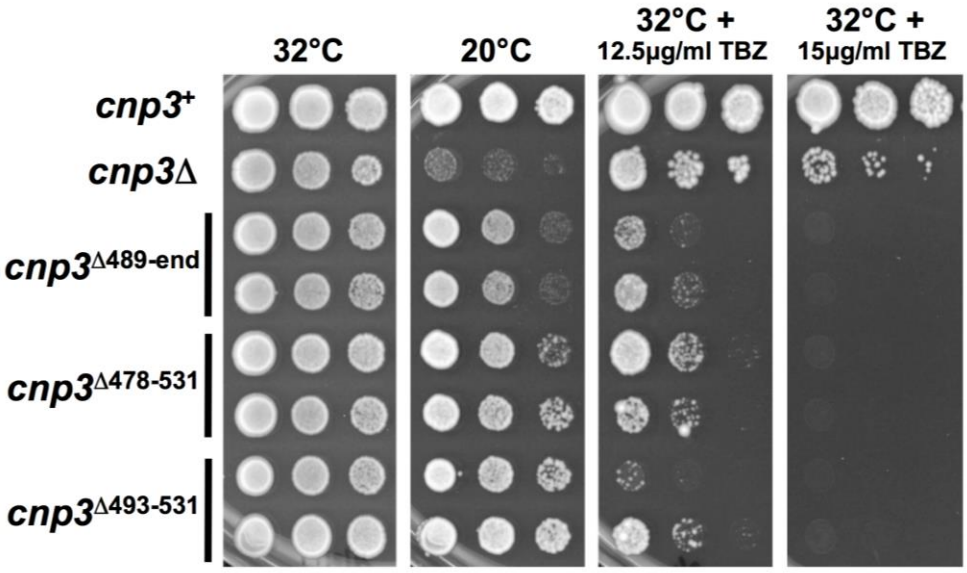

Figure 2.13 The domain swapped region (β-hairpin; DS) promotes *Sp*Cnp3^{CENP-C} function *in vivo*.
cnp3$^{\Delta 478–531}$ and *cnp3*$^{\Delta 493–531}$ DS truncation mutants display hypersensitivity to thiabendazole (TBZ) but show little cold sensitivity in comparison to *cnp3*Δcells. Five-fold serial dilutions of cells of the indicated genotypes were spotted on YES media supplemented with or without the indicated concentrations of TBZ and incubated at the indicated temperatures for 3-7 days. Two independent isolates of each genotype (cupin domain truncation) are shown.

Table 2.1 *S. pombe* strains used in this chapter.

Strain	Figure	Genotype	Source
VM1163	2.13	*h⁺ leu1-32 ura4-D18 ade6-M210 his3-D1 arg3-D4 cnp3⁺:ura4⁺*	This study
LS893	2.13	*h⁺ leu1-32 ura4D18 ade6-M210 his3-D1 arg3-D4 cnp3Δ::ura4⁺*	This study
PG1201	2.13	*h⁺ leu1-32 ura4-D18 ade6-M210 his3-D1 arg3-D4 cnp3$^{\Delta 489\text{-}end}$:natMX*	This study
PG1202	2.13	*h⁺ leu1-32 ura4-D18 ade6-M210 his3-D1 arg3-D4 cnp3$^{\Delta 489\text{-}end}$:natMX*	This study
PG1209	2.13	*h⁺ leu1-32 ura4-D18 ade6-M210 his3-D1 cnp3$^{\Delta 478\text{-}531}$:ura4⁺*	This study
PG1210	2.13	*h⁺ leu1-32 ura4-D18 ade6-M210 his3-D1 arg3-D4 cnp3$^{\Delta 478\text{-}531}$:ura4⁺*	This study
PG1222	2.13	*h⁺ leu1-32 ura4-D18 ade6-M210 his3-D1 arg3-D4 cnp3$^{\Delta 493\text{-}531}$:ura4⁺*	This study
PG1223	2.13	*h⁺ leu1-32 ura4-D18 ade6-M210 his3-D1 arg3-D4 cnp3$^{\Delta 493\text{-}531}$:ura4⁺*	This study

Table 2.2 Data collection and refinement statistics.

	*Sp*Cnp3^{CENP-C} Cupin Domain	*Dm*CENP-C Cupin Domain	
	Cnp3 cupin (489–643)	SeMet CENP-C cupin (1244–1411)	Native CENP-C cupin (1190–1411)
Data collection			
Wavelength (Å)	0.9786	0.9786	0.9786
Space group	P 4_1 2_1 2	P 3_1 2 1	P 2_1 2_1 2_1
Cell dimensions			
a, *b*, *c* (Å)	55.16, 55.16, 206.64	86.24, 86.24, 112.24	51.93, 61.72, 87.92
α, β, γ (°)	90, 90, 90	90, 90, 120	90, 90, 90
Resolution	34.44–2.52 (2.59–2.52)	40.25–2.63 (2.70–2.63)	30.86–1.81 (1.86–1.81)
R_{merge}	0.056 (0.578)	0.257 (2.327)	0.041 (0.469)
R_{pim}	0.016 (0.156)	0.056 (0.502)	0.020 (0.257)
I / σI	32.9 (5.0)	11.8 (1.9)	21.6 (2.8)
Completeness (%)	99.6 (99.3)	99.9 (100.0)	99.6 (99.4)
Redundancy	13.2 (14.5)	21.8 (22.3)	4.8 (4.2)
Refinement			
Resolution (Å)	33.07–2.52		30.86–1.81
No. reflections	11475		25138
R_{work} / R_{free}	0.217/0.251		0.196/0.232
No. atoms			
Protein	2246		2224
Ligand/ion	N/A		N/A
Water	5		128
B-factors			
Protein (average B-factor)	71.68		29.59
Ligand/ion	N/A		N/A
Water	62.60		28.27
R.m.s. deviations			
Bond lengths (Å)	0.008		0.007
Bond angles (°)	1.248		0.902
Ramachandran plot (%)			
Favored	97.43		98.14
Allowed	2.57		1.86
Outliers	0.00		0.00
PDB ID	6O2D		6O2K

Values in parentheses are for the highest-resolution shell.

Chapter 3: The *S. pombe* Cnp3 Cupin Domain has Significant Roles in Meiosis I Fidelity

3.1 Introduction

3.1.1 Regulation of Kinetochores in Mitosis versus Meiosis

Mitosis and meiosis are both forms of cell division that must occur in a highly regulated manner in order to ensure the completion of their respective biological goals. Mitosis occurs in somatic cells and is a purely equational form of cell division, meaning that the cells do not change ploidy during the process. In contrast, meiosis is a unique process that occurs only in germ cells and consists of one reductional division followed by an equational division. As a result of one round of DNA replication and two consecutive rounds of cell division, diploid organisms produce four haploid gametes as products of meiosis. Due to the differing biological roles of mitosis and meiosis, kinetochores must be regulated in a precise manner in order to ensure the fidelity of each process.

An important set of proteins required for the success of both mitosis and meiosis is the cohesin complex. During cell division, the cohesin complex acts to glue sister chromatids together until the appropriate time of separation. Functional cohesin complexes ensure that premature chromosomal separation and subsequent aneuploidy do not occur. The cohesin complex, a well-conserved four-subunit protein complex, is thought to form a ring-like structure that encircles sister chromatids to prevent them

from separating **(Figure 3.1)** [188, 189]. The cohesin core complex consists of four proteins that are required for proper function: Smc1, Smc3, Scc1, and Scc3 [190-193]. The two Smc proteins are members of the structural maintenance of chromosomes (SMC) family and form a heterodimer within the core complex. Each monomer folds upon itself to create a rod-shaped protein with a hinge domain at one end and a globular ATPase domain, created by the N- and C-termini, at the other [188]. The hinge domains of Smc1 and Smc3 mediate the dimerization between the two proteins to form a V-shaped heterodimer [188, 194]. Scc1, also known as MCD1 and Rad21 in *S. cerevisiae* and vertebrates, respectively, is a kleisin protein that functions to bridge the two Smc ATPase domains and form a closed ring [188]. Lastly, Scc3, which has two isoforms in vertebrates (SA1 and SA2), is known to bind to C-terminal region of Scc1 and has implicated roles in destabilizing the cohesin along chromosomal arms during prophase [188, 195-197]. Sister chromatid cohesion is established during S phase and persists until the onset of anaphase in mitosis [191, 198]. For the cohesin complex to be released from the chromosome during mitosis, the Scc1 subunit is cleaved by separase, a cysteine protease, and this is sufficient for promoting the onset of anaphase [199, 200].

Mitotic sister kinetochores exhibit a characteristic “back-to-back” orientation or bi-orientation in order to facilitate their attachment to microtubules emanating from opposite spindle poles **(Figure 3.2)** [201]. In vertebrates, the cohesin complex begins to dissociate from chromosomal arms during prophase [192, 196]. When all chromosomes are bi-oriented and aligned on the metaphase plate, the spindle assembly checkpoint is inactivated, which triggers the onset of anaphase, and the remaining centromeric

cohesin is cleaved by separase [202]. Sister chromatids then evenly segregate to opposite poles and mitosis produces two daughter cells with identical genetic information after cytokinesis.

Because meiosis is composed of a reductional division along with an equational division, the kinetochores must be uniquely regulated during each division in order to ensure the separation of homologous chromosomes during meiosis I **(Figure 3.3)**. There are two important factors that vitally contribute to the success of the first cell division: the mono-orientation of sister kinetochores and the preservation of centromeric cohesion. During meiosis I, sister kinetochores must be mono-oriented, or attached to microtubules emanating from the same spindle pole **(Figure 3.3).** In contrast to the "back-to-back" orientation seen in mitosis, sister kinetochores take on a "fused" or "side-by-side" phenotype in the early stages of meiosis I [203, 204]. During prophase I, homologous chromosomes cross over and form chiasmata to create tension, which ensures correct microtubule attachment. Importantly, meiosis features a unique cohesin subunit, Rec8, which mostly replaces Scc1 and is required to maintain cohesion between sister chromatids [205, 206]. As meiosis I progresses, the cohesin complex is lost in a stepwise manner. During the metaphase to anaphase transition of meiosis I, the cohesin complex is cleaved from the chromosomal arms but is importantly, protected and maintained at the centromere [205, 206]. During meiosis II, the kinetochores return to a bi-oriented manner, similar to mitosis, and the remaining centromeric cohesin is cleaved at the metaphase to anaphase transition to facilitate the separation of sister chromatids and produce four haploid daughter cells **(Figure 3.3)** [205, 206].

3.1.2 Moa1

The Meikin family consists of functional homologs known as Moa1 in *S. pombe*, Spo13 in *S. cerevisiae*, and MEIKIN in mice and humans. While there is little sequence similarity between members of the family, they all have roles in maintaining the mono-orientation of kinetochores, specifically, during meiosis I [207, 208]. Moa1is only expressed during meiosis I and was initially discovered from a screen aiming to find proteins that were critical for monopolar attachment of kinetochores during meiosis I in *S. pombe* [208, 209]. Accordingly, when Moa1 is unable to localize to kinetochores, cells show equational chromosomal division during meiosis I [208]. Interestingly, cells that do not possess functional Moa1 do not possess any abnormal mitotic phenotypes, and as an additional nod to the meiotic specificity of members of the Meikin family, MEIKIN null mice are sterile [60, 207].

In addition to being required for monopolar attachment, Moa1 also plays important roles in protecting centromeric cohesion, a required feature of chromosomes in meiosis I. There are multiple players in the Moa1 triggered cascade that ultimately results in the preservation of centromeric cohesion **(Figure 3.4)**. Previous work has determined that Moa1 is initially recruited to the kinetochore by the *Sp*Cnp3^{CENP-C} cupin domain [60]. Once at the kinetochore, Moa1 recruits Plo1 (polo-like kinase), a kinase that has been shown to phosphorylate the N-terminal MELT (Met-Glu-Leu-Thr) repeats of Spc7 (human KNL1) along with Mph1 (human MPS1) [207, 210]. In turn, the phosphorylated MELT repeats are required for Bub1 kinase accumulation [94, 96, 210]. Bub1 is then able to phosphorylate serine 121 of histone H2A at centromeres, which is a prerequisite for Shugoshin recruitment along with Swi6 (human HP1) [211, 212]. When recruited,

Shugoshin, a protector of the cohesin complex, prevents the cleavage of centromeric cohesin until anaphase II. Shugoshin protects the cohesin complex from being cleaved by recruiting and forming a complex with protein phosphatase 2A (PP2A) [213-215]. Together, they prevent the phosphorylation of Rec8, which is a prerequisite step for the separase mediated proteolytic cleavage of Rec8 and subsequent removal of the cohesin complex from the chromosome [216-218].

While the cupin domain in CENP-C homologs has been established as a dimerization domain, the structural roles of the conserved cupin fold beyond dimerization have not been fully established. Interestingly, previous studies have demonstrated that the centromere-specific localization of Moa1 is driven by the *Sp*Cnp3^{CENP-C} cupin domain [60]. Through structure-guided mutagenesis studies of the *Sp*Cnp3^{CENP-C} cupin domain both *in vitro* and *in vivo*, we have identified the key residues critical for Moa1interaction and recruitment to the centromere. Our work, therefore, further characterizes the *Sp*Cnp3^{CENP-C} cupin domain as a bona fide recruitment factor.

3.2 **Materials and Methods**

3.2.1 Cupin Moa1 Binding Assays

N-terminal tagged His-MBP Cupin and His Moa1 were cloned as a polycistronic construct into the pET3a vector using ligation-independent cloning [219]. Point mutations were introduced to the cupin domain via QuikChange II XL Site-Directed Mutagenesis Kit (Agilent). The proteins were subsequently expressed in 1 L of *Escherichia coli* Rosetta (DE3) cells using PA-5052 auto-inducible media [168]. Harvested cells were resuspended in 30 mL of buffer consisting of 30 mM Tris-HCl (pH

8.0), 500 mM NaCl, 5% glycerol and 3 mM β-mercaptoethanol with protease inhibitor cocktails. After sonication and subsequent spin down, the lysate was applied to affinity columns. Both columns were equilibrated with Buffer B (30 mM Tris-HCl (pH 8.0), 500 mM NaCl, 5% glycerol, 3 mM β-mercaptoethanol) before sample loading. 15 mL of cell lysate was loaded onto 3 mL cobalt resin (Takara) and allowed to drain through. The resin was then washed with 20 mL Buffer B and then bound protein was eluted with 10 mL elution buffer (30 mM Tris-HCl (pH 8.0), 500 mM NaCl, 5% glycerol, 300 mM imidazole, and 3 mM β-mercaptoethanol). The remaining 15 mL of cell lysate was rocked with 2 mL amylose resin (New England Biolabs) at room temperature for one hour. The resin was subsequently washed with 20 mL Buffer B and protein eluted with 5 mL elution buffer (30 mM Tris-HCl (pH 8.0), 500 mM NaCl, 20 mM maltose, 5% glycerol, 3 mM β-mercaptoethanol). Assay was replicated four times for WT cupin domain and each point mutant. Amylose elution gel band intensities (AEI) were quantified using ImageJ [220]. His MBP Cupin AEI/ His Moa1 AEI ratios were calculated for each sample. WT AEI ratios were then divided by the AEI ratio for each sample and this value was subsequently used in GraphPad Prism 7.00 for Windows (GraphPad Software, La Jolla California USA, www.graphpad.com) to run statistical analysis.

3.2.2 Differential Scanning Calorimetry

The transition temperature of WT Cnp3 cupin domain and each significant point mutant was measured using a Nano DSC (TA Instruments, Delaware, USA). Nano DSC was first conditioned with 0.3 mL buffer made of 30 mM Tris-HCl (pH 8.0), 500 mM NaCl, and 1 mM tris(2-carboxyethyl)phosphine (TCEP) in both reference and sample cells. Program for conditioning run consisted of a temperature range of 25 °C to 80 °C,

a scan rate of 2 °C/min, pressure set at 3 atm, and a 60 sec equilibration. The same buffer samples were used for a subsequent baseline run with a temperature range of 25 °C to 80 °C, a scan rate of 1 °C/min, pressure set at 3 atm, and a 60 sec equilibration. Protein sample concentrations ranged from 0.66 mg/mL to 3.17 mg/mL in a buffer consisting of 30 mM Tris-HCl pH (8.0), 500 mM NaCl, and 1 mM tris(2-carboxyethyl)phosphine (TCEP). 1 mL of protein sample was degassed under vacuum for 15 min before loading. Sample cell was loaded with 0.3 mL of protein and same program conditions were used as baseline run. Data was processed using NanoAnalyze Software (TA Instruments, Delaware, USA).

3.2.3 S. pombe Strains and Growth Assays

Standard methods were used for fission yeast growth, genetics and manipulation [181]. Gene deletion, tagging and mutagenesis were carried out by either the lithium acetate transformation method or electroporation. Mutations within the *Sp*Cnp3^{CENP-C} cupin domain were generated by PCR-based methods, and integrated at the endogenous *cnp3* genomic locus using either a *ura4* or *natMX* selection marker targeted to the 3'UTR of *cnp3* [182]. Five-fold serial dilutions of the indicated strains were spotted onto YES media supplemented with or without the indicated concentrations of thiabendazole (TBZ) and incubated at the indicated temperatures for 3–7 days. Genotypes of *S. pombe* strains used in this study are listed in **Table 3.1**.

3.2.4 Cytology

To induce meiosis, homothallic fission yeast cells (h^{90}) expressing GFP-tagged Moa1 in wild type or *cnp3* mutant backgrounds, were grown to exponential phase in

YES, resuspended in 20g/L leucine, and spotted onto SPAS media. Following incubation at 32°C for 24 hours to allow the *mei4Δ* mutation to arrest cells in meiotic prophase I [208], cells were either imaged live using Vectashield with DAPI (Vector Labs) as mounting medium, or processed for immunofluorescence (IF). For IF, cells were fixed in 3.7% formaldehyde for 15 minutes at room temperature. Immunolocalization was performed as previously described [221]. Primary antibodies used for IF were anti-GFP A11122 (1:200) (Thermo Fisher/ Invitrogen) and anti-Cnp1^{CENP-A} antiserum (1:2000) (gift from R. Allshire). Alexa Fluor 488- and 594- coupled secondary antibodies were used at 1:1000 dilution (A21441 & A11016 from Thermo Fisher/ Invitrogen). Fluorescence imaging (live and IF) was performed using a Zeiss Axioimager Z2 microscope (Carl Zeiss AG, Germany) equipped with a Zeiss Colibri LED illumination system and Hamamatsu digital camera C11440. Ten Z sections for GFP (Moa1) and RFP (Cnp1^{CENP-A}) signals acquired using Zen software (Zeiss), as applicable, were converted into single two-dimensional images by projecting the maximum signal at each pixel position using Icy software (Institut Pasteur).

3.3 **Results**

3.3.1 Moa1 Binds to the Inner Pocket of the SpCnp3^{CENP-C} Cupin Domain

A previous study has demonstrated an association between the *Sp*Cnp3^{CENP-C} cupin domain and the meiosis-specific protein Moa1 [60]. In order to elucidate the structural role of the cupin fold and map the binding region required for Moa1 recruitment to centromeres, we introduced ten point mutations within the *Sp*Cnp3^{CENP-C} cupin domain that can be broadly classified into two categories: those within the pocket (N572S, K546D, M574T, A552T, H624A, and F541A) and those on the surface (Y607C,

S609R, T586A, and V566A) of the cupin domain **(Figure 3.5A)**. Mutations Y607C, T586A, M574T, and A552T were used as controls for the binding experiments, as they have already been shown to inhibit *Sp*Cnp3^{CENP-C} interaction with Moa1 *in vivo* [60]. His-MBP-tagged *Sp*Cnp3^{CENP-C} cupin (WT or mutated) and His-tagged Moa1 were co-expressed using a polycistronic construct and subsequently subjected to amylose-resin affinity pulldowns in order to determine the relative amount of mutant complex formation compared to WT protein **(Figure 3.5B)**. Moa1 was only stably expressed and remained soluble when it was co-expressed with the *Sp*Cnp3^{CENP-C} cupin domain. Five *Sp*Cnp3^{CENP-C} cupin domain mutations were found to significantly reduce Moa1 binding: Y607C, M574T, A552T, H624A, and F541A, and notably the latter four mutations are all positioned within the cupin domain binding pocket **(Figure 3.5C)**. Therefore, the affinity pull-down experiments indicate that the pocket within the *Sp*Cnp3^{CENP-C} cupin domain is responsible for Moa1 interaction.

Differential scanning calorimetry (DSC) experiments were performed to confirm that disrupted Moa1 complex formation observed in a subset of *Sp*Cnp3^{CENP-C} cupin mutants is due to the mutation of critical residues required for the interaction, and not due to improper cupin domain folding. DSC experiments show that WT cupin domain has a peak temperature of 48.34 °C while the mutations that significantly disrupted Moa1 binding, Y607C, M574T, A552T, H624A, and F541A, have peak temperatures of 47.34 °C, 42.08 °C, 48.62 °C**,** 51.13 °C, and 47.14 °C, respectively **(Figure 3.6)**. Thus, the DSC experiments indicate that mutations that significantly disrupt the association of the *Sp*Cnp3^{CENP-C} cupin domain with Moa1, do not disturb the structural integrity of the cupin domain, suggesting that they exclusively affect Moa1 binding.

A subset of the ten mutations listed above were also tested for their effects on *Sp*Cnp3^{CENP-C} function and Moa1 localization *in vivo*, as Cnp3^{CENP-C} has been shown to recruit Moa1 to centromeres during *S. pombe* meiosis [60]. Mutations F541A, A552T, M574T (pocket), or Y607C, V566A (surface) were introduced into the endogenous *cnp3* genomic locus. A552T and Y607C served as controls as they have been previously shown to specifically disrupt *Sp*Cnp3^{CENP-C} function in meiosis but not mitosis. Cells expressing Cnp3^{A552T} or Cnp3^{Y607C} display neither cold sensitivity nor TBZ sensitivity, while being unable to recruit Moa1 to centromeres during meiosis I **(Figure 3.7)** [60]. We observed very similar phenotypes for cells expressing Cnp3^{F541A} (pocket) and Cnp3^{V566A} (surface), despite V566A only mildly affecting Moa1 binding *in vitro*. Cnp3^{M574T}-expressing cells additionally displayed mild TBZ sensitivity as has been previously demonstrated **(Figures 3.5C, 3.7, and 3.8)** [60]. Together, these results suggest that mutations in the *Sp*Cnp3^{CENP-C} cupin domain, mainly in the pocket region, disrupt Moa1 association *in vitro*, and consequently Moa1 recruitment to centromeres during meiosis *in vivo*. On the other hand, mutations in the cupin domain have largely no effects on non-meiotic functions of *Sp*Cnp3^{CENP-C}, thus highlighting a largely meiosis-specific role for the *Sp*Cnp3^{CENP-C} cupin fold pocket in *S. pombe*.

3.4 **Discussion**

3.4.1 The SpCnp3^{CENP-C} Cupin Fold Forms a Functional Binding Pocket for Moa1

Using the *Sp*Cnp3^{CENP-C} cupin domain, we further demonstrate that the characteristic cupin fold has structural significance beyond dimerization, by forming a pocket for binding partners. While the majority of residues within the pocket are not structurally conserved among determined CENP-C cupin domain structures, they all

possess a similar pocket that is internally lined with predominantly hydrophobic and aromatic residues. Notably, the crystal packing observed in the *Sp*Cnp3^{CENP-C} cupin domain revealed that the C-terminal tail of an adjacent symmetry mate fits within the pocket opening, likely mimicking the pocket binding with its partner **(Figure 3.9A)**. The utilization of the cupin pocket is not unique to *Sp*Cnp3^{CENP-C} and has been shown to bind metals and sugars in other cupin proteins **(Figure 3.9B)** [185, 222]. It is therefore likely that the residues along the interior of the cupin pocket may be specifically tailored to its respective binding partner(s) to optimize partner binding.

Here, we show that the interaction between the *Sp*Cnp3^{CENP-C} cupin domain and meiosis-specific protein Moa1 occurs at this internal cupin domain pocket. Our *in vitro* pull-downs as well as *in vivo* recruitment studies demonstrate that Moa1 no longer interacts with the cupin domain and fails to localize to the centromere in meiosis I when key residues within the cupin inner pocket are mutated **(Figures 3.5, 3.7, and 3.8)**. However, when these pocket mutants are monitored during mitosis *in vivo,* they display no abnormal phenotypes, further suggesting that the *Sp*Cnp3^{CENP-C} cupin binding pocket is specific for Moa1 recruitment during meiosis I **(Figure 3.7)**. A former study already showed that two mutations A552T and Y607C in the *Sp*Cnp3^{CENP-C} cupin domain severely affect meiotic chromosome segregation [60]. Interestingly, in our pull-down studies, Y607C, a surface mutation, significantly decreased Moa1 binding. As Y607C is the only surface mutation tested to significantly affect Moa1 binding *in vitro*, it is likely that Moa1 uses this residue as a secondary contact point for additional interactions. Interestingly, another tested surface mutation V566A significantly disrupted centromere localization of Moa1 *in vivo* whilst only mildly affecting Moa1 interaction *in*

vitro, much like T586A as previously demonstrated **(Figures 3.5 and 3.7B)** [60]. These observations further support the likelihood of the cupin domain surface being involved in mediating secondary interactions between *Sp*Cnp3^{CENP-C} and Moa1 **(Figure 3.10)**.

3.4.2 The CENP-C Cupin Pocket is Likely to Mediate Crucial Interactions in Metazoans

The *Sp*Cnp3^{CENP-C} cupin Moa1 interaction may be conserved in vertebrates as MEIKIN, the functional mouse homolog of Moa1, has been shown to bind to the C-terminal region of mouse CENP-C [207]. Therefore, it is likely that MEIKIN binds to the cupin domain of CENP-C via the conserved cupin pocket during meiosis. Additionally, there is evidence to suggest that the *Dm*CENP-C cupin pocket likely binds Cal1, an evolutionarily distinct CENP-A chaperone with functions in both mitosis and meiosis [20].

In summary, our study uncovers crucial details about the structure and function of the conserved cupin domain of CENP-C in organisms with point and regional centromeres. Our findings provide insights into how CENP-C proteins might have evolved to interact with and recruit binding partners to centromeres in a wide range of eukaryotes. Our results have important implications for understanding how CENP-C, one of the mostly highly conserved centromere proteins, regulates chromosome segregation in both mitosis and meiosis.

3.5 **Author Contributions**

The data in this chapter has been submitted to the Journal of Biological Chemistry. J.K.C. performed pull-downs, analysed data, and wrote the manuscript; V.M. and P.K.G. generated *S. pombe* strains, performed cold sensitivity and TBZ sensitivity assays; V.M. performed GFP-Moa1 imaging; L.S. designed experiments for *S. pombe in vivo*

analysis, analysed data, and wrote the manuscript; and U-S.C. directed the project, designed experiments, analysed data, and wrote the manuscript.

3.6 **Acknowledgements**

We thank Kathleen Wisser and Joseph Schauerte for their guidance in setting up DSC experiments and Dr. Peter Thorpe for advice, as well as kindly allowing us access to his fluorescence microscope. We are grateful to the Yeast Genetic Resource Center (YGRC), National Bioresource Project (NBRP), Japan for *S. pombe* strains, and Prof. Robin Allshire for the anti-Cnp1^{CENP-A} antibody. This work was supported by grants (N019154-00 and DK111465) to U-S.C, and a QMUL start-up grant and BBSRC grant BB/R00868X/1 to L.S. B.G.M is supported by R01GM-108829. J.K.C. was supported by the NIH Cellular and Molecular Biology Training Grant T-32-GM007315 and the Rackham Graduate Student Precandidate and Candidate Research Grants.

3.7 **Figures**

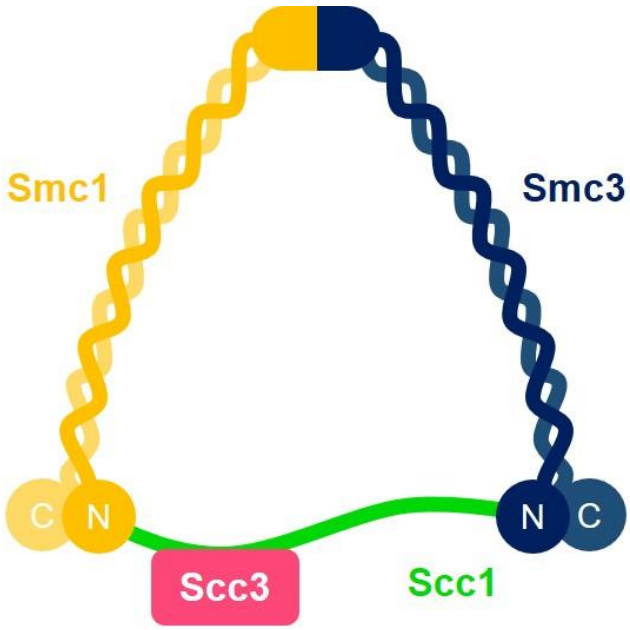

Figure 3.1 The cohesin complex forms a ring-like structure that prevents sister chromatids from separating prematurely during cell division.
Smc1 and Smc3 form a V-shaped heterodimer through their hinge domain interactions. Scc1 connects the Smc1 and Smc3 globular ATPase domains to complete the ring-like shape. Scc3 interacts with Scc1. After the onset of anaphase, separase cleaves Scc1 and subsequently releases the cohesin complex from the chromosome.

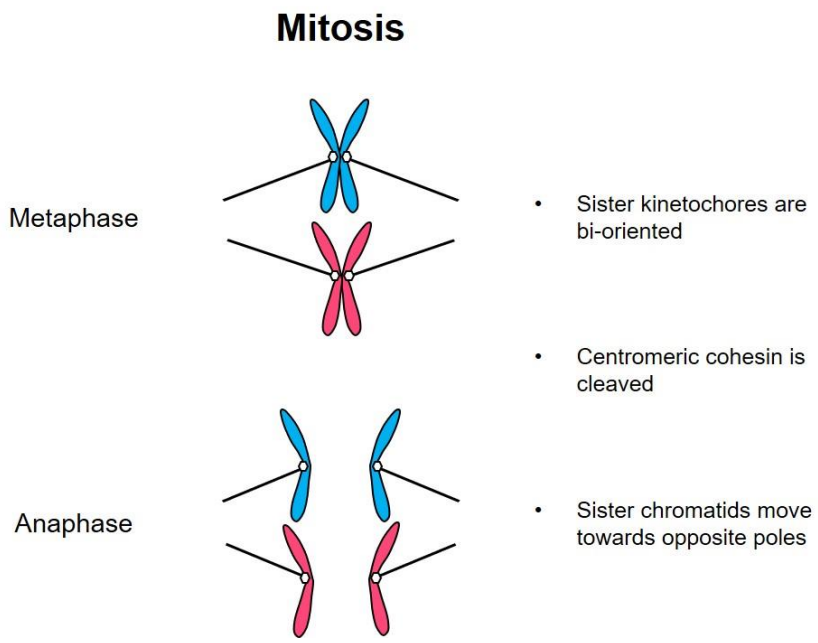

Figure 3.2 Successful mitosis requires bi-oriented sister kinetochores to facilitate microtubule attachments from opposite poles.
During the metaphase to anaphase transition, centromeric cohesin is cleaved and sister chromatids separate to opposite poles.

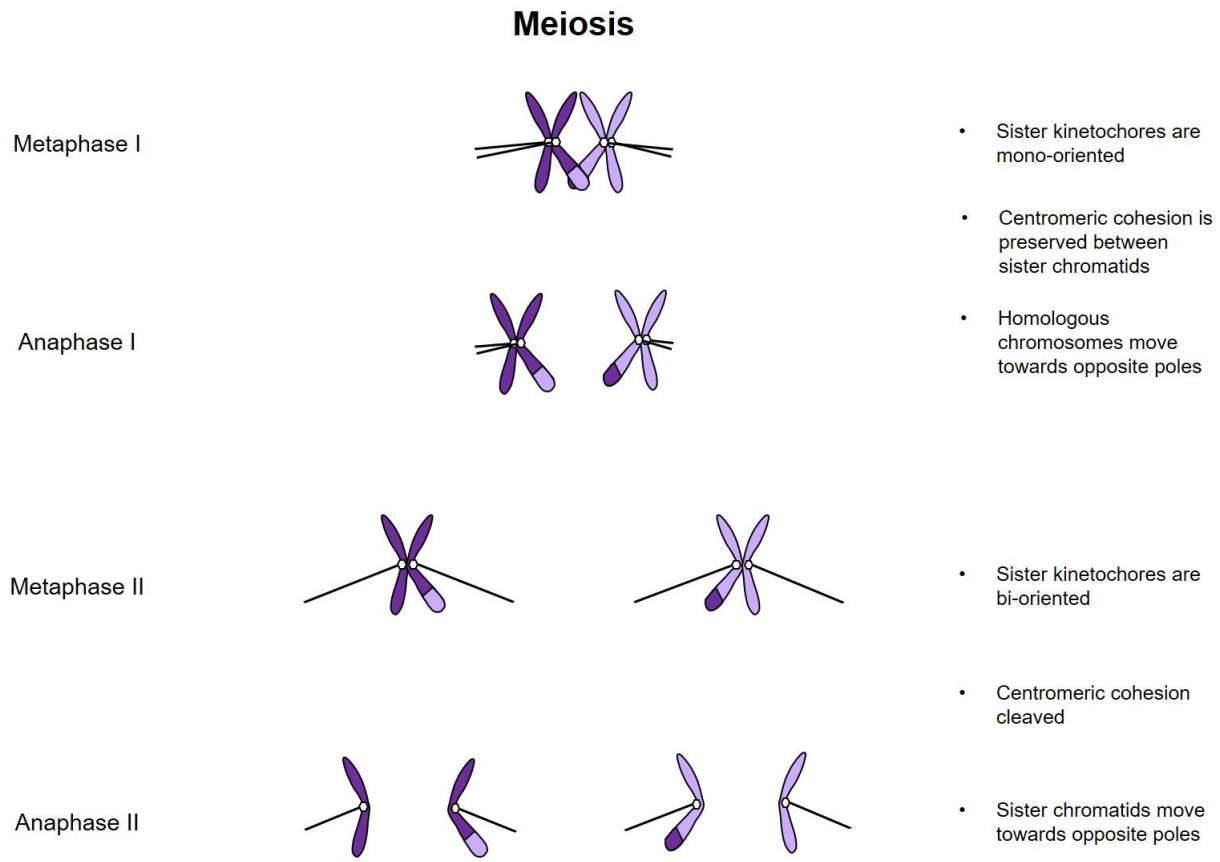

Figure 3.3 Sister kinetochores are regulated differently during meiosis I and meiosis II.
During the transition from metaphase I to anaphase I, sister kinetochores must be mono-oriented to facilitate microtubule attachments from the same pole. Importantly, centromeric cohesion is maintained throughout meiosis I. During meiosis II, kinetochores are bi-oriented, similar to mitosis **(Figure 3.2)**. Metaphase to anaphase transitions for meiosis I and meiosis II are shown.

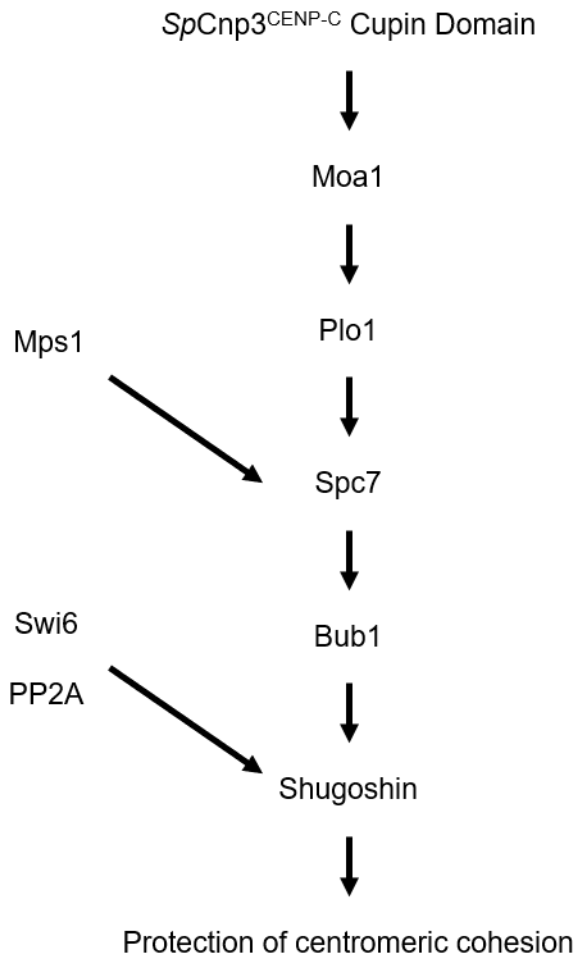

Figure 3.4 Protection of centromeric cohesion during meiosis I.
Moa1 indirectly recruits Shugoshin to ensure the protection of centromeric cohesion during meiosis I in *S. pombe.*

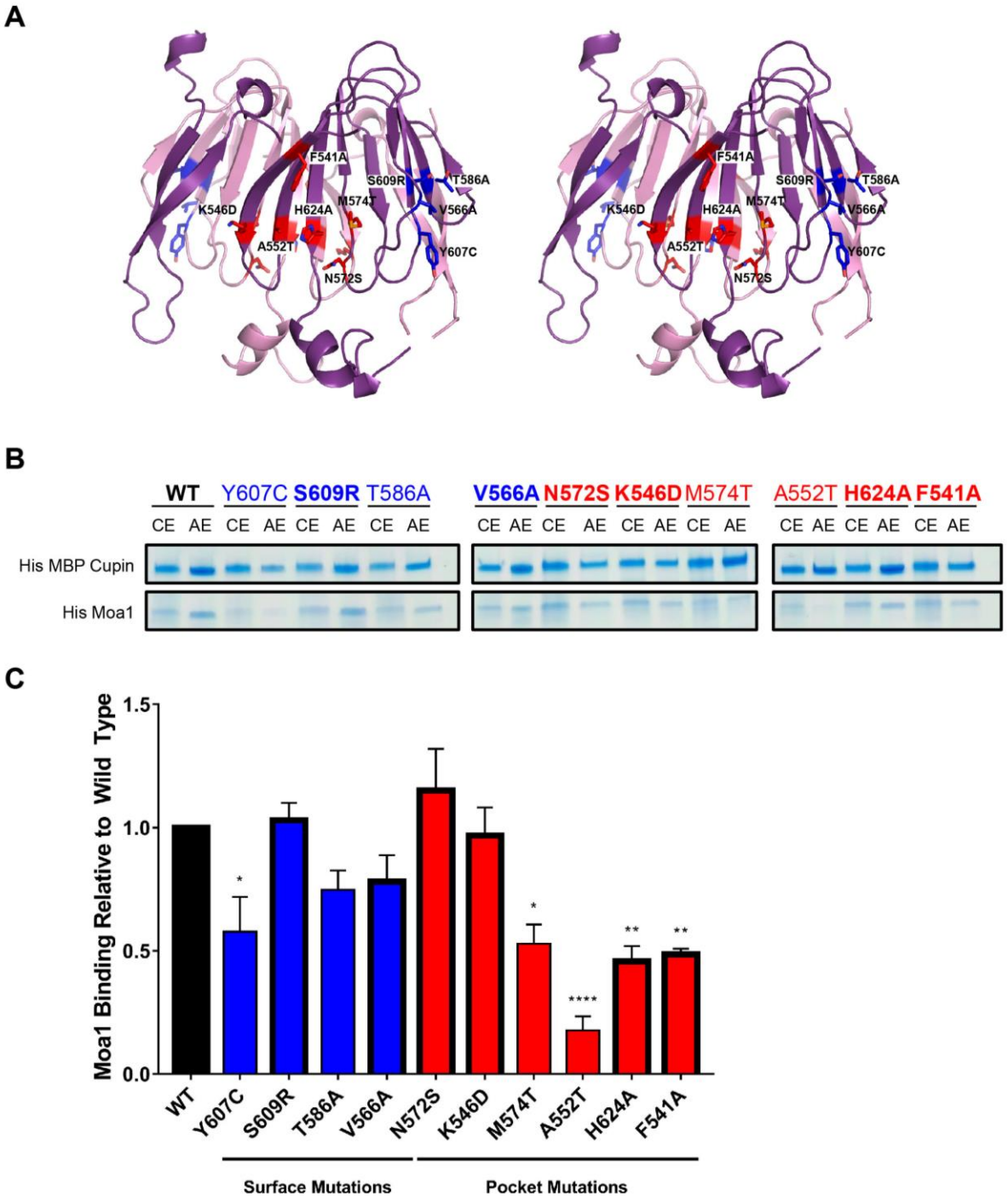

Figure 3.5 Moa1 associates with the inner binding pocket of the *Sp*Cnp3^{CENP-C} cupin domain.
A. Stereoview of *Sp*Cnp3^{CENP-C} cupin domain. Point mutations were designed to determine the Moa1 binding interface in the *Sp*Cnp3^{CENP-C} cupin domain. The mutations (stick sidechains) were split into two categories: pocket mutations (red) and surface mutations (blue). **B.** Amylose affinity pull-downs were performed with the His-MBP-tagged wild type (WT) and mutant *Sp*Cnp3^{CENP-C} cupin domains to determine the binding interface used for His-tagged Moa1 binding. Cobalt affinity column elutions (CE) show the initial expression levels of both components of the complex. Amylose affinity column elutions (AE) show the amount of Moa1 that was able to form a complex with the *Sp*Cnp3^{CENP-C} cupin domain within each sample. Mutations that have been previously shown to disrupt Moa1 recruitment *in vivo* are not shown in bold [60]. **C.** Quantification of the AE pull-down band intensity ratios of each

mutant relative to WT. Five *Sp*Cnp3^{CENP-C} cupin domain point mutations, Y607C, M574T, A552T, H624A, and F541A, significantly reduce complex formation between His-MBP Cupin and His-Moa1. Four of these mutations are located within the cupin domain inner pocket (red). Bars not shown in bold are controls that have been shown to disrupt Moa1 recruitment *in vivo* [60]. One-way ANOVA (n=4, mean ± s.e.m.) *P ≤ 0.05 **P ≤ 0.01 ****P ≤ 0.0001. One outlier was removed from S609R analysis using Grubbs' test.

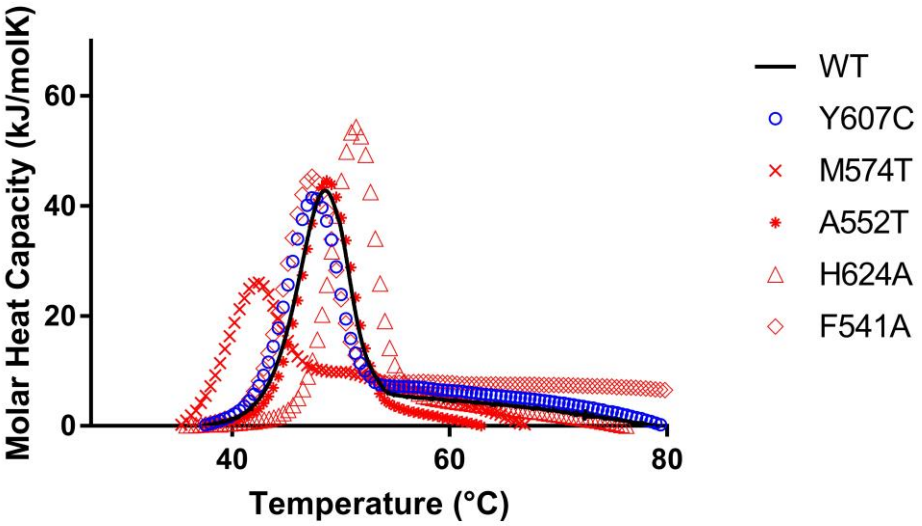

Figure 3.6 *Sp*Cnp3^{CENP-C} cupin domain point mutations that disrupt Moa1 association maintain the structural integrity of the cupin domain.
DSC scans of the WT *Sp*Cnp3^{CENP-C} cupin domain and each point mutation that significantly reduced Moa1 binding *in vitro*.

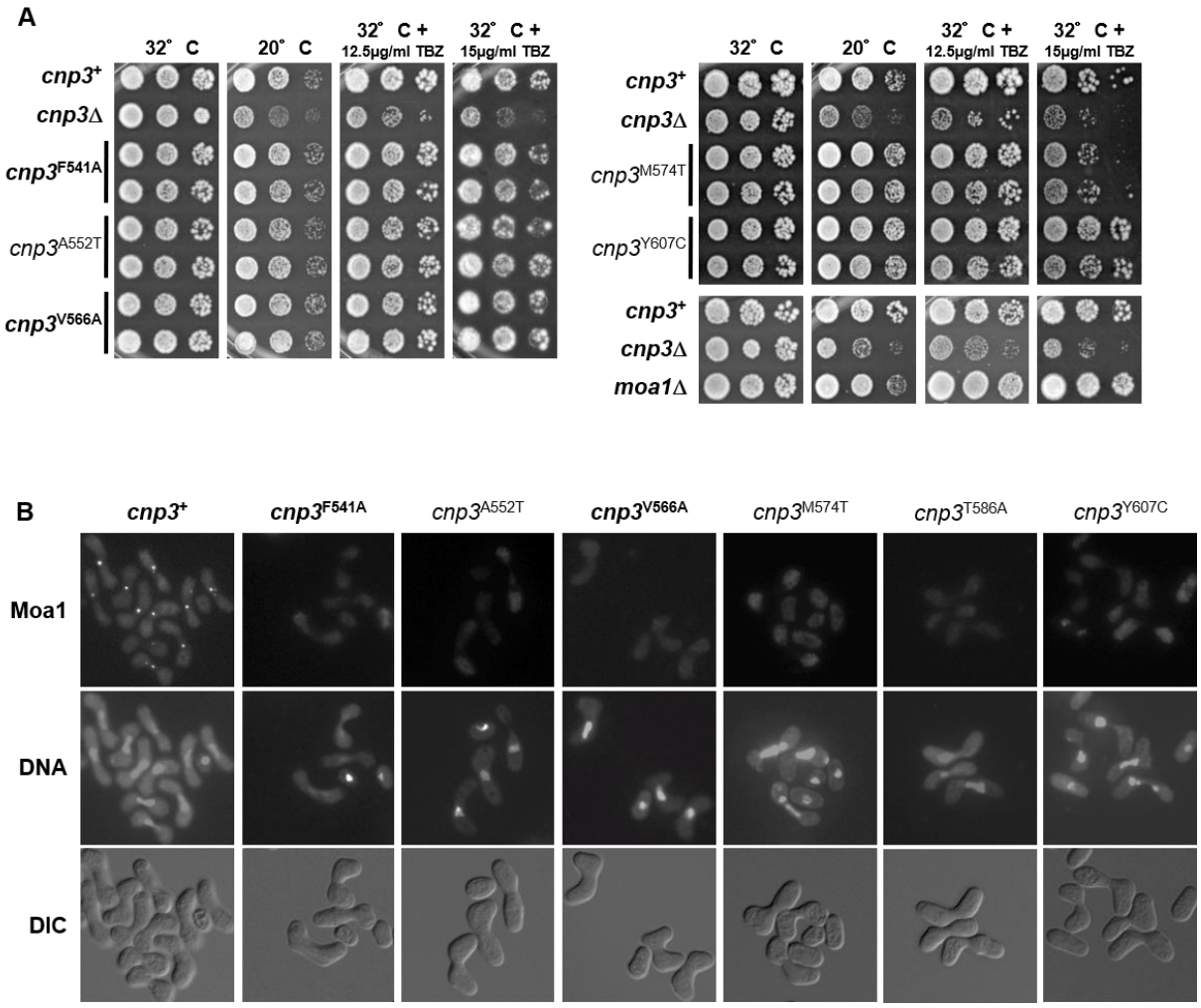

Figure 3.7 Point mutations within the *Sp*Cnp3^{CENP-C} cupin domain exclusively affect its function in meiosis, through disruption of Moa1 recruitment to centromeres.
A. *Sp*Cnp3^{CENP-C} cupin domain point mutants (pocket and surface) largely display no thiabendazole (TBZ) or cold sensitivity when compared with *cnp3*Δ cells (note that *moa1*Δ cells also display no TBZ or cold sensitivity). Five-fold serial dilutions of cells of the indicated genotypes were spotted on YES media supplemented with or without the indicated concentrations of TBZ and incubated at the indicated temperatures for 3-7 days. Two independent isolates of each genotype (cupin domain mutant) are shown. Point mutants unique to this study are bolded, while previously described mutants are not [60]. **B.** Point mutations within the *Sp*Cnp3^{CENP-C} cupin pocket (F541A, A552T, M574T) and surface (V566A, T586A, Y607C) result in failure to recruit Moa1 to centromeres during meiosis I. Homothallic (h^{90}) fission yeast cells of the indicated genotypes expressing GFP-tagged Moa1 were induced into meiosis at 32°C and arrested in meiotic prophase I using a *mei4*Δ allele. DNA was stained with DAPI, following which cells were imaged live. Point mutants unique to this study are bolded, while previously described mutants are not [60]. Also see **Figure 3.8.**

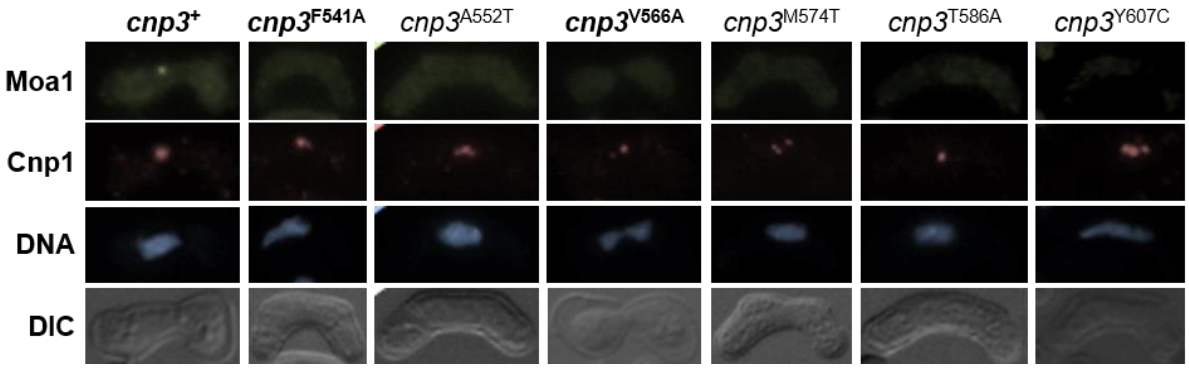

Figure 3.8 *Sp*Cnp3^{CENP-C} cupin domain point mutants fail to recruit Moa1 to centromeres.
Point mutations within the *Sp*Cnp3^{CENP-C} cupin pocket (F541A, A552T, M574T) and surface (V566A, T586A, Y607C) result in failure to recruit Moa1 to centromeres during meiosis I. Homothallic (h^{90}) fission yeast cells of the indicated genotypes expressing GFP-tagged Moa1 were induced into meiosis at 32°C and arrested in meiotic prophase I using a *mei4*Δ allele. Cells were then fixed and immunostained for Moa1 (green) and *Sp*Cnp1^{CENP-A} (red). DNA was stained with DAPI (blue). Mutants unique to this study are bolded, while previously described mutants are not [60].

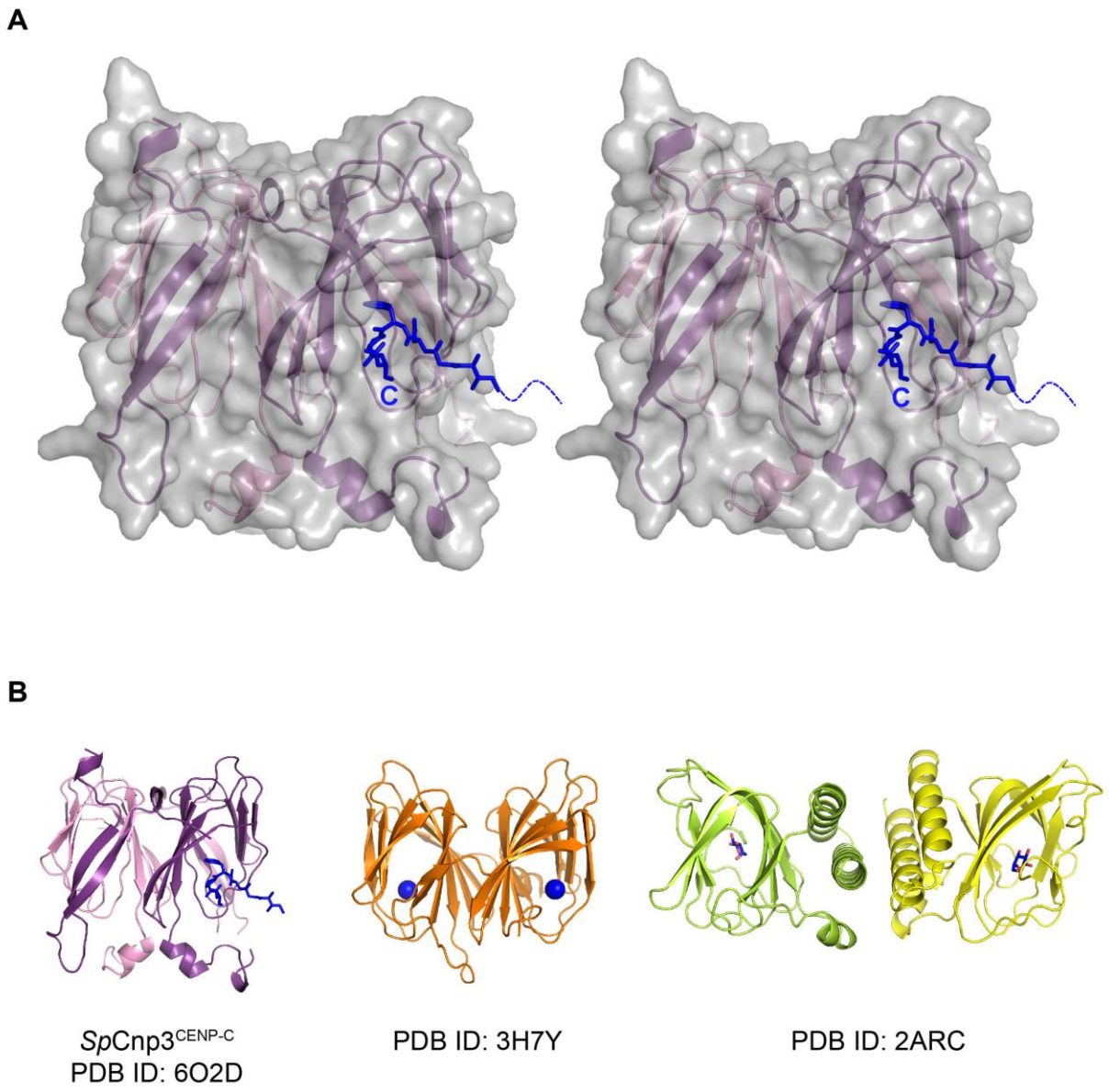

Figure 3.9 A symmetry related copy of the *Sp*Cnp3^{CENP-C} cupin domain may mimic Moa1 binding.
A. The stereoview and crystal packing of the *Sp*Cnp3^{CENP-C} cupin domain provide additional evidence of the inner pocket acting as a functional binding interface. The C-terminal tail of an adjacent symmetry mate (blue sticks) gravitates towards the pocket opening while the continuation of the chain towards the N-terminus is represented by blue dashes. **B.** The *Sp*Cnp3^{CENP-C} cupin domain pocket exhibits similarity to other cupin domain proteins that associate with metals (middle, blue spheres) and sugars (right, blue sticks) [185, 222].

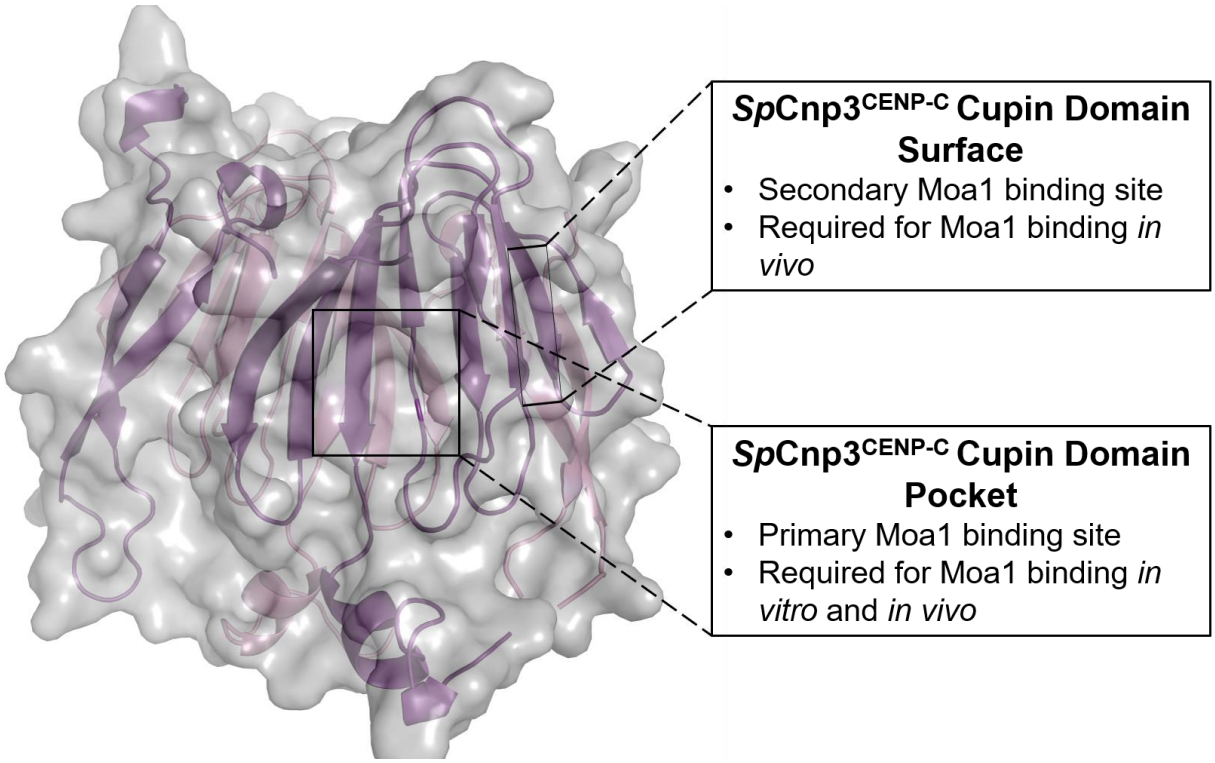

Figure 3.10 Proposed model for the *Sp*Cnp3^{CENP-C} cupin domain Moa1 interaction.
Based on our *in vitro* and *in vivo* analysis, we propose that Moa1 initially recognizes and binds to the *Sp*Cnp3^{CENP-C} cupin domain pocket and then uses the *Sp*Cnp3^{CENP-C} cupin domain surface to further stabilize the interaction.

Table 3.1 *S. pombe* strains used in this chapter.

Strain	Figure	Genotype	Source
VM1163	3.7A	*h^{+} leu1-32 ura4-D18 ade6-M210 his3-D1 arg3-D4 cnp3^{+}:ura4^{+}*	This study
LS893	3.7A	*h^{+} leu1-32 ura4D18 ade6-M210 his3-D1 arg3-D4 cnp3Δ::ura4^{+}*	This study
VM1161	3.7A	*h^{+} leu1-32 ura4-D18 ade6-M210 his3-D1 arg3-D4 cnp3^{F541A}:ura4^{+}*	This study
VM1171	3.7A	*h^{+} leu1-32 ura4-D18 ade6-M210 his3-D1 arg3-D4 cnp3^{F541A}:ura4^{+}*	This study
VM1189	3.7A	*h^{+} leu1-32 ura4-D18 ade6-M210 his3-D1 arg3-D4 cnp3^{A552T}:ura4^{+}*	This study
VM1190	3.7A	*h^{+} leu1-32 ura4-D18 ade6-M210 his3-D1 arg3-D4 cnp3^{A552T}:ura4^{+}*	This study
VM1191	3.7A	*h^{+} leu1-32 ura4-D18 ade6-M210 his3-D1 arg3-D4 cnp3^{V566A}:ura4^{+}*	This study
VM1192	3.7A	*h^{+} leu1-32 ura4-D18 ade6-M210 his3-D1 arg3-D4 cnp3^{V566A}:ura4^{+}*	This study
VM1156	3.7A	*h^{+} leu1-32 ura4-D18 ade6-M210 his3-D1 arg3-D4 cnp3^{M574T}:ura4^{+}*	This study
VM1157	3.7A	*h^{+} leu1-32 ura4-D18 ade6-M210 his3-D1 arg3-D4 cnp3^{M574T}:ura4^{+}*	This study
VM1185	3.7A	*h^{+} leu1-32 ura4-D18 ade6-M210 his3-D1 arg3-D4 cnp3^{Y607C}:ura4^{+}*	This study
VM1186	3.7A	*h^{+} leu1-32 ura4-D18 ade6-M210 his3-D1 arg3-D4 cnp3^{Y607C}:ura4^{+}*	This study
VM1166	3.7A	*h^{+} leu1-32 ura4-D18 ade6-M210 his3-D1 arg3-D4 moa1Δ::kanMX*	This study
VM1197	3.7B, 3.8	*h^{90} leu1-32 ura4-D18 ade6-M210 arg3-D4 GFP-Pk3-moa1 mei4Δ::hphMX cnp3^{+}:ura4^{+}*	This study
VM1194	3.7B, 3.8	*h^{90} leu1-32 ura4-D18 ade6-M210 arg3-D4 GFP-Pk3-moa1 mei4Δ::hphMX cnp3^{F541A}:ura4^{+}*	This study
VM1148	3.7B, 3.8	*h^{90} leu1-32 ura4-D18 ade6-M210 GFP-Pk3-moa1 mei4Δ::hphMX cnp3^{A552T}:ura4^{+}*	Tanaka et al. 2009 / YGRC
VM1206	3.7B, 3.8	*h^{90} leu1-32 ura4-D18 ade6-M210 arg3-D4 GFP-Pk3-moa1 mei4Δ::hphMX cnp3^{V566A}:ura4^{+}*	This study
VM1149	3.7B, 3.8	*h^{90} leu1-32 ura4-D18 ade6-M210 GFP-Pk3-moa1 mei4Δ::hphMX cnp3^{M574T}:ura4^{+}*	Tanaka et al. 2009 / YGRC
VM1150	3.7B, 3.8	*h^{90} leu1-32 ura4-D18 ade6-M210 GFP-Pk3-moa1 mei4Δ::hphMX cnp3^{T586A}:ura4^{+}*	Tanaka et al. 2009 / YGRC
VM1151	3.7B, 3.8	*h^{90} leu1-32 ura4-D18 ade6-M210 GFP-Pk3-moa1 mei4Δ::hphMX cnp3^{Y607C}:ura4^{+}*	Tanaka et al. 2009 / YGRC

Chapter 4: Summary and Future Directions

4.1 Summary

My thesis research focused on multiple facets of CENP-C biology from both evolutionary and biochemical perspectives. Because a wide variety of centromere and kinetochore compositions exist among organisms, it is likely that kinetochore proteins differ in structure due to variations in function and regulation.

Here, I sought to investigate the potential differences in structure between CENP-C homologs in *Saccharromyces cerevisiae*, *Schizosaccharomyces pombe*, and *Drosophila melanogaster*. These three model organisms were chosen due to their varying centromere classification (point centromere: *S. cerevisiae*, regional centromere: *S. pombe* and *D.* melanogaster) and kinetochore makeup (*D. melanogaster* possess a minimal inner kinetochore). Choosing to specifically focus on the conserved C-terminal cupin domain, I first determined the crystal structures the *S. pombe* Cnp3^{CENP-C} and D*. melanogaster* CENP-C cupin domains. These structures revealed that each harbors their own set of unique secondary structures that are not present in the *S. cerevisiae* Mif2^{CENP-C} cupin domain. These additional features mediate unique mechanisms of dimerization and confer stability to the dimeric state.

I further characterized the inner pocket of the *Sp*Cnp3^{CENP-C} cupin domain as a binding region for the meiosis-specific protein, Moa1. These studies therefore classify the *Sp*Cnp3^{CENP-C} cupin domain as a recruitment factor, in addition to its roles as a

dimerization domain. In this chapter, I present the implications of my research within the context of the kinetochore field and the new scientific directions that can be pursued.

4.2 Future Directions

My research shows that underlying centromere organization and kinetochore composition play distinct roles in determining kinetochore protein structure and function. With the addition of my work, the field now has a hold on the structural characteristics of cupin domains from three major model organisms: one from point centromeres (*Sc*Mif2^{CENP-C} cupin; PDB ID: 2VPV) and two from regional centromeres (*Sp*Cnp3^{CENP-C} cupin; PDB ID: 6O2D and *Dm*CENP-C cupin; PDB ID: 6O2K). Because the jelly roll fold is structurally conserved within all known CENP-C cupin structures, this finding would imply that the nature of the core fold plays an important role in cellular function. The next step is to focus on the functional significance of this domain within a broader kinetochore context and parsing out the relative contributions of its dual roles as a dimerization domain and a recruitment factor.

4.2.1 CENP-C and its Role in CENP-A Organization

Previous studies have highlighted a model where CENP-C plays a role in CENP-A organization by using its cupin domain to bridge adjacent CENP-A nucleosomes to create a broad platform for kinetochore recognition [141]. As the *S. cerevisiae* point centromere only possesses one CENP-A nucleosome, it is reasonable that *Sc*Mif2^{CENP-C} might use its C-terminal cupin domain so that the dimer may straddle the nucleosome and subsequently recruit additional kinetochore proteins through its N-terminal domains **(Figure 4.1A)**. Accordingly, quantitative fluorescence microscopy studies have found 1-2 *Sc*Mif2^{CENP-C} per kinetochore at point centromeres [223].

The situation becomes more complicated when we take into account the regional centromeres of other eukaryotes. It has been shown that multiple CENP-A nucleosomes are sporadically interspersed along with canonical H3 nucleosomes within linear centromeric chromatin from organisms with regional centromeres [22, 23]. Interestingly, these CENP-A nucleosomes are clustered toward the chromosomal surface during mitosis, suggesting that there are factors that mediate CENP-A nucleosome clustering **(Figure 4.2)** [22, 24]. As the depletion of CENP-C in HeLa cells shows a disruption of the inner kinetochore structure, and CENP-C is one of two kinetochore components to directly interact with CENP-A nucleosomes, we hypothesize that CENP-C facilitates CENP-A nucleosome clustering to optimize the accessible surface area for kinetochore assembly [59, 108, 141]. Although variable, *S. pombe* kinetochores have shown an approximate ratio of 1:2 CENP-A nucleosome to *Sp*Cnp3^{CENP-C} monomers at their centromere [18]. Additionally, chicken DT40 cells show an approximate ratio of 1:1.6 CENP-A nucleosomes to CENP-C monomers [224]. Because each CENP-A nucleosome contains two copies of CENP-A, dimeric CENP-C can either associate with a single nucleosome or connect two adjacent CENP-A nucleosomes. Therefore, we must determine whether each CENP-C dimer straddles single CENP-A nucleosome or physically connects adjacent CENP-A nucleosomes **(Figure 4.1B)**.

Historically, *in vitro* work concerning the full-length CENP-C protein has been lacking due to the struggle to express and purify the protein from recombinant sources. I have been able to optimize a protocol for the consistent recombinant expression and purification the full-length *Sp*Cnp3^{CENP-C} protein from *E. coli* **(Figure 4.3)**. I have additionally been able to express and purify all of the histones required to assemble

CENP-A nucleosomes. With the combination of these resources, we are in a unique position to examine this question *in vitro*. Specifically, we can determine how many CENP-A nucleosomes a CENP-C dimer can interact with via SV-AUC and visualize the interactions through negative-stain electron microscopy, and potentially cryo-electron microscopy.

Accordingly, our structural characterization of cupin domains from organisms with regional centromeres reveals that they possess dimer interfaces that are approximately doubled in surface area in comparison to that of the *Sc*Mif2^{CENP-C} cupin domain. This interface modification may be required to strengthen CENP-C dimerization so the protein can span a larger distance to link a greater number of CENP-A nucleosomes. As each cupin domain can be purified with relative ease, it would be worthwhile to determine whether interface size is indicative of the strength of each dimer interaction. Additionally, the *in vivo* characterization of CENP-C C-terminal chimeras or an artificial dimerization domain would determine whether an increased dimerization interface is indeed required for optimal kinetochore and overall cellular function.

4.2.2 Further Characterization of the CENP-C Cupin Inner Pocket

While we have determined that the inner pocket of the *Sp*Cnp3^{CENP-C} cupin domain is the primary binding site for Moa1 binding, we still do not have a clear picture of how this interaction is mediated at the atomic level. I have also optimized a purification protocol for the *Sp*Cnp3^{CENP-C} cupin domain and Moa1 complex using a polycistronic expression system and have begun initial screens for crystallization conditions **(Figure 4.4)**. It would be worthwhile to continue co-crystallization studies to gain a better

understanding of the cupin Moa1 interaction and the implications it may have for other CENP-C cupin domains and their binding partners.

Throughout my work, we have seen time and time again that centromere and kinetochore composition affect the structure and function of kinetochore proteins. Therefore, while Moa1 binds to the *Sp*Cnp3^{CENP-C} cupin domain, the binding partners are likely not conserved between organisms where centromere and kinetochore makeup greatly differ. Currently, there is no obvious candidate for a binding partner to the *Sc*Mif2^{CENP-C} cupin domain. Spo13, a meiosis specific protein that acts upstream of the monopolin complex in *S. cerevisiae*, has implicated roles as the *S. cerevisiae* Meikin family functional homolog [207, 225, 226]. While the function between Spo13 and other members of the Meikin family is not completely conserved, it remains a potential candidate as a Mif2 cupin domain binding partner by way of both the *Sp*Cnp3^{CENP-C} and mouse CENP-C cupin domains binding to their respective Meikin homologs [207].

As stated in the previously, it is likely that the *Dm*CENP-C cupin domain pocket binds to the unique CENP-A chaperone, Cal1 [20]. As the Mis18 complex has not been identified, Cal1 is likely the functional homolog in *D. melanogaster.* While the minimum binding region required for the interaction between the C-terminus of Cal1 and the cupin domain does not include the CENP-C motif, we cannot completely disregard its contribution as the motif is required for Mis18BP1 binding in other organisms [20, 155, 156]. It would be interesting to further characterize this interaction to determine whether the CENP-C motif does indeed play a role in this interaction, and if not, to determine if the CENP-C motif plays a different role within the CENP-A deposition process.

Lastly, as each cupin domain structure contains a pocket lined with predominantly aromatic and hydrophobic residues, we can determine whether all cupin domain partners are recruited through a similar mechanism or if each pocket is tailored specifically toward their respective binding partners. This question could be investigated more thoroughly by co-expressing cupin domains and binding partners from different organisms. Here, we can determine whether binding is preserved *in vitro* via pulldowns and subsequently test recruitment *in vivo.*

4.3 **Figures**

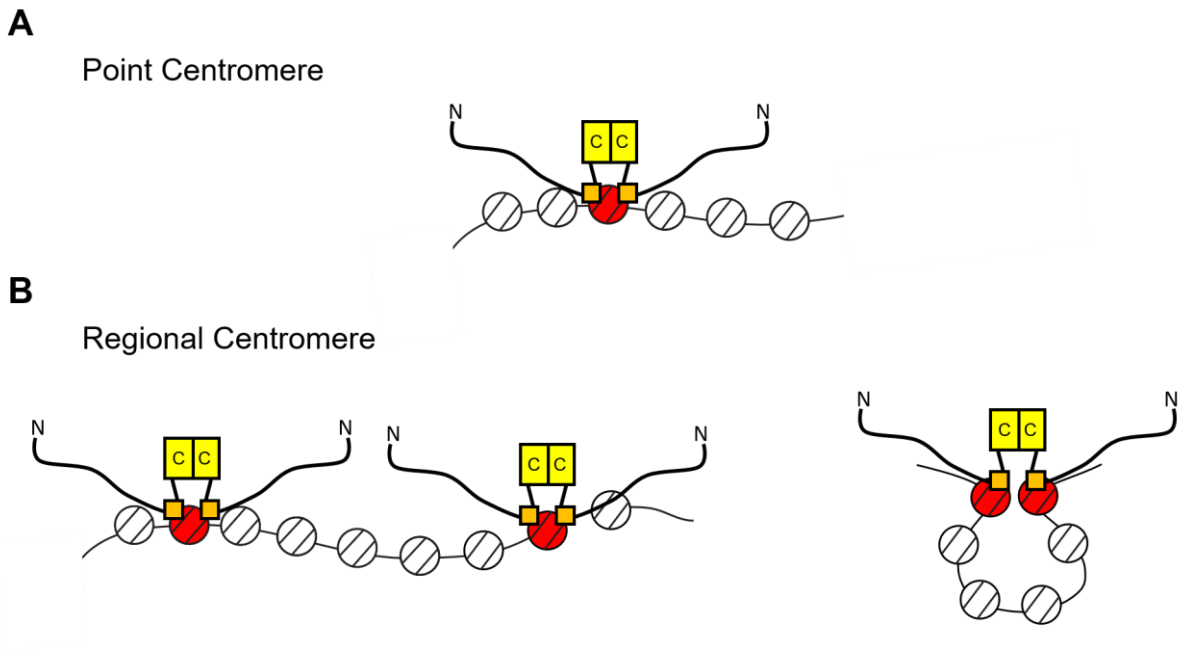

Figure 4.1 Models for dimeric CENP-C and its interaction with CENP-A nucleosomes.
A. At point centromeres, the *Sc*Mif2^{CENP-C} dimer likely interacts with the two CENP-A histones within a single nucleosome. **B.** At regional centromeres, two models are possible as more than one CENP-A nucleosome exists at the centromere. A CENP-C dimer can interact with adjacent nucleosomes (right) or with a single nucleosome (left) similar to what occurs at the point centromere. Canonical H3 nucleosomes and CENP-A nucleosomes are shown in white and red, respectively. The CENP-C motif is represented in orange and the cupin domain in yellow.

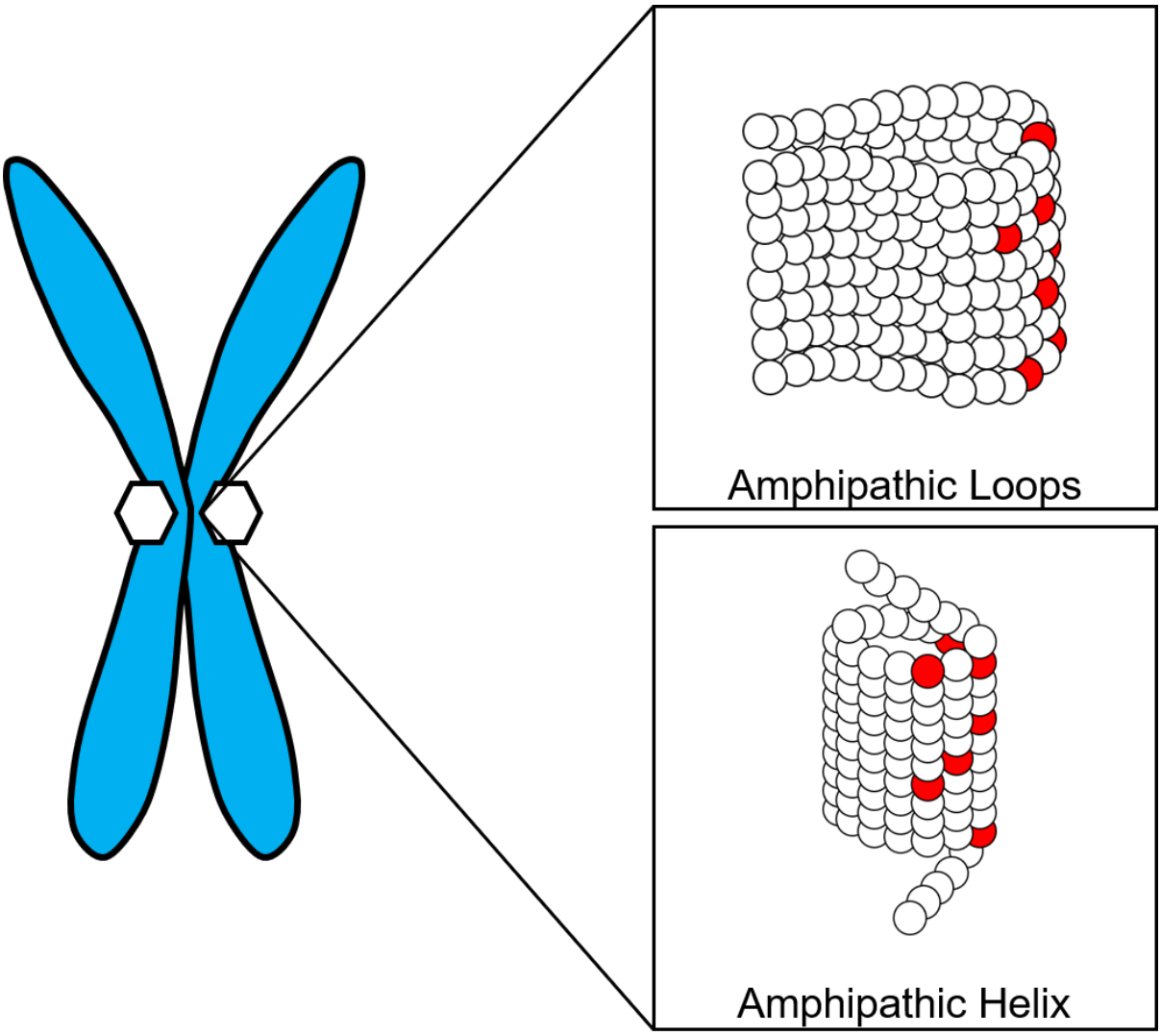

Figure 4.2 Proposed models of mitotic centromeric chromatin organization that would allow CENP-A nucleosomes to cluster towards the chromosomal surface.
Canonical H3 containing nucleosomes are represented in white, while CENP-A nucleosomes are shown in red. Modified from [187].

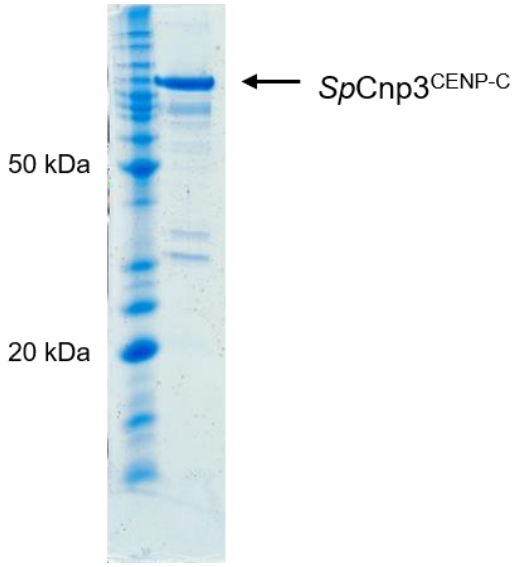

Figure 4.3 Full-length *Sp*Cnp3^{CENP-C} can be purified recombinantly from *E. coli.*
Coomassie-stained SDS-PAGE gel showing purified *Sp*Cnp3^{CENP-C} (72 kDa).

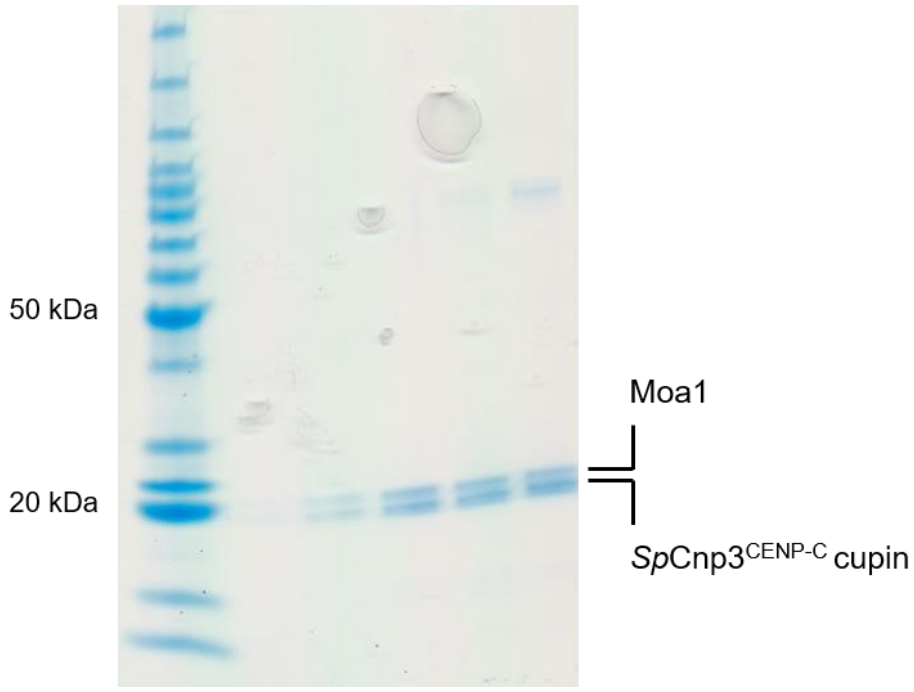

Figure 4.4 The *Sp*Cnp3^{CENP-C} cupin domain and Moa1 complex can be purified recombinantly from *E. coli*. Coomassie-stained SDS-PAGE gel showing purified size exclusion column fractions of the *Sp*Cnp3^{CENP-C} cupin domain (16.8 kDa) and Moa1 (19.6 kDa) complex.

References

1. Darlington, C.D., *The external mechanics of the chromosomes I—The scope of enquiry*, A.D. Hall, Editor. 1936: Proceedings of the Royal Society of London. Series B, Biological Sciences. p. 264-273.
2. Tachiwana, H., et al., *Crystal structure of the human centromeric nucleosome containing CENP-A.* Nature, 2011. **476**(7359): p. 232-5.
3. Stoler, S., et al., *A mutation in CSE4, an essential gene encoding a novel chromatin-associated protein in yeast, causes chromosome nondisjunction and cell cycle arrest at mitosis.* Genes Dev, 1995. **9**(5): p. 573-86.
4. Kim, D.U., et al., *Analysis of a genome-wide set of gene deletions in the fission yeast Schizosaccharomyces pombe.* Nat Biotechnol, 2010. **28**(6): p. 617-623.
5. Buchwitz, B.J., et al., *A histone-H3-like protein in C. elegans.* Nature, 1999. **401**(6753): p. 547-8.
6. Blower, M.D. and G.H. Karpen, *The role of Drosophila CID in kinetochore formation, cell-cycle progression and heterochromatin interactions.* Nat Cell Biol, 2001. **3**(8): p. 730-9.
7. Fachinetti, D., et al., *A two-step mechanism for epigenetic specification of centromere identity and function.* Nat Cell Biol, 2013. **15**(9): p. 1056-66.
8. Warburton, P.E., et al., *Immunolocalization of CENP-A suggests a distinct nucleosome structure at the inner kinetochore plate of active centromeres.* Curr Biol, 1997. **7**(11): p. 901-4.
9. Earnshaw, W.C. and B.R. Migeon, *Three related centromere proteins are absent from the inactive centromere of a stable isodicentric chromosome.* Chromosoma, 1985. **92**(4): p. 290-6.
10. Tyler-Smith, C., et al., *Transmission of a fully functional human neocentromere through three generations.* Am J Hum Genet, 1999. **64**(5): p. 1440-4.
11. Lo, A.W., et al., *A novel chromatin immunoprecipitation and array (CIA) analysis identifies a 460-kb CENP-A-binding neocentromere DNA.* Genome Res, 2001. **11**(3): p. 448-57.
12. Alonso, A., et al., *Genomic microarray analysis reveals distinct locations for the CENP-A binding domains in three human chromosome 13q32 neocentromeres.* Hum Mol Genet, 2003. **12**(20): p. 2711-21.
13. Shelby, R.D., O. Vafa, and K.F. Sullivan, *Assembly of CENP-A into centromeric chromatin requires a cooperative array of nucleosomal DNA contact sites.* J Cell Biol, 1997. **136**(3): p. 501-13.
14. Black, B.E., et al., *Structural determinants for generating centromeric chromatin.* Nature, 2004. **430**(6999): p. 578-82.
15. Van Hooser, A.A., et al., *Specification of kinetochore-forming chromatin by the histone H3 variant CENP-A.* J Cell Sci, 2001. **114**(Pt 19): p. 3529-42.

16. Heun, P., et al., *Mislocalization of the Drosophila centromere-specific histone CID promotes formation of functional ectopic kinetochores.* Dev Cell, 2006. **10**(3): p. 303-15.
17. Gascoigne, K.E., et al., *Induced ectopic kinetochore assembly bypasses the requirement for CENP-A nucleosomes.* Cell, 2011. **145**(3): p. 410-22.
18. Joglekar, A.P., et al., *Molecular architecture of the kinetochore-microtubule attachment site is conserved between point and regional centromeres.* J Cell Biol, 2008. **181**(4): p. 587-94.
19. Lando, D., et al., *Quantitative single-molecule microscopy reveals that CENP-A(Cnp1) deposition occurs during G2 in fission yeast.* Open Biol, 2012. **2**(7): p. 120078.
20. Schittenhelm, R.B., et al., *Detrimental incorporation of excess Cenp-A/Cid and Cenp-C into Drosophila centromeres is prevented by limiting amounts of the bridging factor Cal1.* J Cell Sci, 2010. **123**(Pt 21): p. 3768-79.
21. Sullivan, B.A. and G.H. Karpen, *Centromeric chromatin exhibits a histone modification pattern that is distinct from both euchromatin and heterochromatin.* Nat Struct Mol Biol, 2004. **11**(11): p. 1076-83.
22. Blower, M.D., B.A. Sullivan, and G.H. Karpen, *Conserved organization of centromeric chromatin in flies and humans.* Dev Cell, 2002. **2**(3): p. 319-30.
23. Bergmann, J.H., et al., *Epigenetic engineering shows H3K4me2 is required for HJURP targeting and CENP-A assembly on a synthetic human kinetochore.* EMBO J, 2011. **30**(2): p. 328-40.
24. Marshall, O.J., A.T. Marshall, and K.H. Choo, *Three-dimensional localization of CENP-A suggests a complex higher order structure of centromeric chromatin.* J Cell Biol, 2008. **183**(7): p. 1193-202.
25. Polizzi, C. and L. Clarke, *The chromatin structure of centromeres from fission yeast: differentiation of the central core that correlates with function.* J Cell Biol, 1991. **112**(2): p. 191-201.
26. Takahashi, K., et al., *A low copy number central sequence with strict symmetry and unusual chromatin structure in fission yeast centromere.* Mol Biol Cell, 1992. **3**(7): p. 819-35.
27. Takahashi, K., E.S. Chen, and M. Yanagida, *Requirement of Mis6 centromere connector for localizing a CENP-A-like protein in fission yeast.* Science, 2000. **288**(5474): p. 2215-9.
28. Hayashi, T., et al., *Mis16 and Mis18 are required for CENP-A loading and histone deacetylation at centromeres.* Cell, 2004. **118**(6): p. 715-29.
29. Cottarel, G., et al., *A 125-base-pair CEN6 DNA fragment is sufficient for complete meiotic and mitotic centromere functions in Saccharomyces cerevisiae.* Mol Cell Biol, 1989. **9**(8): p. 3342-9.
30. Clarke, L. and J. Carbon, *Isolation of a yeast centromere and construction of functional small circular chromosomes.* Nature, 1980. **287**(5782): p. 504-9.
31. Fitzgerald-Hayes, M., L. Clarke, and J. Carbon, *Nucleotide sequence comparisons and functional analysis of yeast centromere DNAs.* Cell, 1982. **29**(1): p. 235-44.

32. Furuyama, S. and S. Biggins, *Centromere identity is specified by a single centromeric nucleosome in budding yeast.* Proc Natl Acad Sci U S A, 2007. **104**(37): p. 14706-11.
33. Peterson, J.B. and H. Ris, *Electron-microscopic study of the spindle and chromosome movement in the yeast Saccharomyces cerevisiae.* J Cell Sci, 1976. **22**(2): p. 219-42.
34. Winey, M., et al., *Three-dimensional ultrastructural analysis of the Saccharomyces cerevisiae mitotic spindle.* J Cell Biol, 1995. **129**(6): p. 1601-15.
35. Cai, M.J. and R.W. Davis, *Purification of a yeast centromere-binding protein that is able to distinguish single base-pair mutations in its recognition site.* Mol Cell Biol, 1989. **9**(6): p. 2544-50.
36. Krassovsky, K., J.G. Henikoff, and S. Henikoff, *Tripartite organization of centromeric chromatin in budding yeast.* Proc Natl Acad Sci U S A, 2012. **109**(1): p. 243-8.
37. Lechner, J. and J. Carbon, *A 240 kd multisubunit protein complex, CBF3, is a major component of the budding yeast centromere.* Cell, 1991. **64**(4): p. 717-25.
38. Pidoux, A.L. and R.C. Allshire, *Kinetochore and heterochromatin domains of the fission yeast centromere.* Chromosome Res, 2004. **12**(6): p. 521-34.
39. Aldrup-Macdonald, M.E. and B.A. Sullivan, *The past, present, and future of human centromere genomics.* Genes (Basel), 2014. **5**(1): p. 33-50.
40. Sun, X., J. Wahlstrom, and G. Karpen, *Molecular structure of a functional Drosophila centromere.* Cell, 1997. **91**(7): p. 1007-19.
41. Sun, X., et al., *Sequence analysis of a functional Drosophila centromere.* Genome Res, 2003. **13**(2): p. 182-94.
42. Nakayama , J., et al., *Role of histone H3 lysine 9 methylation in epigenetic control of heterochromatin assembly.* Science, 2001. **292**(5514): p. 110-3.
43. Cam, H.P., et al., *Comprehensive analysis of heterochromatin- and RNAi-mediated epigenetic control of the fission yeast genome.* Nat Genet, 2005. **37**(8): p. 809-19.
44. Ding, R., K.L. McDonald, and J.R. McIntosh, *Three-dimensional reconstruction and analysis of mitotic spindles from the yeast, Schizosaccharomyces pombe.* J Cell Biol, 1993. **120**(1): p. 141-51.
45. Lin, H.P., J.G. Ault, and K. Church, *Meiosis in Drosophila melanogaster. I. Chromosome identification and kinetochore microtubule numbers during the first and second meiotic divisions in males.* Chromosoma, 1981. **83**(4): p. 507-21.
46. McEwen, B.F., et al., *CENP-E is essential for reliable bioriented spindle attachment, but chromosome alignment can be achieved via redundant mechanisms in mammalian cells.* Mol Biol Cell, 2001. **12**(9): p. 2776-89.
47. Wood, V., et al., *The genome sequence of Schizosaccharomyces pombe.* Nature, 2002. **415**(6874): p. 871-80.
48. Yao, J., et al., *Plasticity and epigenetic inheritance of centromere-specific histone H3 (CENP-A)-containing nucleosome positioning in the fission yeast.* J Biol Chem, 2013. **288**(26): p. 19184-96.
49. Yamada, T., et al., *The nucleation and maintenance of heterochromatin by a histone deacetylase in fission yeast.* Mol Cell, 2005. **20**(2): p. 173-85.

50. Willard, H.F., *Chromosome-specific organization of human alpha satellite DNA.* Am J Hum Genet, 1985. **37**(3): p. 524-32.
51. Guerra, M., et al., *Mitotic microtubule development and histone H3 phosphorylation in the holocentric chromosomes of Rhynchospora tenuis (Cyperaceae).* Genetica, 2006. **126**(1-2): p. 33-41.
52. Moroi, Y., et al., *Autoantibody to centromere (kinetochore) in scleroderma sera.* Proc Natl Acad Sci U S A, 1980. **77**(3): p. 1627-31.
53. Earnshaw, W.C. and N. Rothfield, *Identification of a family of human centromere proteins using autoimmune sera from patients with scleroderma.* Chromosoma, 1985. **91**(3-4): p. 313-21.
54. Brinkley, B.R. and E. Stubblefield, *The fine structure of the kinetochore of a mammalian cell in vitro.* Chromosoma, 1966. **19**(1): p. 28-43.
55. Jokelainen, P.T., *The ultrastructure and spatial organization of the metaphase kinetochore in mitotic rat cells.* J Ultrastruct Res, 1967. **19**(1): p. 19-44.
56. Foltz, D.R., et al., *The human CENP-A centromeric nucleosome-associated complex.* Nat Cell Biol, 2006. **8**(5): p. 458-69.
57. Okada, M., et al., *The CENP-H-I complex is required for the efficient incorporation of newly synthesized CENP-A into centromeres.* Nat Cell Biol, 2006. **8**(5): p. 446-57.
58. McKinley, K.L., et al., *The CENP-L-N Complex Forms a Critical Node in an Integrated Meshwork of Interactions at the Centromere-Kinetochore Interface.* Mol Cell, 2015. **60**(6): p. 886-98.
59. Kato, H., et al., *A conserved mechanism for centromeric nucleosome recognition by centromere protein CENP-C.* Science, 2013. **340**(6136): p. 1110-3.
60. Tanaka, K., et al., *CENP-C functions as a scaffold for effectors with essential kinetochore functions in mitosis and meiosis.* Dev Cell, 2009. **17**(3): p. 334-43.
61. Hinshaw, S.M. and S.C. Harrison, *An Iml3-Chl4 heterodimer links the core centromere to factors required for accurate chromosome segregation.* Cell Rep, 2013. **5**(1): p. 29-36.
62. Klare, K., et al., *CENP-C is a blueprint for constitutive centromere-associated network assembly within human kinetochores.* J Cell Biol, 2015. **210**(1): p. 11-22.
63. Screpanti, E., et al., *Direct binding of Cenp-C to the Mis12 complex joins the inner and outer kinetochore.* Curr Biol, 2011. **21**(5): p. 391-8.
64. Przewloka, M.R., et al., *CENP-C is a structural platform for kinetochore assembly.* Curr Biol, 2011. **21**(5): p. 399-405.
65. Dimitrova, Y.N., et al., *Structure of the MIND Complex Defines a Regulatory Focus for Yeast Kinetochore Assembly.* Cell, 2016. **167**(4): p. 1014-1027.e12.
66. Petrovic, A., et al., *Structure of the MIS12 Complex and Molecular Basis of Its Interaction with CENP-C at Human Kinetochores.* Cell, 2016. **167**(4): p. 1028-1040.e15.
67. Cohen, R.L., et al., *Structural and functional dissection of Mif2p, a conserved DNA-binding kinetochore protein.* Mol Biol Cell, 2008. **19**(10): p. 4480-91.
68. Carroll, C.W., et al., *Centromere assembly requires the direct recognition of CENP-A nucleosomes by CENP-N.* Nat Cell Biol, 2009. **11**(7): p. 896-902.
69. Chittori, S., et al., *Structural mechanisms of centromeric nucleosome recognition by the kinetochore protein CENP-N.* Science, 2018. **359**(6373): p. 339-343.

70. Nagpal, H., et al., *Dynamic changes in CCAN organization through CENP-C during cell-cycle progression.* Mol Biol Cell, 2015. **26**(21): p. 3768-76.
71. Weir, J.R., et al., *Insights from biochemical reconstitution into the architecture of human kinetochores.* Nature, 2016. **537**(7619): p. 249-253.
72. Nishino, T., et al., *CENP-T-W-S-X forms a unique centromeric chromatin structure with a histone-like fold.* Cell, 2012. **148**(3): p. 487-501.
73. Takeuchi, K., et al., *The centromeric nucleosome-like CENP-T-W-S-X complex induces positive supercoils into DNA.* Nucleic Acids Res, 2014. **42**(3): p. 1644-55.
74. Nishino, T., et al., *CENP-T provides a structural platform for outer kinetochore assembly.* EMBO J, 2013. **32**(3): p. 424-36.
75. Basilico, F., et al., *The pseudo GTPase CENP-M drives human kinetochore assembly.* Elife, 2014. **3**: p. e02978.
76. Sugata, N., E. Munekata, and K. Todokoro, *Characterization of a novel kinetochore protein, CENP-H.* J Biol Chem, 1999. **274**(39): p. 27343-6.
77. Nishihashi, A., et al., *CENP-I is essential for centromere function in vertebrate cells.* Dev Cell, 2002. **2**(4): p. 463-76.
78. Pesenti, M.E., et al., *Reconstitution of a 26-Subunit Human Kinetochore Reveals Cooperative Microtubule Binding by CENP-OPQUR and NDC80.* Mol Cell, 2018. **71**(6): p. 923-939.e10.
79. Schmitzberger, F. and S.C. Harrison, *RWD domain: a recurring module in kinetochore architecture shown by a Ctf19-Mcm21 complex structure.* EMBO Rep, 2012. **13**(3): p. 216-22.
80. Hornung, P., et al., *A cooperative mechanism drives budding yeast kinetochore assembly downstream of CENP-A.* J Cell Biol, 2014. **206**(4): p. 509-24.
81. Amaro, A.C., et al., *Molecular control of kinetochore-microtubule dynamics and chromosome oscillations.* Nat Cell Biol, 2010. **12**(4): p. 319-29.
82. Hua, S., et al., *CENP-U cooperates with Hec1 to orchestrate kinetochore-microtubule attachment.* J Biol Chem, 2011. **286**(2): p. 1627-38.
83. Hinshaw, S.M., et al., *The Kinetochore Receptor for the Cohesin Loading Complex.* Cell, 2017. **171**(1): p. 72-84.e13.
84. Cheeseman, I.M., et al., *The conserved KMN network constitutes the core microtubule-binding site of the kinetochore.* Cell, 2006. **127**(5): p. 983-97.
85. Cheeseman, I.M. and A. Desai, *Molecular architecture of the kinetochore-microtubule interface.* Nat Rev Mol Cell Biol, 2008. **9**(1): p. 33-46.
86. Petrovic, A., et al., *The MIS12 complex is a protein interaction hub for outer kinetochore assembly.* J Cell Biol, 2010. **190**(5): p. 835-52.
87. Huis In 't Veld, P.J., et al., *Molecular basis of outer kinetochore assembly on CENP-T.* Elife, 2016. **5**.
88. Kline, S.L., et al., *The human Mis12 complex is required for kinetochore assembly and proper chromosome segregation.* J Cell Biol, 2006. **173**(1): p. 9-17.
89. Espeut, J., et al., *Microtubule binding by KNL-1 contributes to spindle checkpoint silencing at the kinetochore.* J Cell Biol, 2012. **196**(4): p. 469-82.

90. Kiyomitsu, T., C. Obuse, and M. Yanagida, *Human Blinkin/AF15q14 is required for chromosome alignment and the mitotic checkpoint through direct interaction with Bub1 and BubR1.* Dev Cell, 2007. **13**(5): p. 663-76.
91. Liu, D., et al., *Regulated targeting of protein phosphatase 1 to the outer kinetochore by KNL1 opposes Aurora B kinase.* J Cell Biol, 2010. **188**(6): p. 809-20.
92. Kiyomitsu, T., H. Murakami, and M. Yanagida, *Protein interaction domain mapping of human kinetochore protein Blinkin reveals a consensus motif for binding of spindle assembly checkpoint proteins Bub1 and BubR1.* Mol Cell Biol, 2011. **31**(5): p. 998-1011.
93. Krenn, V., et al., *Structural analysis reveals features of the spindle checkpoint kinase Bub1-kinetochore subunit Knl1 interaction.* J Cell Biol, 2012. **196**(4): p. 451-67.
94. London, N., et al., *Phosphoregulation of Spc105 by Mps1 and PP1 regulates Bub1 localization to kinetochores.* Curr Biol, 2012. **22**(10): p. 900-6.
95. Primorac, I., et al., *Bub3 reads phosphorylated MELT repeats to promote spindle assembly checkpoint signaling.* Elife, 2013. **2**: p. e01030.
96. Yamagishi, Y., et al., *MPS1/Mph1 phosphorylates the kinetochore protein KNL1/Spc7 to recruit SAC components.* Nat Cell Biol, 2012. **14**(7): p. 746-52.
97. Petrovic, A., et al., *Modular assembly of RWD domains on the Mis12 complex underlies outer kinetochore organization.* Mol Cell, 2014. **53**(4): p. 591-605.
98. Kops, G.J., et al., *ZW10 links mitotic checkpoint signaling to the structural kinetochore.* J Cell Biol, 2005. **169**(1): p. 49-60.
99. Wang, H., et al., *Human Zwint-1 specifies localization of Zeste White 10 to kinetochores and is essential for mitotic checkpoint signaling.* J Biol Chem, 2004. **279**(52): p. 54590-8.
100. Gassmann, R., et al., *A new mechanism controlling kinetochore-microtubule interactions revealed by comparison of two dynein-targeting components: SPDL-1 and the Rod/Zwilch/Zw10 complex.* Genes Dev, 2008. **22**(17): p. 2385-99.
101. Griffis, E.R., N. Stuurman, and R.D. Vale, *Spindly, a novel protein essential for silencing the spindle assembly checkpoint, recruits dynein to the kinetochore.* J Cell Biol, 2007. **177**(6): p. 1005-15.
102. Varma, D., et al., *Spindle assembly checkpoint proteins are positioned close to core microtubule attachment sites at kinetochores.* J Cell Biol, 2013. **202**(5): p. 735-46.
103. Wei, R.R., J. Al-Bassam, and S.C. Harrison, *The Ndc80/HEC1 complex is a contact point for kinetochore-microtubule attachment.* Nat Struct Mol Biol, 2007. **14**(1): p. 54-9.
104. Wei, R.R., P.K. Sorger, and S.C. Harrison, *Molecular organization of the Ndc80 complex, an essential kinetochore component.* Proc Natl Acad Sci U S A, 2005. **102**(15): p. 5363-7.
105. Ciferri, C., et al., *Implications for kinetochore-microtubule attachment from the structure of an engineered Ndc80 complex.* Cell, 2008. **133**(3): p. 427-39.
106. Wei, R.R., et al., *Structure of a central component of the yeast kinetochore: the Spc24p/Spc25p globular domain.* Structure, 2006. **14**(6): p. 1003-9.

107. DeLuca, J.G., et al., *Hec1 and nuf2 are core components of the kinetochore outer plate essential for organizing microtubule attachment sites.* Mol Biol Cell, 2005. **16**(2): p. 519-31.
108. Liu, S.T., et al., *Mapping the assembly pathways that specify formation of the trilaminar kinetochore plates in human cells.* J Cell Biol, 2006. **175**(1): p. 41-53.
109. Rago, F., K.E. Gascoigne, and I.M. Cheeseman, *Distinct organization and regulation of the outer kinetochore KMN network downstream of CENP-C and CENP-T.* Curr Biol, 2015. **25**(5): p. 671-7.
110. Malvezzi, F., et al., *A structural basis for kinetochore recruitment of the Ndc80 complex via two distinct centromere receptors.* EMBO J, 2013. **32**(3): p. 409-23.
111. Drinnenberg, I.A., S. Henikoff, and H.S. Malik, *Evolutionary Turnover of Kinetochore Proteins: A Ship of Theseus?* Trends Cell Biol, 2016. **26**(7): p. 498-510.
112. Przewloka, M.R. and D.M. Glover, *The kinetochore and the centromere: a working long distance relationship.* Annu Rev Genet, 2009. **43**: p. 439-65.
113. Drinnenberg, I.A., et al., *Recurrent loss of CenH3 is associated with independent transitions to holocentricity in insects.* Elife, 2014. **3**.
114. Przewloka, M.R., et al., *Molecular analysis of core kinetochore composition and assembly in Drosophila melanogaster.* PLoS One, 2007. **2**(5): p. e478.
115. Schittenhelm, R.B., et al., *Spatial organization of a ubiquitous eukaryotic kinetochore protein network in Drosophila chromosomes.* Chromosoma, 2007. **116**(4): p. 385-402.
116. Liu, Y., et al., *Insights from the reconstitution of the divergent outer kinetochore of Drosophila melanogaster.* Open Biol, 2016. **6**(2): p. 150236.
117. Hornung, P., et al., *Molecular architecture and connectivity of the budding yeast Mtw1 kinetochore complex.* J Mol Biol, 2011. **405**(2): p. 548-59.
118. Maskell, D.P., X.W. Hu, and M.R. Singleton, *Molecular architecture and assembly of the yeast kinetochore MIND complex.* J Cell Biol, 2010. **190**(5): p. 823-34.
119. Hassold, T. and P. Hunt, *To err (meiotically) is human: the genesis of human aneuploidy.* Nat Rev Genet, 2001. **2**(4): p. 280-91.
120. Weaver, B.A. and D.W. Cleveland, *Does aneuploidy cause cancer?* Curr Opin Cell Biol, 2006. **18**(6): p. 658-67.
121. Tomonaga, T., et al., *Overexpression and mistargeting of centromere protein-A in human primary colorectal cancer.* Cancer Res, 2003. **63**(13): p. 3511-6.
122. Sun, X., et al., *Elevated expression of the centromere protein-A(CENP-A)-encoding gene as a prognostic and predictive biomarker in human cancers.* Int J Cancer, 2016. **139**(4): p. 899-907.
123. Tomonaga, T., et al., *Centromere protein H is up-regulated in primary human colorectal cancer and its overexpression induces aneuploidy.* Cancer Res, 2005. **65**(11): p. 4683-9.
124. Chen, Y., et al., *HEC, a novel nuclear protein rich in leucine heptad repeats specifically involved in mitosis.* Mol Cell Biol, 1997. **17**(10): p. 6049-56.
125. Bièche, I., et al., *Expression analysis of mitotic spindle checkpoint genes in breast carcinoma: role of NDC80/HEC1 in early breast tumorigenicity, and a two-gene signature for aneuploidy.* Mol Cancer, 2011. **10**: p. 23.

126. Durfee, T., et al., *The retinoblastoma protein associates with the protein phosphatase type 1 catalytic subunit.* Genes Dev, 1993. **7**(4): p. 555-69.
127. Diaz-Rodríguez, E., et al., *Hec1 overexpression hyperactivates the mitotic checkpoint and induces tumor formation in vivo.* Proc Natl Acad Sci U S A, 2008. **105**(43): p. 16719-24.
128. Tischkowitz, M.D. and S.V. Hodgson, *Fanconi anaemia.* J Med Genet, 2003. **40**(1): p. 1-10.
129. Singh, T.R., et al., *MHF1-MHF2, a histone-fold-containing protein complex, participates in the Fanconi anemia pathway via FANCM.* Mol Cell, 2010. **37**(6): p. 879-86.
130. Black, B.E., *Centromeres and kinetochores : discovering the molecular mechanisms underlying chromosome inheritance*. Progress in molecular and subcellular biology. xi, 554 pages.
131. Meeks-Wagner, D., et al., *Isolation of two genes that affect mitotic chromosome transmission in S. cerevisiae.* Cell, 1986. **44**(1): p. 53-63.
132. Kalitsis, P., et al., *Targeted disruption of mouse centromere protein C gene leads to mitotic disarray and early embryo death.* Proc Natl Acad Sci U S A, 1998. **95**(3): p. 1136-41.
133. Heeger, S., et al., *Genetic interactions of separase regulatory subunits reveal the diverged Drosophila Cenp-C homolog.* Genes Dev, 2005. **19**(17): p. 2041-53.
134. Moore, L.L. and M.B. Roth, *HCP-4, a CENP-C-like protein in Caenorhabditis elegans, is required for resolution of sister centromeres.* J Cell Biol, 2001. **153**(6): p. 1199-208.
135. Oegema, K., et al., *Functional analysis of kinetochore assembly in Caenorhabditis elegans.* J Cell Biol, 2001. **153**(6): p. 1209-26.
136. Brown, M.T., L. Goetsch, and L.H. Hartwell, *MIF2 is required for mitotic spindle integrity during anaphase spindle elongation in Saccharomyces cerevisiae.* J Cell Biol, 1993. **123**(2): p. 387-403.
137. Fukagawa, T., V. Regnier, and T. Ikemura, *Creation and characterization of temperature-sensitive CENP-C mutants in vertebrate cells.* Nucleic Acids Res, 2001. **29**(18): p. 3796-803.
138. Tomkiel, J., et al., *CENP-C is required for maintaining proper kinetochore size and for a timely transition to anaphase.* J Cell Biol, 1994. **125**(3): p. 531-45.
139. Xue, B., et al., *PONDR-FIT: a meta-predictor of intrinsically disordered amino acids.* Biochim Biophys Acta, 2010. **1804**(4): p. 996-1010.
140. Uversky, V.N., *Intrinsic Disorder, Protein-Protein Interactions, and Disease.* Adv Protein Chem Struct Biol, 2018. **110**: p. 85-121.
141. Carroll, C.W., K.J. Milks, and A.F. Straight, *Dual recognition of CENP-A nucleosomes is required for centromere assembly.* J Cell Biol, 2010. **189**(7): p. 1143-55.
142. Talbert, P.B., T.D. Bryson, and S. Henikoff, *Adaptive evolution of centromere proteins in plants and animals.* J Biol, 2004. **3**(4): p. 18.
143. Falk, S.J., et al., *Chromosomes. CENP-C reshapes and stabilizes CENP-A nucleosomes at the centromere.* Science, 2015. **348**(6235): p. 699-703.

144. Falk, S.J., et al., *CENP-C directs a structural transition of CENP-A nucleosomes mainly through sliding of DNA gyres.* Nat Struct Mol Biol, 2016. **23**(3): p. 204-208.
145. Sugimoto, K., et al., *Characterization of internal DNA-binding and C-terminal dimerization domains of human centromere/kinetochore autoantigen CENP-C in vitro: role of DNA-binding and self-associating activities in kinetochore organization.* Chromosome Res, 1997. **5**(2): p. 132-41.
146. Yang, C.H., et al., *Identification of overlapping DNA-binding and centromere-targeting domains in the human kinetochore protein CENP-C.* Mol Cell Biol, 1996. **16**(7): p. 3576-86.
147. Song, K., et al., *Mutational analysis of the central centromere targeting domain of human centromere protein C, (CENP-C).* Exp Cell Res, 2002. **275**(1): p. 81-91.
148. Trazzi, S., et al., *In vivo functional dissection of human inner kinetochore protein CENP-C.* J Struct Biol, 2002. **140**(1-3): p. 39-48.
149. Lanini, L. and F. McKeon, *Domains required for CENP-C assembly at the kinetochore.* Mol Biol Cell, 1995. **6**(8): p. 1049-59.
150. Milks, K.J., B. Moree, and A.F. Straight, *Dissection of CENP-C-directed centromere and kinetochore assembly.* Mol Biol Cell, 2009. **20**(19): p. 4246-55.
151. Sugimoto, K., et al., *Human centromere protein C (CENP-C) is a DNA-binding protein which possesses a novel DNA-binding motif.* J Biochem, 1994. **116**(4): p. 877-81.
152. Politi, V., et al., *CENP-C binds the alpha-satellite DNA in vivo at specific centromere domains.* J Cell Sci, 2002. **115**(Pt 11): p. 2317-27.
153. Kwon, M.S., et al., *CENP-C is involved in chromosome segregation, mitotic checkpoint function, and kinetochore assembly.* Mol Biol Cell, 2007. **18**(6): p. 2155-68.
154. Fukagawa, T., et al., *CENP-H, a constitutive centromere component, is required for centromere targeting of CENP-C in vertebrate cells.* EMBO J, 2001. **20**(16): p. 4603-17.
155. Moree, B., et al., *CENP-C recruits M18BP1 to centromeres to promote CENP-A chromatin assembly.* J Cell Biol, 2011. **194**(6): p. 855-71.
156. Dambacher, S., et al., *CENP-C facilitates the recruitment of M18BP1 to centromeric chromatin.* Nucleus, 2012. **3**(1): p. 101-10.
157. Fujita, Y., et al., *Priming of centromere for CENP-A recruitment by human hMis18alpha, hMis18beta, and M18BP1.* Dev Cell, 2007. **12**(1): p. 17-30.
158. McKinley, K.L. and I.M. Cheeseman, *Polo-like kinase 1 licenses CENP-A deposition at centromeres.* Cell, 2014. **158**(2): p. 397-411.
159. Dunwell, J.M., *Cupins: a new superfamily of functionally diverse proteins that include germins and plant storage proteins.* Biotechnol Genet Eng Rev, 1998. **15**: p. 1-32.
160. Dunwell, J.M. and P.J. Gane, *Microbial relatives of seed storage proteins: conservation of motifs in a functionally diverse superfamily of enzymes.* J Mol Evol, 1998. **46**(2): p. 147-54.
161. Dunwell, J.M., et al., *Evolution of functional diversity in the cupin superfamily.* Trends Biochem Sci, 2001. **26**(12): p. 740-6.

162. Dunwell, J.M., S. Khuri, and P.J. Gane, *Microbial relatives of the seed storage proteins of higher plants: conservation of structure and diversification of function during evolution of the cupin superfamily.* Microbiol Mol Biol Rev, 2000. **64**(1): p. 153-79.
163. Clissold, P.M. and C.P. Ponting, *JmjC: cupin metalloenzyme-like domains in jumonji, hairless and phospholipase A2beta.* Trends Biochem Sci, 2001. **26**(1): p. 7-9.
164. Swan, M.K., et al., *Structural evidence for a hydride transfer mechanism of catalysis in phosphoglucose isomerase from Pyrococcus furiosus.* J Biol Chem, 2003. **278**(47): p. 47261-8.
165. Stipanuk, M.H., et al., *Thiol dioxygenases: unique families of cupin proteins.* Amino Acids, 2011. **41**(1): p. 91-102.
166. Woo, E.J., et al., *Germin is a manganese containing homohexamer with oxalate oxidase and superoxide dismutase activities.* Nat Struct Biol, 2000. **7**(11): p. 1036-40.
167. Agarwal, G., et al., *Structure-based phylogeny as a diagnostic for functional characterization of proteins with a cupin fold.* PLoS One, 2009. **4**(5): p. e5736.
168. Studier, F.W., *Protein production by auto-induction in high density shaking cultures.* Protein Expr Purif, 2005. **41**(1): p. 207-34.
169. Kabsch, W., *Integration, scaling, space-group assignment and post-refinement.* Acta Crystallogr D Biol Crystallogr, 2010. **66**(Pt 2): p. 133-44.
170. Kabsch, W., *XDS.* Acta Crystallogr D Biol Crystallogr, 2010. **66**(Pt 2): p. 125-32.
171. Terwilliger, T.C., et al., *Decision-making in structure solution using Bayesian estimates of map quality: the PHENIX AutoSol wizard.* Acta Crystallogr D Biol Crystallogr, 2009. **65**(Pt 6): p. 582-601.
172. Terwilliger, T.C., et al., *Iterative model building, structure refinement and density modification with the PHENIX AutoBuild wizard.* Acta Crystallogr D Biol Crystallogr, 2008. **64**(Pt 1): p. 61-9.
173. Emsley, P., et al., *Features and development of Coot.* Acta Crystallogr D Biol Crystallogr, 2010. **66**(Pt 4): p. 486-501.
174. Adams, P.D., et al., *PHENIX: a comprehensive Python-based system for macromolecular structure solution.* Acta Crystallogr D Biol Crystallogr, 2010. **66**(Pt 2): p. 213-21.
175. Chen, V.B., et al., *MolProbity: all-atom structure validation for macromolecular crystallography.* Acta Crystallogr D Biol Crystallogr, 2010. **66**(Pt 1): p. 12-21.
176. Battye, T.G., et al., *iMOSFLM: a new graphical interface for diffraction-image processing with MOSFLM.* Acta Crystallogr D Biol Crystallogr, 2011. **67**(Pt 4): p. 271-81.
177. Evans, P.R. and G.N. Murshudov, *How good are my data and what is the resolution?* Acta Crystallogr D Biol Crystallogr, 2013. **69**(Pt 7): p. 1204-14.
178. McCoy, A.J., et al., *Phaser crystallographic software.* J Appl Crystallogr, 2007. **40**(Pt 4): p. 658-674.
179. Demeler, B., *UltraScan - A Comprehensive Data Analysis Software Package for Analytical Ultracentrifugation Experiments*, in *Analytical Ultracentrifugation: Techniques and Methods*, D.J. Scott, S.E. Harding, and A.J. Rowe, Editors. 2005, The Royal Society of Chemistry. p. 210-230.

180. Brookes, E., W. Cao, and B. Demeler, *A two-dimensional spectrum analysis for sedimentation velocity experiments of mixtures with heterogeneity in molecular weight and shape.* Eur Biophys J, 2010. **39**(3): p. 405-14.
181. Moreno, S., A. Klar, and P. Nurse, *Molecular genetic analysis of fission yeast Schizosaccharomyces pombe.* Methods Enzymol, 1991. **194**: p. 795-823.
182. Bähler, J., et al., *Heterologous modules for efficient and versatile PCR-based gene targeting in Schizosaccharomyces pombe.* Yeast, 1998. **14**(10): p. 943-51.
183. Pang, H., et al., *Crystal structure of human pirin: an iron-binding nuclear protein and transcription cofactor.* J Biol Chem, 2004. **279**(2): p. 1491-8.
184. Simmons, C.R., et al., *Crystal structure of mammalian cysteine dioxygenase. A novel mononuclear iron center for cysteine thiol oxidation.* J Biol Chem, 2006. **281**(27): p. 18723-33.
185. Rajavel, M., A. Mitra, and B. Gopal, *Role of Bacillus subtilis BacB in the synthesis of bacilysin.* J Biol Chem, 2009. **284**(46): p. 31882-92.
186. Krissinel, E. and K. Henrick, *Inference of macromolecular assemblies from crystalline state.* J Mol Biol, 2007. **372**(3): p. 774-97.
187. Fukagawa, T. and W.C. Earnshaw, *The centromere: chromatin foundation for the kinetochore machinery.* Dev Cell, 2014. **30**(5): p. 496-508.
188. Haering, C.H., et al., *Molecular architecture of SMC proteins and the yeast cohesin complex.* Mol Cell, 2002. **9**(4): p. 773-88.
189. Gruber, S., C.H. Haering, and K. Nasmyth, *Chromosomal cohesin forms a ring.* Cell, 2003. **112**(6): p. 765-77.
190. Strunnikov, A.V., V.L. Larionov, and D. Koshland, *SMC1: an essential yeast gene encoding a putative head-rod-tail protein is required for nuclear division and defines a new ubiquitous protein family.* J Cell Biol, 1993. **123**(6 Pt 2): p. 1635-48.
191. Michaelis, C., R. Ciosk, and K. Nasmyth, *Cohesins: chromosomal proteins that prevent premature separation of sister chromatids.* Cell, 1997. **91**(1): p. 35-45.
192. Losada, A., M. Hirano, and T. Hirano, *Identification of Xenopus SMC protein complexes required for sister chromatid cohesion.* Genes Dev, 1998. **12**(13): p. 1986-97.
193. Tóth, A., et al., *Yeast cohesin complex requires a conserved protein, Eco1p(Ctf7), to establish cohesion between sister chromatids during DNA replication.* Genes Dev, 1999. **13**(3): p. 320-33.
194. Hirano, M. and T. Hirano, *Hinge-mediated dimerization of SMC protein is essential for its dynamic interaction with DNA.* EMBO J, 2002. **21**(21): p. 5733-44.
195. Losada, A., et al., *Identification and characterization of SA/Scc3p subunits in the Xenopus and human cohesin complexes.* J Cell Biol, 2000. **150**(3): p. 405-16.
196. Sumara, I., et al., *Characterization of vertebrate cohesin complexes and their regulation in prophase.* J Cell Biol, 2000. **151**(4): p. 749-62.
197. Hauf, S., et al., *Dissociation of cohesin from chromosome arms and loss of arm cohesion during early mitosis depends on phosphorylation of SA2.* PLoS Biol, 2005. **3**(3): p. e69.
198. Uhlmann, F. and K. Nasmyth, *Cohesion between sister chromatids must be established during DNA replication.* Curr Biol, 1998. **8**(20): p. 1095-101.

199. Uhlmann, F., F. Lottspeich, and K. Nasmyth, *Sister-chromatid separation at anaphase onset is promoted by cleavage of the cohesin subunit Scc1.* Nature, 1999. **400**(6739): p. 37-42.
200. Uhlmann, F., et al., *Cleavage of cohesin by the CD clan protease separin triggers anaphase in yeast.* Cell, 2000. **103**(3): p. 375-86.
201. Tanaka, T.U., M.J. Stark, and K. Tanaka, *Kinetochore capture and bi-orientation on the mitotic spindle.* Nat Rev Mol Cell Biol, 2005. **6**(12): p. 929-42.
202. Waizenegger, I.C., et al., *Two distinct pathways remove mammalian cohesin from chromosome arms in prophase and from centromeres in anaphase.* Cell, 2000. **103**(3): p. 399-410.
203. Goldstein, L.S., *Kinetochore structure and its role in chromosome orientation during the first meiotic division in male D. melanogaster.* Cell, 1981. **25**(3): p. 591-602.
204. Parra, M.T., et al., *Involvement of the cohesin Rad21 and SCP3 in monopolar attachment of sister kinetochores during mouse meiosis I.* J Cell Sci, 2004. **117**(Pt 7): p. 1221-34.
205. Watanabe, Y. and P. Nurse, *Cohesin Rec8 is required for reductional chromosome segregation at meiosis.* Nature, 1999. **400**(6743): p. 461-4.
206. Klein, F., et al., *A central role for cohesins in sister chromatid cohesion, formation of axial elements, and recombination during yeast meiosis.* Cell, 1999. **98**(1): p. 91-103.
207. Kim, J., et al., *Meikin is a conserved regulator of meiosis-I-specific kinetochore function.* Nature, 2015. **517**(7535): p. 466-71.
208. Yokobayashi, S. and Y. Watanabe, *The kinetochore protein Moa1 enables cohesion-mediated monopolar attachment at meiosis I.* Cell, 2005. **123**(5): p. 803-17.
209. Mata, J., et al., *The transcriptional program of meiosis and sporulation in fission yeast.* Nat Genet, 2002. **32**(1): p. 143-7.
210. Miyazaki, S., et al., *Meikin-associated polo-like kinase specifies Bub1 distribution in meiosis I.* Genes Cells, 2017. **22**(6): p. 552-567.
211. Kawashima, S.A., et al., *Phosphorylation of H2A by Bub1 prevents chromosomal instability through localizing shugoshin.* Science, 2010. **327**(5962): p. 172-7.
212. Yamagishi, Y., et al., *Heterochromatin links to centromeric protection by recruiting shugoshin.* Nature, 2008. **455**(7210): p. 251-5.
213. Kitajima, T.S., et al., *Shugoshin collaborates with protein phosphatase 2A to protect cohesin.* Nature, 2006. **441**(7089): p. 46-52.
214. Riedel, C.G., et al., *Protein phosphatase 2A protects centromeric sister chromatid cohesion during meiosis I.* Nature, 2006. **441**(7089): p. 53-61.
215. Tang, Z., et al., *PP2A is required for centromeric localization of Sgo1 and proper chromosome segregation.* Dev Cell, 2006. **10**(5): p. 575-85.
216. Brar, G.A., et al., *Rec8 phosphorylation and recombination promote the step-wise loss of cohesins in meiosis.* Nature, 2006. **441**(7092): p. 532-6.
217. Attner, M.A., et al., *Polo kinase Cdc5 is a central regulator of meiosis I.* Proc Natl Acad Sci U S A, 2013. **110**(35): p. 14278-83.

218. Katis, V.L., et al., *Rec8 phosphorylation by casein kinase 1 and Cdc7-Dbf4 kinase regulates cohesin cleavage by separase during meiosis.* Dev Cell, 2010. **18**(3): p. 397-409.
219. Schmid-Burgk, J.L., Z. Xie, and Y. Benenson, *Hierarchical ligation-independent assembly of PCR fragments.* Methods Mol Biol, 2014. **1116**: p. 49-58.
220. Schneider, C.A., W.S. Rasband, and K.W. Eliceiri, *NIH Image to ImageJ: 25 years of image analysis.* Nat Methods, 2012. **9**(7): p. 671-5.
221. Subramanian, L., et al., *Eic1 links Mis18 with the CCAN/Mis6/Ctf19 complex to promote CENP-A assembly.* Open Biol, 2014. **4**: p. 140043.
222. Soisson, S.M., et al., *Structural basis for ligand-regulated oligomerization of AraC.* Science, 1997. **276**(5311): p. 421-5.
223. Joglekar, A.P., et al., *Molecular architecture of a kinetochore-microtubule attachment site.* Nat Cell Biol, 2006. **8**(6): p. 581-5.
224. Johnston, K., et al., *Vertebrate kinetochore protein architecture: protein copy number.* J Cell Biol, 2010. **189**(6): p. 937-43.
225. Buckingham, L.E., et al., *Nucleotide sequence and promoter analysis of SPO13, a meiosis-specific gene of Saccharomyces cerevisiae.* Proc Natl Acad Sci U S A, 1990. **87**(23): p. 9406-10.
226. Katis, V.L., et al., *Spo13 facilitates monopolin recruitment to kinetochores and regulates maintenance of centromeric cohesion during yeast meiosis.* Curr Biol, 2004. **14**(24): p. 2183-96.